UNIVERSITY OF SOUTHAMPTON

FACULTY OF SCIENCE

OCEANOGRAPHY

The Use of ERS-1 Synthetic Aperture Radar for Measurement and Modeling of the Directional Wave Spectrum

by Nelson Violante-Carvalho

Thesis submitted in partial fulfillment of the requirements for the degree of Doctor of Philosophy

November 2002

Dedico esse trabalho ao meu melhor amigo, Seu Armandão.

Cais - Milton Nascimento e Ronaldo Bastos

Para quem quer se soltar
Invento o cais
Invento mais que a solidão me dá
Invento lua nova a clarear
Invento o amor
E sei a dor de encontrar
Eu queria ser feliz
Invento o mar
Invento em mim o sonhador
Para quem quer me seguir
Eu quero mais
Tenho o caminho do que sempre quis
E um saveiro pronto pra partir
Invento o cais
E sei a vez de me lançar

A Terceira Margem do Rio - Guimarães Rosa

Nosso pai era homem cumpridor, ordeiro, positivo; e sido assim desde mocinho e menino, pelo que testemunharam as diversas sensatas pessoas, quando indaguei a informação. Do que eu mesmo me alembro, ele não figurava mais estúrdio nem mais triste do que os outros, conhecidos nossos. Só quieto. Nossa mãe era quem regia, e que ralhava no diário com a gente - minha irmã, meu irmão e eu. Mas se deu que, certo dia, nosso pai mandou fazer para si uma canoa.

Era a sério. Encomendou a canoa especial, de pau de vinhático, pequena, mal com a tabuinha da popa, como para caber justo o remador. Mas teve de ser toda fabricada, escolhida forte e arqueada em rijo, própria para dever durar na água por uns vinte ou trinta anos. Nossa mãe jurou muito contra a idéia. Seria que, ele, que nessas artes não vadiava, se ia propor agora para pescarias e caçadas? Nosso pai nada não dizia. Nossa casa, no tempo, ainda era mais próxima do rio, obra de nem quarto de légua: o rio por aí se estendendo grande, fundo, calado que sempre. Largo, de não se poder ver a forma da outra beira. E esquecer não posso, do dia em que a canoa ficou pronta.

Sem alegria nem cuidado, nosso pai encalcou o chapéu e decidiu um adeus para a gente. Nem falou outras palavras, não pegou matula e trouxa, não fez a alguma recomendação. Nossa mãe, a gente achou que ela ia esbravejar, mas persistiu somente alva de pálida, mascou o beiço e bramou: - "Cê vai, ocê fique, você nunca volte!" Nosso pai suspendeu a resposta. Espiou manso para mim, me acenando de vir também, por uns passos. Temi a ira de nossa mãe, mas obedeci, de vez de jeito. O rumo daquilo me animava, chega que um propósito perguntei: - "Pai, o senhor me leva junto, nessa sua canoa?" Ele só retornou o olhar em mim, e me botou a bênção, com gesto me mandando para trás. Fiz que vim, mas ainda virei, na grota do mato, para saber. Nosso pai entrou na canoa e desamarrou, pelo remar. E a canoa saiu se indo - a sombra dela por igual, feito um jacaré, comprida longa.

Nosso pai não voltou. Ele não tinha ido a nenhuma parte. Só executava a invenção de se permanecer naqueles espaços do rio, de meio a meio, sempre dentro da canoa, para dela não saltar, nunca mais. A estranheza dessa verdade deu para estarrecer de todo a gente. Aquilo que não havia, acontecia. Os parentes, vizinhos e conhecidos nossos, se reuniram, tomaram juntamente conselho.

Nossa mãe, vergonhosa, se portou com muita cordura; por isso, todos pensaram de nosso pai a razão em que não queriam falar: doideira. Só uns achavam o entanto de poder também ser pagamento de promessa; ou que, nosso pai, quem sabe, por escrúpulo de estar com alguma feia doença, que seja, a lepra, se desertava para outra sina de existir, perto e longe de sua família dele. As vozes das notícias se dando pelas certas pessoas - passadores, moradores das beiras, até do afastado da outra banda - descrevendo que nosso pai nunca

se surgia a tomar terra, em ponto nem canto, de dia nem de noite, da forma como cursava no rio, solto solitariamente. Então, pois, nossa mãe e os aparentados nossos, assentaram: que o mantimento que tivesse, ocultado na canoa, se gastava; e, ele, ou desembarcava e viajava s'embora, para jamais, o que ao menos se condizia mais correto, ou se arrependia, por uma vez, para casa.

No que num engano. Eu mesmo cumpria de trazer para ele, cada dia, um tanto de comida furtada: a idéia que senti, logo na primeira noite, quando o pessoal nosso experimentou de acender fogueiras em beirada do rio, enquanto que, no alumiado delas, se rezava e se chamava. Depois, no seguinte, apareci, com rapadura, broa de pão, cacho de bananas. Enxerguei nosso pai, no enfim de uma hora, tão custosa para sobrevir: só assim, ele no ao-longe, sentado no fundo da canoa, suspendida no liso do rio. Me viu, não remou para cá, não fez sinal. Mostrei o de comer, depositei num oco de pedra do barranco, a salvo de bicho mexer e a seco de chuva e orvalho. Isso, que fiz, e refiz, sempre, tempos a fora. Surpresa que mais tarde tive: que nossa mãe sabia desse meu encargo, só se encobrindo de não saber; ela mesma deixava, facilitado, sobra de coisas, para o meu conseguir. Nossa mãe muito não se demonstrava.

Mandou vir o tio nosso, irmão dela, para auxiliar na fazenda e nos negócios. Mandou vir o mestre, para nós, os meninos. Incumbiu ao padre que um dia se revestisse, em praia de margem, para esconjurar e clamar a nosso pai o dever de desistir da tristonha teima. De outra, por arranjo dela, para medo, vieram os dois soldados. Tudo o que não valeu de nada. Nosso pai passava ao largo, avistado ou diluso, cruzando na canoa, sem deixar ninguém se chegar à pega ou à fala. Mesmo quando foi, não faz muito, dos homens do jornal, que trouxeram a lancha e tencionavam tirar retrato dele, não venceram: nosso pai se desaparecia para a outra banda, aproava a canoa no brejão, de léguas, que há, por entre juncos e mato, e só ele conhecesse, a palmos, a escuridão, daquele.

A gente teve de se acostumar com aquilo. Às penas, que, com aquilo, a gente mesmo nunca se acostumou, em si, na verdade. Tiro por mim, que, no que queria, e no que não queria, só com nosso pai me achava: assunto que jogava para trás meus pensamentos. O severo que era, de não se entender, de maneira nenhuma, como ele agüentava. De dia e de noite, com sol ou aguaceiros, calor, sereno, e nas friagens terríveis de meio-do-ano, sem arrumo, só com o chapéu velho na cabeça, por todas as semanas, e meses, e os anos - sem fazer conta do se-ir do viver. Não pojava em nenhuma das duas beiras, nem nas ilhas e croas do rio, não pisou mais em chão nem capim. Por certo, ao menos, que, para dormir seu tanto, ele fizesse amarração da canoa, em alguma ponta-de-ilha, no esconso. Mas não armava um foguinho em praia, nem dispunha de sua luz feita, nunca mais riscou um fósforo. O que consumia de comer, era só um quase; mesmo do que a gente depositava, no entre as raízes da gameleira, ou na lapinha de pedra do barranco, ele

recolhia pouco, nem o bastável. Não adoecia? E a constante força dos braços, para ter tento na canoa, resistido, mesmo na demasia das enchentes, no subimento, aí quando no lanço da correnteza enorme do rio tudo rola o perigoso, aqueles corpos de bichos mortos e paus-de-árvore descendo - de espanto de esbarro. E nunca falou mais palavra, com pessoa alguma. Nós, também, não falávamos mais nele. Só se pensava. Não, de nosso pai não se podia ter esquecimento; e, se, por um pouco, a gente fazia que esquecia, era só para se despertar de novo, de repente, com a memória, no passo de outros sobressaltos.

Minha irmã se casou; nossa mãe não quis festa. A gente imaginava nele, quando se comia uma comida mais gostosa; assim como, no gasalhado da noite, no desamparo dessas noites de muita chuva, fria, forte, nosso pai só com a mão e uma cabaça para ir esvaziando a canoa da água do temporal. Às vezes, algum conhecido nosso achava que eu ia ficando mais parecido com nosso pai. Mas eu sabia que ele agora virara cabeludo, barbudo, de unhas grandes, mal e magro, ficado preto de sol e dos pêlos, com o aspecto de bicho, conforme quase nu, mesmo dispondo das peças de roupas que a gente de tempos em tempos fornecia.

Nem queria saber de nós; não tinha afeto? Mas, por afeto mesmo, de respeito, sempre que às vezes me louvavam, por causa de algum meu bom procedimento, eu falava: - "Foi pai que um dia me ensinou a fazer assim..."; o que não era o certo, exato; mas, que era mentira por verdade. Sendo que, se ele não se lembrava mais, nem queria saber da gente, por que, então, não subia ou descia o rio, para outras paragens, longe, no não-encontrável? Só ele soubesse. Mas minha irmã teve menino, ela mesma entestou que queria mostrar para ele o neto. Viemos, todos, no barranco, foi num dia bonito, minha irmã de vestido branco, que tinha sido o do casamento, ela erguia nos braços a criancinha, o marido dela segurou, para defender os dois, o guarda-sol. A gente chamou, esperou. Nosso pai não apareceu. Minha irmã chorou, nós todos aí choramos, abraçados.

Minha irmã se mudou, com o marido, para longe daqui. Meu irmão resolveu e se foi, para uma cidade. Os tempos mudavam, no devagar depressa dos tempos. Nossa mãe terminou indo também, de uma vez, residir com minha irmã, ela estava envelhecida. Eu fiquei aqui, de resto. Eu nunca podia querer me casar. Eu permaneci, com as bagagens da vida. Nosso pai carecia de mim, eu sei - na vagação, no rio no ermo - sem dar razão de seu feito. Seja que, quando eu quis mesmo saber, e firme indaguei, me diz-que-disseram: que constava que nosso pai, alguma vez, tivesse revelado a explicação, ao homem que para ele aprontara a canoa. Mas, agora, esse homem já tinha morrido, ninguém soubesse, fizesse recordação, de nada mais. Só as falsas conversas, sem senso, como por ocasião, no começo, na vinda das primeiras cheias do rio, com chuvas que não estiavam, todos temeram o fim-do-mundo, diziam: que nosso pai fosse o avisado que nem Noé, que, por tanto, a canoa ele tinha antecipado; pois agora me entrelembro. Meu pai, eu não podia

malsinar. E apontavam já em mim uns primeiros cabelos brancos.

Sou homem de tristes palavras. De que era que eu tinha tanta, tanta culpa? Se o meu pai, sempre fazendo ausência: e o rio-rio-rio, o rio - pondo perpétuo. Eu sofria já o começo de velhice - esta vida era só o demoramento. Eu mesmo tinha achaques, ânsias, cá de baixo, cansaços, perrenguice de reumatismo. E ele? Por quê? Devia de padecer demais. De tão idoso, não ia, mais dia menos dia, fraquejar do vigor, deixar que a canoa emborcasse, ou que bubuiasse sem pulso, na levada do rio, para se despenhar horas abaixo, em tororoma e no tombo da cachoeira, brava, com o fervimento e morte. Apertava o coração. Ele estava lá, sem a minha tranqüilidade. Sou o culpado do que nem sei, de dor em aberto, no meu foro. Soubesse - se as coisas fossem outras. E fui tomando idéia.

Sem fazer véspera. Sou doido? Não. Na nossa casa, a palavra doido não se falava, nunca mais se falou, os anos todos, não se condenava ninguém de doido. Ninguém é doido. Ou, então, todos. Só fiz, que fui lá. Com um lenço, para o aceno ser mais. Eu estava muito no meu sentido. Esperei. Ao por fim, ele apareceu, aí e lá, o vulto. Estava ali, sentado à popa. Estava ali, de grito. Chamei, umas quantas vezes. E falei, o que me urgia, jurado e declarado, tive que reforçar a voz: - "Pai, o senhor está velho, já fez o seu tanto... Agora, o senhor vem, não carece mais... O senhor vem, e eu, agora mesmo, quando que seja, a ambas vontades, eu tomo o seu lugar, do senhor, na canoa!..." E, assim dizendo, meu coração bateu no compasso do mais certo.

Ele me escutou. Ficou em pé. Manejou remo n'água, proava para cá, concordado. E eu tremi, profundo, de repente: porque, antes, ele tinha levantado o braço e feito um saudar de gesto - o primeiro, depois de tamanhos anos decorridos! E eu não podia... Por pavor, arrepiados os cabelos, corri, fugi, me tirei de lá, num procedimento desatinado. Porquanto que ele me pareceu vir: da parte de além. E estou pedindo, pedindo, pedindo um perdão.

Sofri o grave frio dos medos, adoeci. Sei que ninguém soube mais dele. Sou homem, depois desse falimento? Sou o que não foi, o que vai ficar calado. Sei que agora é tarde, e temo abreviar com a vida, nos rasos do mundo. Mas, então, ao menos, que, no artigo da morte, peguem em mim, e me depositem também numa canoinha de nada, nessa água que não pára, de longas beiras: e, eu, rio abaixo, rio a fora, rio a dentro - o rio.

PREFACE

Living abroad is a trip of self discovery. Weakness, fears, limits and strengths, it seems that your inner self is revealed in, many times, surprising ways. Doing a PhD is not exactly easy, either. And if I managed to do so is because I relied on many people, old and new friends that I've made along this long road.

Jamais conseguirei expressar com palavras a gratidão que tenho pelos meus pais, Seu Armando e Dona Emilia. O esforço de uma vida de trabalho para dar a mim e aos meus irmãos a educação que eles nunca tiveram condições de desfrutar. Pessoas simples mas que sempre perceberam que há algo que nunca será tomado de você, por mais que essa vida venha a lhe maltratar.

Professor Dr Ian S. Robinson, my supervisor and now my friend. He always believed in me, even at the very beginning when all the ideas that I had seemed almost unattainable, he did everything possible to make me get there.

I sincerely want to give thanks to the Brazilian People for this lifetime opportunity. I have to be proud of the chance that I was awarded by the Brazilian Research Funding Agency CNPq.

Meu pobre português, tenho que admitir, não evoluiu muito durante esses quatro anos de Inglaterra. O processo de aprendizado de uma língua, às vezes com uma quase imersão numa cultura diferente, é bastante frustrante. Porém vários compatriotas ajudaram a manter viva minha chama brasileira, mesmo vivendo num país e numa cultura tão diferentes da minha própria. Queria deixar aqui minha gratidão a alguns deles. Marcia, talvez você nunca vá ter idéia de como você foi importante para a realização deste trabalho. Seu apoio incondicional, especialmente no início da minha vida aqui, foi o estímulo que eu precisava para seguir em frente. Voce me mostrou que ainda tenho muito que esperar dos anos que vem por aí. Ao Rodrigão e a Dhesi, minha família no Hemisfério Norte, obrigado por tudo. Quando a solidão apertava mais forte lá era sempre um porto seguro para me sentir em um lar mais uma vez, sempre com a chance de matar as saudades de um feijão preto ou simplesmente falar sobre tudo ou nada. Ao Israel, ao Andrezinho e à Celina, fazendo com que a Bahia fosse aqui. Ao Cesar 'mad doc' pela inacreditável paciência toda vez que eu ligava pedindo um reboque do meu clássico Santana 1983 pelas ruas de Southampton (carro de colecionador, gostava de pensar...).

More rewarding than doing a PhD, I have to say, was the chance to meet people from all

over the world and with some of them I have built relationships that I'm sure I'll take with me forever. Adrian, since the month we spent on Discovery studying the ocean circulation of the North Atlantic in between our gin and tonics, showed me how the British people can be very warm and friendly. Ed Boy 'echale ganas' Possani, mi cabronissimo hermano mexicano, always there for me. Vaso, Marina, Sally, Kirstin, Stuart, Helko, Carlita and Spiros, Doortje, this thesis could be finished with the special help of all of you. I won't forget that....

UNIVERSITY OF SOUTHAMPTON

ABSTRACT

FACULTY OF SCIENCE

OCEANOGRAPHY

Doctor of Philosophy

The Use of ERS-1 Synthetic Aperture Radar for Measurement and Modeling of the Directional Wave Spectrum

by Nelson Violante-Carvalho

The study presented in this work examines the use of Synthetic Aperture Radar (SAR) onboard the first European Remote Sensing Satellite (ERS-1) for the measurement of wind waves and discusses its applications such as wave data assimilation and inverse modeling. Since the launch of ERS-1 in 1991 the directional wave spectrum became available with high spatial and temporal global coverage. With the subsequent launch of its successors ERS-2 and ENVISAT millions of SAR wave mode (SWM) imagettes have been and are still being acquired providing a unique data set for the improvement of the understanding of the dynamics of surface gravity waves.

Over four years of directional measurements acquired by a heave-pitch-roll buoy moored in tropical deep waters around 150 km offshore are employed to investigate the mechanisms of SAR wave imaging and the retrievals of wave spectra from SAR images. A new approach for the partitioning of the frequency spectrum is implemented and applied to isolate the wind sea from the swell contaminated spectra. Specifically the influence of swell on wind sea growth is analyzed in terms of their direction of propagation and separation in frequency space, with direct connection on how long waves modulate short ones. The relatively poorly understood Hydrodynamic and Tilt Modulation Transfer Functions (MTF) are discussed in the light of the findings.

For the first time the most widely implemented Max-Planck Institut (MPI) SWM retrieval scheme was assessed through detailed statistical intercomparisons and selected qualitative validations against directional buoy data and against the third generation wave model WAM data—which was used as first guess to the inversion. The MPI scheme deteriorates the first guess increasing the bias and the error of the retrievals of significant wave height, mean wave length and mean direction of propagation of short waves. Nevertheless for waves longer than 225 m—the part of the spectrum directly mapped onto SAR images—the performance of the retrieval scheme is superior to the wave model. The directional spreading retrieved by the MPI scheme is also investigated with results in close agreement with the spreading obtained from the Fourier coefficients directly measured by the buoy. The performance of the WAM model, the ECMWF Atmospheric Model and of the Maximum Entropy Method for the retrieval of the buoy directional spectrum are also discussed through several cross-validation exercises.

RESUMO

Uso de Radar de Abertura Sintética para Medições e Modelagem do Espectro de Ondas Direcional

O presente trabalho examina o uso de Radar de Abertura Sintética (Synthetic Aperture Radar SAR da sigla em inglês) a bordo do primeiro Satélite Europeu de Sensoriamento Remoto (ERS-1) para medições de ondas superficiais de gravidade e suas aplicações como por exemplo em assimilação de dados e em técnicas de modelagem inversa. Medições do espectro direcional de onda com elevada cobertura espacial e temporal estão agora disponíveis desde o lançamento do ERS-1 em 1991. Com o subsequente lançamento de seus sucessores ERS-2 e ENVISAT milhões de imagens SAR no modo onda (SAR wave mode) foram e ainda estão sendo aquisitadas gerando uma oportunidade única para o aperfeiçoamento da compreensão da dinâmica de ondas superficias de gravidade.

Medições direcionais aquisitadas por uma bóia do tipo heave-pitch-roll fundeada em água profunda compreendendo mais de quatro anos de dados são empregadas na investigação dos mecanismos de imageamento de ondas por SAR e na extração do espectro direcional de ondas. Uma nova abordagem é desenvolvida e aplicada para o particionamento do espectro de freqêuncia para possibilitar a separação da vaga do resto do espectro contendo ondulação. Em particular a influência da ondulação no desenvolvimento das vagas é analizada em termos das suas direções de propagação e separação em frequência, estando diretamente relacionado em como ondas mais longas modulam ondas relativamente mais curtas. A relativamente pouco compreendidada Função de Transferência de Modulação Hidrodinâmica e de Inclinação (Tilt) são discutidas baseadas nos resultados obtidos.

Pela primeira vez o amplamente difundido esquema de extração do Max-Planck Institut (MPI) é avaliado através de detalhadas intercomparações estatísticas com dados da bóia e com dados do modelo de ondas de terceira geração WAM—que foi usado como primeira estimativa para a inversão. O esquema MPI deteriora a qualidade do dado do modelo usado como entrada para a inversão aumentando o erro e a tendência (bias) da altura significativa de onda, direção média de propagação e frequência média das ondas relativamente mais curtas. Contudo para ondas mais longas que 225 m—a parte do espectro diretamente mapeado nas imagens SAR—o esquema MPI não deteriora o espectro usado como estimativa inicial, com resultados comparando com a bóia tão bem quanto o modelo WAM. O espalhamento direcional calculado pelo esquema MPI também é investigado com resultados próximos com o espalhamento obtido dos coeficientes de Fourier diretamente medidos pela bóia. O desempenho do modelo de ondas WAM, do modelo atmosférico do ECMWF e do Método de Máxima Entropia para a recuperação do espectro direcional da bóia são também discutidos através de vários execícios de intercomparação.

Contents

List of Figures

List of Tables

Chapter 1

Introduction and Objectives

1.1 Overview

The launch of the first European Remote Sensing Satellite (ERS-1) in 1991 was a turning point for the investigation of the climatology and for the continuous observation of the detailed spectral properties of the wind waves. For the first time the two-dimensional directional wave spectrum became available with high spatial and temporal coverage over all oceanic basins through the wave mode of the Synthetic Aperture Radar (SAR). With the subsequent launch of its successors ERS-2 and ENVISAT, over ten years of global measurements and millions of SAR wave mode (SWM) imagettes have been and are still being acquired in quasi-real time yielding a unique opportunity for the improvement of our understanding of the mechanisms that govern the growth and evolution of waves.

The potentialities of such data are enormous. The better estimation through numerical simulations of the wave field using past forcing winds to compute the climatologies (hindcasts) or for wave forecasts has practical importance such as for ship routing, offshore activities, coastal management and fisheries among several others. To achieve such improvements wave models have to rely on detailed spectral measurements which are available, on such a spatial and temporal coverage, only from sensors onboard satellites.

The interest in this field of research is, however, not only limited to the economic and engineering concerns. Wind waves are the interface between the ocean and the atmosphere and are therefore closely connected to the exchange processes like for example transfer of mechanical energy, momentum, sensible and latent heat and gases (Donelan, 1990; Komen et al., 1994; Csanady, 2001). Energy is transferred from the atmosphere to the ocean driving

the circulation of the upper ocean. Energy from the ocean, on the other hand, is fed back to the atmosphere affecting the atmospheric circulation and the climate. The wind drag coefficient is affected by the wave age and by the wave spectrum but there is still, however, considerable uncertainty on how to model its dependency on the sea state. A better description of air-sea interaction and its consequences, for example on the the world climate, has to take into account the role played by the waves on the fluxes across the interface. The studies using sophisticated numerical climate simulations considering the coupling between ocean and atmosphere and its interface using wave models are increasingly expanding. This is a field of exciting possibilities and several forecasting centers are investigating the feasibility of combining such models.

Over the last 30 years major research efforts have been made and we now have suitable parameterizations of the source terms that describe the dynamics of wind waves. This has been reflected in the development of advanced third generation wave models such as WAM, WaveWatch and SWAN that compute the directional spectrum by direct integration of the energy balance equation based on the structure of the terms that describe the input of energy from the wind, the nonlinear interaction among wave components and the dissipation of energy due to whitecapping. Although their performances have already been demonstrated by several validation tests (see for example the comparisons of the WAM estimates against buoy and satellite measurements in Komen et al., 1994) these wave models have room for improvement where their main deficiencies lay in: 1. the numerical resolution; 2. the numerics, such as the propagation schemes and the integration of the nonlinear interactions; 3. the physical representation of the terms of input and dissipation of energy.

Advances in our understanding of surface processes translating into better estimates through numerical simulations will necessarily require improvements in satellite remote sensing retrievals and more comprehensive schemes for the assimilation of this information into wave models. Present operational methods are still based on the relatively simple optimal interpolation schemes (Lionello et al., 1992; Hasselmann et al., 1997; Voorrips et al., 1997). So far only significant wave heights obtained from altimeters have been assimilated operationally into wave models. However with positive impact the use of an integral parameter such as H_s imposes severe limitations since the averaged energy has to be distributed somehow over the entire spectrum. The use of more sophisticated methods (such as the Green's Function Method proposed by Bauer et al., 1996) that take advantage of the detailed spectral information yielded by SAR have not yet been implemented operationally but have already

shown the potentialities of the technique. Variational methods are able to track back in time and space swell components and correct the forcing wind at a time preceding the available observations which would reflect into better forecasts in coupled atmosphere-ocean models. More advanced methods using the adjoint technique and the Kalman filter should be further explored although their feasibility has already been demonstrated (de las Heras et al., 1994; Voorrips et al., 1999).

The high spatial and temporal variability of surface processes needs to be properly considered in any investigation of the dynamics of wind waves. High resolution models combined with detailed spectral satellite data seem to offer the best opportunity to provide global analysis and predictions. The use of wave spectra retrieved from ERS-1 SAR wave mode and the WAM wave model together with in situ measurements are the main constituents of the present study.

1.2 Description of the Data Used

1.2.1 ERS-1 SAR Wave Mode Spectra

SAR is the only instrument that has been so far deployed from satellites that is capable of measuring the full directional wave spectrum and therefore allowing the complete characterization of a sea state. In SAR image mode the instrument acquires 100 x 100 km images with resolution around 30 x 30 m but due to onboard storage limitations it can be operated only with a ground station in sight. The SAR wave mode (SWM) was introduced to overcome this coverage limitation since the much smaller 10 x 5 km imagettes are storage onboard and transmitted once per orbit to ground stations. With similar resolution to the image mode, SWM are acquired every 30 seconds yielding an along track resolution of 200 km and a cross track resolution of 1000–2000 km with a total of around 15 hundred images collected every day.

The retrieval of the directional wave spectrum from SAR images is not, however, a trivial exercise. There are two main limitations in the SAR ocean wave imaging mechanisms. Firstly there is a 180° directional ambiguity observed in frozen images. This problem has been solved with the launch of ENVISAT carrying the Advanced Synthetic Aperture Radar (ASAR) which computes two successive images resolving the propagation direction. In second place the SAR imaging mechanism is strongly nonlinear due to the vertical orbital movements induced by the waves which causes a Doppler offset in the image plane with smearing and

loss of information beyond a high wavenumber cut-off. These limitations impose the use of additional information, in general a first guess wave spectrum from a model, to solve the ambiguity and to augment the spectral information in the high wavenumber part of the spectrum.

Several schemes to extract the wave spectrum from SAR images have been proposed (Hasselmann and Hasselmann, 1991; Krogstad et al., 1994; Hasselmann et al., 1996; Mastenbroek and de Valk, 2000), however the breakthrough in the retrieval of ocean wave spectra from SAR was the work by Hasselmann and Hasselmann (1991). Since the imaging mechanisms are reasonably well understood (Hasselmann et al., 1985), K. Hasselmann and S. Hasselmann realized that the mapping of a wave spectrum into a SAR image spectrum can be numerically computed. Furthermore they proposed a computationally efficient way of inverting the mapping relation in order to extend the missing information in the high wavenumber band and to solve the directional ambiguity. An improved algorithm developed at the Max-Planck Institut (MPI) was later implemented (Hasselmann et al., 1996) which is the version used in the present work. For the first time a retrieval algorithm will be statistically validated against directional buoy data allowing the assessment of the directional and spectral capabilities of the SAR measurements.

1.2.2 The WAM Model

In the present study a workstation version of the wave model WAM cycle 4 is run to yield the first guess for the MPI scheme. WAM is a third generation wave model and has been so far the most validated model running operationally at several forecasting centers (see the 'WAM book' for more details about the validation exercises and the model characteristics: Komen et al., 1994). The version of the WAM model that runs operationally at the European Centre for Medium-Range Weather Forecasts (ECMWF) has been assimilating significant wave heights obtained from altimeters continuously since August 1993.

Since we are also comparing the estimates of the wave model used as first guess to the retrieval against buoy measurements, the possible influence of the assimilation on the final results of the retrieval could be assessed using in addition spectra from the ECMWF WAM. However in our period of interest the only data set including 2D spectra is the ERA (ECMWF Re-analysis) but currently only the year 1993 has been validated and released. Although the investigation of the influence of the assimilation on the MPI retrievals comparing runs with and without assimilation would be of great value, the use of the results of the WAM model

without any sort of modification on the estimates of significant wave height (SWH) has an extra appeal. If one seeks to search for deficiencies in the numerical model through detailed spectral comparisons against buoy measurements the spurious influence of the assimilation of altimeter data would make the interpretation of the discrepancies more complicated.

1.2.3 In Situ Measurements

Campos Basin, in the coast off Rio de Janeiro, is the most important petrolic basin in Brazil. Tens of platforms are located in this area responsible for over 75% of the oil produced by the country with several offshore operations taking place daily. In addition the surrounding area holds a high urban concentration with strong commercial and industrial activities. Due to the remarkable importance of this region, the Brazilian Oil Company PETROBRAS carried out an extensive experiment to study the main meteo-oceanographic features of Campos Basin deploying a heave-pitch-roll buoy—in addition to mooring lines—during a period of more than four years in a depth over 1000 m around 150 km offshore.

This data set yields a unique opportunity to investigate the mechanisms of ocean wave SAR imaging and the retrievals of wave spectra from SAR images. In the first place directional buoy measurements in deep water are scarce. The buoys under the supervision of the National Oceanic and Atmospheric Administration (NOAA) are located mainly in relatively shallow waters and are almost all omni-directional. The location of buoys in shallow waters imposes an additional complication to any sort of analysis due to the spatially high gradients of the wave parameters compared to the more homogeneous situations encountered in the open ocean. The other well known source of wave measurements is the network deployed in relatively shallow waters in the North Sea which are in their majority directional buoys. Nevertheless when passing over this region the ERS SAR is often switched to image mode which yielded only a few SWM imagettes during the several years of SAR measurements (Mastenbroek and de Valk, 2000).

Another interesting characteristic of the wave measurements used in this work is their geographical location. Right under the line of the Tropic of Capricorn Campos Basin is strongly affect by swell all the year round with the low frequency band containing most of the spectral energy measured by the buoy. As pointed out by Voorrips et al. (2001) the larger the energy in the part of the spectrum unobserved by SAR the more difficult the retrieval schemes have in estimating the low-frequency swell. Consequently one would expect a better performance of the retrieval in this area.

Thirdly the data set shows the ubiquitous presence of a young swell component propagating closely in direction and frequency with the wind sea (in range direction), as well as a much longer, opposing swell propagating in azimuth direction. These characteristics are ideal for the study of the influence of swell on wind sea growth in the open sea, with direct connection on how short waves are modulated by longer ones.

1.3 Objectives

The interest in the energy balance of short gravity waves has increased substantially in the last 20 years. These decimetric waves play an important role in small scale air-sea interactions that are responsible for the exchange processes through the interface. Furthermore the electromagnetic waves emitted by microwave instruments interact with the short ocean gravity waves in a process called Bragg resonance (see for example Robinson, 1985, chapter 12) responsible for the modulation of the radar backscatter and therefore for the imaging mechanisms. The Real Aperture Radar (RAR) modulation, composed by the Hydrodynamic and Tilt modulation, is particularly sensitive to the behavior of the Bragg (ripple) waves. Just for a brief description, the Tilt Modulation Transfer Function (MTF) assumes that these Bragg waves are represented by a high frequency tail proportional to the wave number vector $\mathbf{k}$ to the power of -4. The Hydrodynamic MTF, on the other hand, describes the modulation of the ripples by the phase of the longer waves.

The question that arises is how the investigation of waves propagating in the open ocean will contribute to the understanding of the modulation mechanisms, since they are in general much longer than the decimetric Bragg waves. As pointed out by Komen (1988), for low wind speeds and at early stages of development, the Bragg waves are within the spectral range analyzed by Komen et al. (1984) and consequently the energy balance in the equilibrium range described by the interaction of the source functions applies. Likewise, the results of the investigation of the influence of swell on wind sea waves can be extrapolated to shorter waves thus contributing to the discussion.

Several experimental studies have been presented aimed at a better understanding of the processes of modulation of short wind waves generated in tanks by longer, paddled waves (see a review of such experiments in Hanson and Phillips, 1999). Nevertheless the evidence for the influence of longer (swell) waves on wind waves in the open ocean is difficult to demonstrate, partially due to the need for reliable spectral methods to isolate the wind sea

from the swell contaminated spectra. Some spectral methods have been proposed lately, from the pioneering JONSWAP to the more sophisticated methods for the partitioning of the directional spectrum (Gerling, 1992). The high frequency spectral tail is, however, sensitive to the spectral width of the directional spectrum (as demonstrated by Banner and Young, 1994) and the reconstruction of the 2D spectrum from heave-pitch-roll buoy measurements is subject to a degree of uncertainty. As a consequence we believe that the results from the partitioning of the frequency spectrum—yielded directly from the heave measurements without any assumption about the directional spreading—are more robust.

One of the main issues addressed in this work therefore is the influence on short waves by longer waves in the open ocean. To attain this goal we propose a new method for the partitioning and adjustment of the spectral parameters of the frequency spectrum. This method is applied to a large data set of buoy measurements obtained in a tropical region where the influence of swell on wind sea waves is investigated in terms of their direction of propagation and in terms of their distance in frequency space.

The second main ingredient in our study is the retrieval of wave spectra from SAR images. The MPI scheme is the most widely used retrieval algorithm which runs operationally at several forecasting centers, many of them developing techniques for the assimilation of the directional spectrum retrieved from the inversion—as for example the ECMWF (Janssen and Bidlot, 2001) and the British Met Office (Jim Gunson, personal communication). Surprisingly, however, the statistical validation of the algorithm against directional buoy measurements has not been done yet. As discussed earlier one of the main reasons is the lack of continuous directional buoy wave measurements, in particular in deep waters.

A comprehensive intercomparison of the directional wave spectra retrieved from the MPI scheme, estimated by the WAM wave model and measured by a heave-pitch-roll buoy is carried out for a period of one year using over one hundred spectra. When possible the strength of one method is used to assess the performance of the others, pointing out their weakness. Thus, for example, the linearly mapped swell components from SAR measurements are used to check the quality of the Maximum Entropy Method in the reconstruction of the directional spectra from buoy measurements and in addition to validate the estimation of long waves by the model. Moreover the wind sea components measured by the buoy can assess the quality of the model estimates in more complicated conditions, such as turning winds or on early stages of development when the performance of the approximation of the nonlinear interactions and the numerical resolution of the model, respectively, can be analyzed.

Since the advent of satellite oceanography the field of wave data assimilation has experienced a fast development. So far only SWH from altimeters have been assimilated by operational forecasting centers but with the improvement of the schemes for the retrieval of the wave spectrum from SAR images the natural trend is that this picture is going to change. The cumbersome task of redistributing the energy from an integral parameter like SWH over the spectrum seems pointless since reliable global estimates of the full directional spectrum are becoming available. With this picture in mind we present a review of the techniques for the assimilation of the two-dimensional directional spectrum into wave models.

1.4 Organization of the Work

The structure of the work is the following. In Chapter 2 and 3 the buoy measurements and the characteristics of the WAM model that we are working with are respectively presented. The scheme for the partitioning and spectral adjustment of the frequency spectrum is described in Chapter 4 and its application to buoy measurements to investigate the influence of swell on wind sea growth in the open sea is carried out in Chapter 5.

Chapter 6 is focused on a comprehensive description of the Max-Planck Institut (MPI) retrieval scheme of wave spectra from SAR images. In addition a review of the SAR ocean wave imaging mechanisms is presented together with discussions about the strengths and the weakness of the algorithm.

The intercomparison of the directional spectra yielded by the MPI scheme, from the model and by the buoy together with a statistical validation of the retrievals and estimates against buoy measurements is presented in Chapter 7.

The conclusions and ideas for future work are presented in Chapter 8 whereas the Appendix provides an overview of assimilation schemes of directional wave data published up to the present.

This work has been organized in such a way that every chapter has the format of a scientific paper, therefore the fundamental background concepts are within chapters rather than in a single, in general introductory chapter.

Chapter 2

Buoy Measurements

2.1 Buoy Wave Data Analysis

Campos Basin, off Rio de Janeiro (Figure 2.1), is the most important oil and gas basin in Brazil. More than 70% of the petroleum prospected in the country comes from the tens of platforms located in this area. Every day several offshore operations take place in the region, which operatively depend on the sea state, in particular on the surface waves. This is one of the most important regions in Brazil with huge urban concentrations and strong commercial, industrial and touristic activities.

The South Atlantic Deep Water Program (PROCAP) was an extensive experiment carried out by the Brazilian Oil Company PETROBRAS in Campos Basin to study the main oceanographic features of the region. In terms of wind and wave measurements a heave-pitch-roll buoy (Figure 2.2) was moored in a depth over 1000 meters at position $22°31' S$ and $39°58' W$ from March 1991 to March 1993 and from January 1994 to July 1995. The wind speed and direction were measured hourly from the buoy by two Young propeller-vane anemometers at a height of $3.78\,m$ and $4.43\,m$ and later converted for the standard height of $10\,m$. Each measurement is the average of a ten minute record, obtained one per hour.

The wave buoy acquired three time series, the vertical displacement (η) and two slopes (η_x and η_y) in the east and north directions, respectively. These time series are the starting point for the spectral analysis performed. The displacements were sampled at a rate of $1\,Hz$ during 20 minutes eight times a day every three hours. The spectral estimators were obtained using the Welch Method (see for example Marple Jr., 1987). Records consisting of 1024 data points (with a sample length of approximately 17 minutes) were segmented in 16 partitions

Page 10
missing from
this Thesis

Figure 2.2: Heave-pitch-roll buoy in operation in Campos Basin. The hull has a diameter of 3 m, the structure has a height of 6 m with a total weight of 1500 kg.

Following the original work of Longuet-Higgins et al. (1963), applying auto and cross-

spectral analysis on the three components yields

$$\begin{aligned}
C_{11}(f) &= \int_{-\pi}^{+\pi} F(f,\theta)\, d\theta, \\
C_{22}(f) &= k^2 \int_{-\pi}^{+\pi} F(f,\theta) \cos^2(\theta)\, d\theta, \\
C_{33}(f) &= k^2 \int_{-\pi}^{+\pi} F(f,\theta) \sin^2(\theta)\, d\theta, \\
Q_{12}(f) &= k \int_{-\pi}^{+\pi} F(f,\theta) \cos(\theta)\, d\theta, \\
Q_{13}(f) &= k \int_{-\pi}^{+\pi} F(f,\theta) \sin(\theta)\, d\theta, \\
C_{23}(f) &= k^2 \int_{-\pi}^{+\pi} F(f,\theta) \sin(\theta)\cos(\theta)\, d\theta, \\
C_{12}(f) &= C_{13}(f) = Q_{23}(f) = 0
\end{aligned} \tag{2.1}$$

where

$$\theta = \tan^{-1} \frac{Q_{13}(f)}{Q_{12}(f)} \tag{2.2}$$

is the direction of propagation and where the wave number is represented by

$$k = k(f) = \left\{ \frac{C_{22}(f) + C_{33}(f)}{C_{11}(f)} \right\}^{\frac{1}{2}}. \tag{2.3}$$

The directional wave spectrum $F(f,\theta)$ describes how energy propagates in frequency and direction and is represented by the product of the one dimensional spectrum $F(f)$ and the energy spreading function $D(f,\theta)$ as

$$F(f,\theta) = F(f)D(f,\theta) \tag{2.4}$$

where

$$\int_{-\pi}^{+\pi} D(f,\theta)\, d\theta = 1. \tag{2.5}$$

The spreading function $D(f,\theta)$ can be expanded as a Fourier series as follows:

$$D(f,\theta) = \frac{1}{\pi}\left\{ \frac{1}{2} + \sum_{n=1}^{2} (a_n(f)\cos n\theta + b_n(f)\sin n\theta) \right\} \tag{2.6}$$

where

$$
\begin{aligned}
a_1(f) &= \int_{-\pi}^{+\pi} D(f,\theta)\cos(\theta)\,d\theta = \frac{Q_{12}(f)}{k\,C_{11}(f)}, \\
b_1(f) &= \int_{-\pi}^{+\pi} D(f,\theta)\sin(\theta)\,d\theta = \frac{Q_{13}(f)}{k\,C_{11}(f)}, \\
a_2(f) &= \int_{-\pi}^{+\pi} D(f,\theta)\cos(2\theta)\,d\theta = \frac{C_{22}(f)-C_{33}(f)}{k^2 C_{11}(f)}, \\
b_2(f) &= \int_{-\pi}^{+\pi} D(f,\theta)\sin(2\theta)\,d\theta = \frac{2\,C_{23}(f)}{k^2 C_{11}(f)}.
\end{aligned}
\tag{2.7}
$$

The Fourier expansion (2.6) is truncated at $n = 2$ given the limitation that only three components are measured by the buoy, that is the vertical displacement and two slopes. This truncation causes negative lobes in $D(f,\theta)$, which is always positive definite. Longuet-Higgins et al. (1963) proposed the application of weighting functions to solve this limitation, which causes an undesirable broadening of the spreading function.

The application of Fourier analysis to obtain the spreading function $D(f,\theta)$ is limited to the small number of components used in the expansion. Due to this limitation alternative approaches are applied to estimate the spreading function. Among them the non-parametric Maximum Entropy Method (MEM) produces reasonable results, particularly in the reconstruction of directional double-peaked wave spectra (Lygre and Krogstad, 1986). MEM is a non-parametric model in the sense that there is no fixed analytical form. In contrast to MEM, parametric models such as the forms proposed by Longuet-Higgins et al. (1963) and Donelan et al. (1985) have a predetermined form and a controlling parameter (respectively s and β) which is dependent on a single peak frequency. These parametric models are not consistent with reconstructing the two dimensional spectrum $F(f,\theta)$ when wind sea and swell co-exist, since they attempt to fit a single peak centered between the two wave directions (Young, 1994). Hence MEM is more suitable for the present purpose and was applied for the estimation of $D(f,\theta)$.

2.2 Wind Measurements

The buoy was equipped with meteorological instruments for measuring wind, barometric pressure, air temperature, relative humidity and precipitation. Wind speed and direction were measured by two Young propeller-vane anemometers at a height of 3.78 m and 4.43m and the speed value later corrected for the standard height of 10 m using a logarithmic

relationship. Each wind measurement is an average of a 10-min record obtained hourly.

Gaps in the wind recorded by the anemometers on the buoy correspond to less than 10% of the total amount of measurements, and were filled with observations obtained on the nearby Enchova Platform located at $22°40'36''$ S and $40°36'20''$ W, about 60 km west from the buoy mean position. The wind measurements obtained from the buoy and from the oil platform present a high correlation, both in direction and speed as described in Violante-Carvalho et al. (1997), which is attributed to the spatial homogeneity of the wind fields encountered in the region. This is not true for situations associated with the passage of cold fronts with winds varying rapidly in both vertical and horizontal speed and direction.

2.3 The Wave Climate in Campos Basin

The wave climate in Campos Basin can be described by the main meteorological situations encountered over the South Atlantic. The area is strongly affected all the year round by relatively long swell waves responsible for most of the spectral energy measured by the buoy. For completeness a brief description of the most important meteorological events and the characteristics of the waves generated by them is presented (see more details in Violante-Carvalho, 1998).

Over one third of the spectra measured in the area present 3 or more peaks which can be explained on the grounds of the prevailing meteorological conditions. The decomposition of the spectra into different wave systems (wind sea, swell and young swell) and the information of how energy is distributed in frequency and direction is valuable information for the characterization of the wave climate of the region. Some of the characteristics of the wave spectra analyzed appear in table 2.1, which shows the occurrence of spectral peaks as a function of the significant wave height H_s. The dataset spans a period of 26 months during which 5807 wave spectra were measured. The data indicate that about 25% of the spectra are unimodal whereas the vast majority presents two or more peaks.

The semi-stationary South Atlantic Subtropical High pressure center (SASH) has a fundamental role in the climatology over the continent and in the wave climate in Campos Basin (represented by H in Figure 2.3). The anticyclonic circulation usually creates good weather conditions and is associated in the study area with northeasterly or easterly winds generating wind seas with SWH spanning from 0.25 to 1.25 m and peak periods from 3 to 5 s. Another wave system is also associated with the SASH although not related to the local wind measured

Table 2.1: Occurrence of Spectral Peaks in Campos Basin.

H_s(m)	1 peak	2 peaks	3 or more	*num. obs.*	*% obs.*
$H_s \leq 1.5$	236	533	706	1475	25.40
$1.5 < H_s \leq 2.5$	776	1468	1176	3420	58.89
$2.5 < H_s \leq 3.5$	312	298	121	731	12.59
$3.5 < H_s \leq 4.5$	116	24	3	143	2.46
$4.5 < H_s \leq 5.5$	25	9	0	34	0.59
$5.5 < H_s$	4	0	0	4	0.07
num. obs.	1469	2332	2006	5807	
% obs.	25.30	40.16	34.54		100

by the buoy. Due to the curved form of the isobars around the high pressure center waves are generated near the buoy with propagation directions slightly more easterly (in general 20 to 40° higher clockwise), as can be seen by the arrows indicating the wind direction in Figure 2.3. This young swell component presents typical values of SWH ranging from 0.5 to 2.0 m and peak periods from 5 to 8 s. The young swell is generally associated with longer fetches and more energetic waves than the wind sea and is responsible for severe situations in the area (Parente et al., 2001).

Frontal systems act in the South American continent throughout the whole year associated with the large scale undulatory flow. The dislocation of these systems has two main preferential trajectories—with a zonal or meridional component (Gan and Rao, 1991)—that are determinant in the direction of the waves that propagate towards Campos Basin. Frontal systems with a meridional component dislocate typically from southwest to northeast over the American continent. The passage of cold fronts over Campos Basin is combined with winds turning anticlockwise from southwest to northeast and more severe wave conditions (Parente et al., 2001). On the other hand the dislocation of these systems with a more pronounced zonal component, preferentially from west to east within a latitude band between 35° and 55°S, is responsible for long waves from the south quadrant with typical values of SWH from 0.5 to 2.0 m and peak periods from 8 to 15 s. Figure 2.3 also presents a typical situation of waves generated over 3000 km from the buoy. A cold front represented by black triangles associated with a low-pressure center in the southern extreme of the continent generates a distant swell. This is a common situation in Campos Basin, that is, a distant swell propagating in the opposite direction to the wind sea and a young swell propagating close to the wind sea both in direction and frequency.

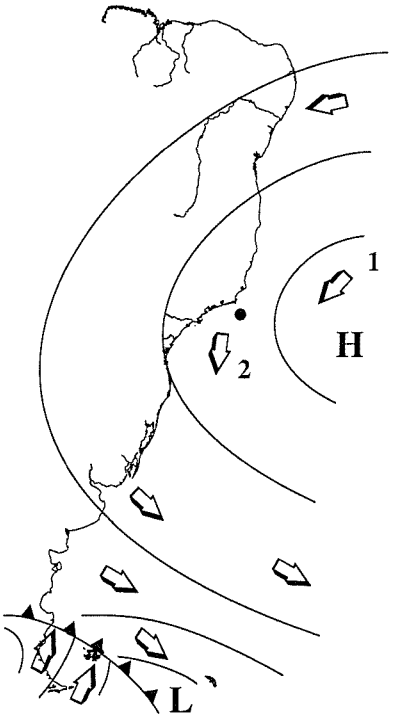

Figure 2.3: Schematic representation of the semi-stationary South Atlantic Subtropical High pressure center and its influence over the South American continent. The position of the buoy at Campos Basin is represented by the black spot and the direction of the wind responsible for the generation of a young swell and the wind sea is represented respectively by the arrows 1 and 2. At the south extreme of the continent there is a cold front plotted as black triangles associated with the progression of an extratropical cyclone (low pressure center L) generating swell from the southern quadrant.

Chapter 3

The Wave Model WAM

3.1 WAM Data

In this work the directional spectra from WAM are used as a first-guess by the MPI retrieval scheme to remove the 180° ambiguity and to augment the wave spectral information beyond the azimuthal cut-off wavenumber. A brief summary of the main characteristics of the third generation WAM model follows but more detailed information is presented by WAMDI Group (1988); Günther et al. (1992); Komen et al. (1994) and in the web site at www.dkrz.de/forschung/reports/report4/wamh-1.html.

In contrast with second generation wave models, a third generation model such as WAM does not introduce assumptions about the shape of the spectrum (SWAMP Group, 1985). The 2D wave spectrum is determined by the integration of the transport equation :

$$\begin{aligned} \frac{D}{Dt}F &\equiv \frac{\partial F}{\partial t} + \frac{1}{cos\phi}\frac{\partial}{\partial \phi}(\dot{\phi}\cos\phi F) + \frac{\partial}{\partial \lambda}(\dot{\lambda}F) + \frac{\partial}{\partial \theta}(\dot{\theta}F) \\ &= S_{in} + S_{nl} + S_{ds} \end{aligned} \tag{3.1}$$

where $F = F(f, \theta, \phi, \lambda, t)$ the two-dimensional wave spectrum is a function of the frequency f, the direction θ on a spherical grid of latitude ϕ and longitude λ and

$$\dot{\phi} = \frac{d\phi}{dt} \tag{3.2}$$

$$\dot{\lambda} = \frac{d\lambda}{dt} \tag{3.3}$$

$$\dot{\theta} = \frac{d\theta}{dt} \tag{3.4}$$

represent the rate of change of the position and direction along a great circle path for a wave packet in water of infinite depth. The source terms are represented by the wind input (S_{in}), the nonlinear transfer (S_{nl}) and the dissipation term (S_{ds}).

Since August 1993 ERS-1 altimeter wave height data have been assimilated by ECMWF into their WAM wave model using an optimal interpolation scheme. We are running a workstation version of the WAM without the implementation of any sort of data assimilation. That means that the outputs from the wave model used in this work are the direct result of integration of the energy balance equation (3.1) which makes the comparison of the model against buoy data much more meaningful. The ocean wave spectra are computed using the WAM cycle 4 every hour on a latitude-longitude grid with a spatial resolution of 1° covering the whole South Atlantic basin from the Equator line to 72° S and from 74° W to 30° E, which totals 7488 grid points. Both the source and the advection terms have a time step of 12 minutes for all the 600 spectral components (25 frequencies and 24 directions). The spectrum is evaluated up to a high frequency cut-off, and beyond this point an f^{-5} tail is added with the same directional distribution as the cut-off region.

The WAM model runs operationally at most forecasting centers and has been validated on statistical basis against buoy data (see for example the results presented in Komen et al., 1994). The comparisons of significant wave height estimated by the model against Geosat altimeter measurements show an overall good correlation with small values of bias (Romeiser, 1993). However significant discrepancies were encountered in some individual cases and have been attributed to errors in the forcing wind or to inadequate spectral resolution of the model.

3.1.1 The Wind Input Source Term

The wind input term represents the transfer of energy from the wind to the ocean, producing waves. Short waves are produced in the high frequency part of the spectrum whenever the wind is blowing on the sea surface. The wind input source term S_{in} adopted in the WAM cycle 4 is based on Miles' theory for laminar flow given by the expression presented by Snyder et al. (1981) and later modified (Janssen, 1989; 1991) which describes the wind-wave momentum transfer. In this theory the wind input depends in a a *quasi-linear* way on the wave spectrum:

$$S_{in} = \gamma_{in} F \tag{3.5}$$

where γ_{in} is the growth rate parameter. The stress in the air surface layer is affected by the waves through their orbital velocity, the so-called wave-induced stress. Therefore the momentum transfer from air to ocean is dependent on the sea state, which is taken into account in the model.

3.1.2 The Nonlinear Wave-Wave Interactions

The nonlinear wave-wave interactions are extremely important for the understanding of the evolution of the directional spectrum. The role of the nonlinear term is to redistribute energy from the short wave components to the long ones resulting in waves that otherwise would not be generated directly by the wind. The term S_{nl} describes the energy transfer due to nonlinear wave-wave interactions when a set of four waves of different wave lengths, called a quadruplet, interact with each other satisfying the resonance conditions

$$\mathbf{k}_1 + \mathbf{k}_2 = \mathbf{k}_3 + \mathbf{k}_4 \tag{3.6}$$

$$\omega_1 + \omega_2 = \omega_3 + \omega_4 \tag{3.7}$$

where $\mathbf{k}$ is the wavenumber vector and ω is the angular frequency ($2\pi f$). The exact calculation of S_{nl} is too time consuming to be used in operational models so a parameterization is employed, the discrete interaction approximation (DIA) (Hasselmann and Hasselmann, 1985; Hasselmann et al., 1985a). It is still not very clear whether the DIA represents correctly the nonlinear interactions in more complex sea states such as in situations of turning or ceasing winds where wind sea-swell transition and turning wind sea are present (Young, 1999).

3.1.3 Dissipation Due to Whitecapping

Dissipation of energy may occur in deep water by wave breaking in a process called whitecapping when the wave amplitude increases beyond a certain level—this term was introduced to differentiate it from depth-induced wave breaking. The dissipation term S_{ds} implemented in WAM cycle 4 is based on the whitecapping theory (Hasselmann, 1974), uses the parameterization proposed by Komen et al. (1984) and takes into account the wave induced stress (Janssen, 1991). Like the wind input, S_{ds} is quasi linear in the wave spectrum and is represented by

$$S_{ds} = \gamma_{ds} F \tag{3.8}$$

with the dissipation rate γ_{ds} depending on integral spectral parameters. The parameter S_{ds} is the least well known of the three source functions and its value was adjusted to ensure that the action balance equation (3.1) achieves an agreement with measurements in fetch-limited growth.

3.2 The Forcing Wind

The wind input is from the Atmospheric General Circulation Model (AGCM) which is run operationally by the European Centre for Medium-Range Weather Forecasts (ECMWF). Two different data sets were obtained from the British Atmospheric Data Centre (BADC). The first one is the ECMWF Re-Analysis (ERA) from 1991 to February 1994. The AGCM has a variable altitude resolution divided in 31 levels with maximum altitude of 30 km, it has a latitude-longitude resolution of 1.125° and the wind field is computed every 6 hours. The second data set is the ECMWF Operational Analysis (from March 1994 to December 1995) and includes the same parameters with same resolution as ERA. The wind field at 10 meters height (u_{10}) is used to drive the wave model. More details are presented at the web page http://www.badc.rl.ac.uk/.

Chapter 4

A Spectral Scheme for the Partitioning of the Frequency Spectrum into Wave Systems

A spectral approach is applied in a novel method for the partitioning of the frequency wave spectrum into wave systems and for the adjustment of the spectral parameters. The method described in this chapter is employed on the investigation of the growth of surface gravity waves in an open sea region dominated by swell.

4.1 Introduction

It is fundamental to be able to properly separate swell from wind sea in order to study whether or how the interactions between them modify the growth relations of wind waves obtained in swell-free environments. Spectral methods are necessary for the partitioning and adjustment of the multi-modal wave spectra in order to determine how energy distributes in frequency and direction. Most of the known spectral formulations are for the adjustment of unimodal spectra and so it is not possible to apply them for the common cases when more than one spectral peak is present. To overcome this limitation a technique for the representation and partitioning of multi-peaked spectra is proposed.

Detailed knowledge of the shape of the ocean wave spectrum and its growth is important information for offshore engineering purposes. Among numerous examples are the estimation of induced loads on marine structures and the response of floating bodies to the wave action.

In the last 50 years several works have sought to properly describe and parameterize the wave spectrum. Most of them have produced spectral models that aim to describe only the wind sea part of the spectrum, generated by the local wind, and hence unimodal. Furthermore the greatest part of these studies are based on measurements on wave tanks in laboratories or in swell-free environments with well defined fetches like lakes or sheltered coastal areas. Undoubtedly such work has clarified the understanding of the physical mechanisms behind wave generation and growth but there is a lack of studies in open sea regions. From the operational perspective it is important to confirm whether the theoretical relationships, for example correlating wave energy and wind, apply to the most common cases, that is areas in the open ocean where swell is present.

Donelan et al. (1992) carried out a detailed field experiment in Lake Saint Clair to explore the wave growth in a fetch-limited swell-free environment. They found a high correlation between the reciprocal wave age U_c/c_p and the dimensionless wave energy $\epsilon = m_0 g^2/U_c^4$ where m_0 is the wave energy variance, U_c is the component of the wind in the wave direction and c_p is the phase velocity at the peak frequency. But the modification of the wind sea growth by swell is not completely clear and the results from laboratory waves show some disagreements among experiments. It is clear however that there is a reduction in the amplitude of laboratory wind waves when longer (swell) waves are added.

In the North Atlantic Dobson et al. (1989) found no significant influence on the fetch laws proposed by Donelan et al. (1985) after removing the swell from the spectra. However both works were carried out in short-fetched coastal areas and some questions still remain about the influence of swell on wind sea growth in the open ocean.

4.2 Spectral Formulations

The spectrum measured in a particular point of the ocean is the sum of wave systems generated by events apart either in space and in time. Although the wave spectrum is quite complex there is a remarkable similarity of its shape in different locations under an enormous variety of wind speeds, spanning from small waves in lakes up to storm waves generated by hurricanes. It is believed that the evolution of the waves in deep water is a function of three dynamical processes (Komen et al., 1994): the nonlinear wave-wave interaction (S_{nl}), the gain of energy from the wind input (S_{in}) and the dissipation due to wave breaking (S_{ds}). Among the three processes the non-linear interactions play a very important role in the shape

stabilization of the wave spectrum $F(f)$ forcing its high frequency portion beyond the peak frequency to decay in a manner inversely proportional to frequency to a power n in the form $F(f) \propto f^{-n}$.

The similarity hypothesis proposed by Kitaigorodskii (1962) enabled the description of the development of the wave spectrum under fetch limited conditions. A key argument in his hypothesis was the existence of a high frequency 'equilibrium range'. In this equilibrium range the dynamical processes balance each other, that is $S_{nl} + S_{in} + S_{ds} = 0$, rates of energy gain due to wind input is balanced by energy loss due to breaking and nonlinear wave-wave interactions and hence the spectrum remains stable. Phillips (1958) suggested that in the portion of higher energy within the equilibrium range (in the band of frequencies from $1.5f_p$ to $3.0f_p$ where f_p is the peak frequency) the spectrum is a function of f^{-5} decay expressed as:

$$F(f) = \alpha g^2 (2\pi)^{-4} f^{-5} \tag{4.1}$$

where f is frequency, g is the gravitational acceleration and α is a constant scale parameter set equal to 0.0081. Phillips' work was based on dimensional considerations and on the fact that due to the wave steepness the high frequency part of the spectrum is limited due to wave breaking. Any wind input in these frequencies is lost in wave breaking and hence (4.1) escribes the high frequency part of the wave spectrum.

Pierson and Moskowitz (1964) proposed a spectral form for fully developed seas from analysis of measurements in the North Atlantic. They added an exponential term to Phillips' expression (4.1) to generate a low frequency spectral face

$$F(f) = \alpha g^2 (2\pi)^{-4} f^{-5} \exp\left[-\frac{5}{4}\left(\frac{f}{f_p}\right)^{-4} \right]. \tag{4.2}$$

The Pierson-Moskowitz spectrum (4.2) describes the waves developed under no limitations in fetch and time. But fully developed seas are not very common in nature as they require a steady wind blowing for a long period over a large area. Seeking to clarify the development of growing seas under fetch limited conditions researchers from Europe and USA carried out the Joint North Sea Wave Project (JONSWAP). The location of these extensive observations was carefully chosen based on the simple situations suggested by Kitaigorodskii, that is a steady offshore wind over a strait beach in a region not contaminated by swell. Hasselmann et al. (1973) proposed the JONSWAP spectrum that described fetch-limited waves very well

using five parameters ($f_p, \alpha_j, \gamma_j, \sigma_a$ and σ_b):

$$F(f) = \alpha_j g^2 (2\pi)^{-4} f^{-5} \exp\left[-\frac{5}{4}\left(\frac{f}{f_p}\right)^{-4}\right] \gamma_j^{\exp\left[\frac{-(f-f_p)^2}{2\sigma^2 f_p^2}\right]} \tag{4.3}$$

where

$$\sigma = \begin{cases} \sigma_a & for f \leq f_p \\ \sigma_b & for f > f_p. \end{cases}$$

The JONSWAP spectrum (4.3) is based on the Pierson-Moskowitz spectrum with an enhancement factor γ_j added. This enhancement is only significant in the region near the spectral peak and at higher frequencies the decay is inversely proportional to frequency to the fifth power as suggested by Phillips (1958). The peak frequency f_p is the frequency at the maximum of the spectrum. The left and right-side widths of the peak region are represented respectively by σ_a and σ_b. The high frequency scale parameter α_j is not constant as initially proposed by Phillips (1958). Hasselmann et al. (1973) found a relationship between α_j and fetch which confirmed the suggestion of Longuet-Higgins (1969) that α_j decreases with increasing fetch X given by

$$\alpha_j = 0.076\left(\frac{Xg}{U_{10}^2}\right)^{-0.22}$$

where U_{10} is the wind speed at 10 meters height. They found no correlation of γ_j, σ_a and σ_b with fetch and proposed mean values for their representation ($\gamma_j = 3.3$, $\sigma_a = 0.07$ and $\sigma_b = 0.09$).

The high frequency form $F(f) \propto f^{-5}$ present in the JONSWAP spectrum has been questioned by recent researches (see for example Phillips, 1985) that reanalyzed the equilibrium spectral balances coming up with a f^{-4} power law rather than f^{-5}. Toba (1973) postulated a different formulation for the high frequency tail represented by a f^{-4} decay which seems to be more consistent with observations. Based on detailed field measurements in Lake Ontario Donelan et al. (1985) proposed a new spectral form:

$$F(f) = \alpha_d g^2 (2\pi)^{-4} f_p^{-1} f^{-4} \exp\left[\left(\frac{f}{f_p}\right)^{-4}\right] \gamma_d^{\exp\left[\frac{-(f-f_p)^2}{2\sigma^2 f_p^2}\right]}. \tag{4.4}$$

The Donelan spectrum (4.4) is a modified version of the JONSWAP spectrum to allow a f^{-4} frequency tail. Unlike Hasselmann et al. (1973) who presented spectral parameters dependent

on fetch, Donelan et al. (1985) parameterized them in terms of the reciprocal wave age U_c/c_p. For the high frequency scale parameter they proposed:

$$\alpha_d = 0.006(U_c/c_p)^{0.55}; \quad 0.83 < U_c/c_p < 5.$$

Furthermore Donelan et al. (1985) suggested that, in contrast to Hasselmann et al. (1973), γ_d and σ depend on wave age:

$$\gamma_d = \begin{cases} 1.7, & 0.83 < U_c/c_p < 1; \\ 1.7 + 6.0\log(U_c/c_p), & 1 \leq U_c/c_p < 5 \end{cases}$$

and

$$\sigma = 0.08[1 + 4/(U_c/c_p)^3]; \quad 0.83 < U_c/c_p < 5.$$

The exponent n of the high frequency tail that best describes the spectrum decay $F(f) \propto f^{-n}$ is still an open question. In many studies (Toba, 1973; Mitsuyasu et al., 1975; Donelan et al., 1985; Rodriguez and Guedes Soares, 1999b; Liu, 1989; Young, 1998) the value of n varied between -3.5 and -5. Rodriguez et al. (1999), following Kitaigorodskii (1983) considerations, point out the existence of a transitional frequency at which the decay changes from f^{-4} to a f^{-5} tail. These works raise the question of whether there is a universal high frequency decay in the form $F(f) \propto f^{-n}$, but also give strong evidence that n lies between -4 and -5.

4.3 The Method for the Spectral Adjustment

Formulations of the type (4.2, 4.3, 4.4) are for unimodal spectra and cannot represent the sea state when there is wind sea and swell. However they form the theoretical basis for the representation of multi-peaked spectra (Ochi and Hubble, 1976; Guedes Soares, 1984; McCarthy, 1989). In these papers it is assumed that the wave spectrum is composed of wave systems generated by different sources and there is no interaction between each spectral component. Hence the methods for representing a bimodal spectrum assume that the one dimensional spectrum $F(f)$ is the sum of a high frequency $F_{hf}(f)$ and a low frequency $F_{lf}(f)$ component yielding

$$F(f) = F_{hf}(f) + F_{lf}(f). \tag{4.5}$$

Ochi and Hubble (1976) proposed a method for the adjustment of bimodal spectra where each part is expressed by three parameters. They represented the high and low spectral components using a modified version of the Pierson-Moskowitz spectrum. Guedes Soares (1984) adopted the same approach to model double-peaked wave spectra but using a spectrum derived from JONSWAP. The justification for modeling the high frequency part of the spectrum is straightforward since the JONSWAP form was originally developed for wind sea. However this spectral formulation does not apply for swell. His explanation for adjusting the low frequency using a JONSWAP model was due to the narrowness of the swell, which can be well represented by the sharp spectral shape of (4.3).

The spectral representation suggested by Guedes Soares (1984) seems to be more appropriate. The good fit of the JONSWAP type formulations (4.3 and 4.4) has been confirmed by numerous experiments and the power laws for wave growth were obtained applying these spectral forms. Nevertheless, as has already been pointed out, the exponent n that best describes the high frequency part of the spectrum in the form $F(f) \propto f^{-n}$ is not exactly known. McCarthy (1989) also applied a modified version of JONSWAP to adjust double-peaked spectra. His approach was based on a more flexible spectral form where the logarithmic decay is allowed to vary and he added a new parameter to adjust the low frequency region before the peak.

In order to investigate the behavior of the high frequency tail decay we employed a spectral method based on JONSWAP using a variable exponent n:

$$F(f) = (2\pi)\alpha g^2 (2\pi f)^{-n} \exp\left[-\frac{5}{4}\left(\frac{f}{f_p}\right)^{-4}\right] \gamma_j^{\exp\left[\frac{-(f-f_p)^2}{2\sigma^2 f_p^2}\right]}. \tag{4.6}$$

The values of σ are the same as in (4.3) and hence there are four parameters to be determined for the spectral adjustment: f_p, n, α and γ.

The first step in the fitting procedure is to select the spectral peaks (see flow chart in Figure 4.1). As discussed by Rodriguez and Guedes Soares (1999a) the correct identification of the points of maximum ordinates might be masked by random fluctuations arising from the spectral estimators. Pierson (1977) pointed out that 70% of the spectral peaks that are 4 bands wide are double-peaked due to sampling variability. Therefore this selection requires additional tests to identify whether a separate peak corresponds to a different wave system or not.

A balance must be found between resolution and variance, or in other words a compromise

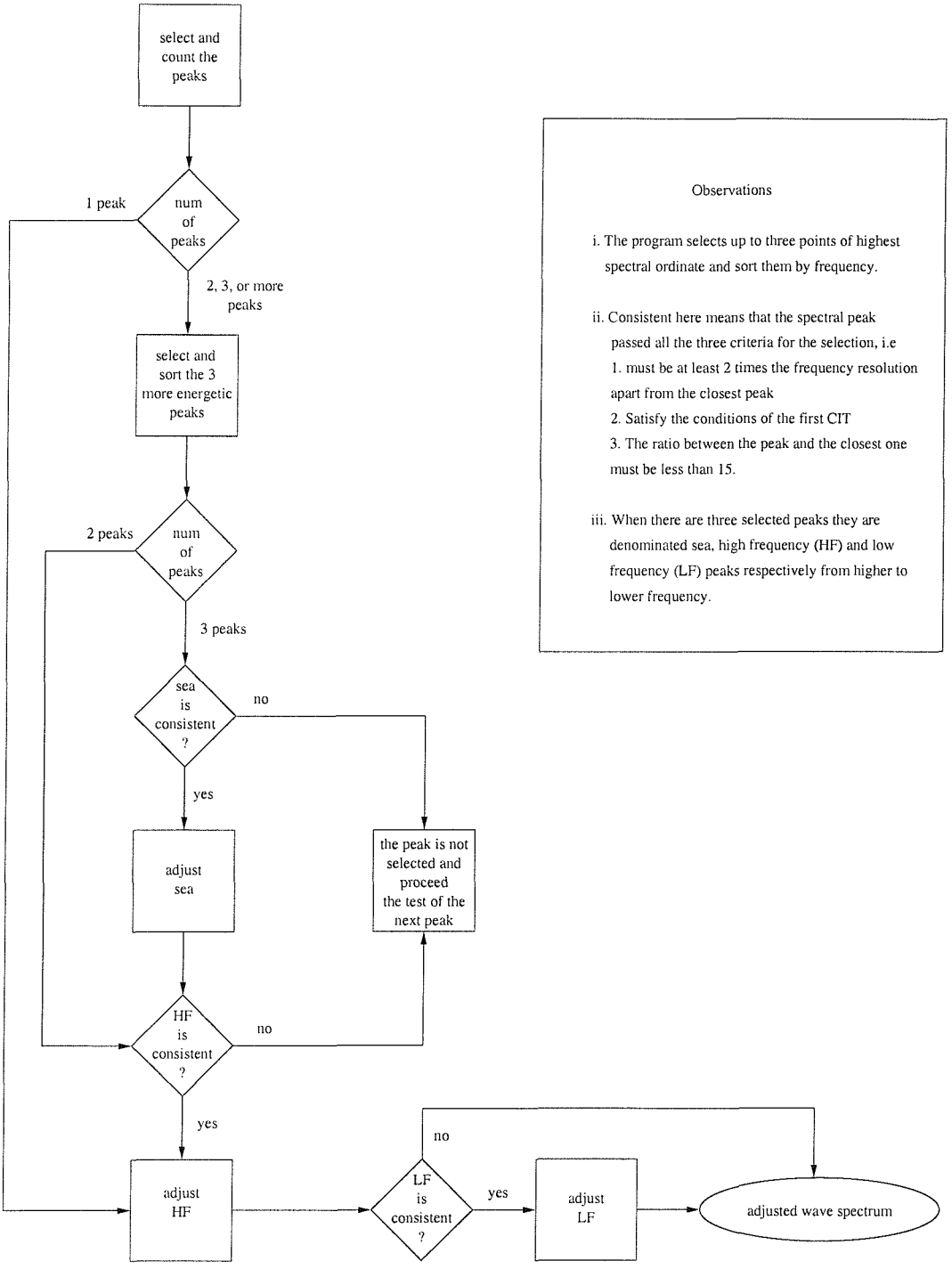

Figure 4.1: Flow chart of the algorithm for the spectral adjustment of the 1-D wave spectrum.

between increasing the number of degrees of freedom (and hence reducing the variance) and the capability to identify small nuances in the smoothed spectrum. The spectra with 32

degrees of freedom and 50% overlap yielded a satisfactory relation between resolution and variance, although additional criteria are applied to check whether the peaks are due to the sampling variability. Guedes Soares and Nolasco (1992) presented some criteria for the selection of the peaks, in which two of them are based on the 90% confidence interval test (CIT). In that paper the first CIT used by them imposes the condition that the two peaks will be accepted if the ordinate of lower limit of the 90% confidence interval of the greater peak is higher than the ordinate of the upper limit of the confidence interval of the trough between the peaks. In addition they proposed a second CIT that imposes that the ordinate of the trough between the two peaks must be lower than the lower limit of the 90% confidence interval of the smaller peak.

We adopted three criteria which must all be satisfied for the selection of the spectral peaks. The first criterion requires that the peaks must be 2 times the frequency resolution (0.03 Hz) apart. This was considered the best value after several tests using distances spanning from $0.02\,Hz$ to $0.05\,Hz$. The second criterion is based on the 90% confidence intervals and the peaks will be accepted if they satisfy the conditions of the first CIT in Guedes Soares and Nolasco (1992). The second CIT proposed by them is too restrictive eliminating many peaks that were visually accepted. The third criterion applied for peak selection is that the ratio between the two spectral peaks must be less than 15. This requirement eliminates peaks that are below an arbitrary threshold value and hence contaminated by background noise.

The next step in the fitting procedure is to adjust the high frequency spectrum $F_{hf}(f)$. The decay n is determined by logarithmic regression of the points greater than $2f_p$. To obtain α the value of γ was set to 1 in (4.6) because its effect at frequencies higher than $f/f_p > 1.37$ is negligible. The value of α was obtained by iterating from 0.0001 to 0.1 in order to minimize the total square error for the range between 1.37 and 2 times the peak frequency (Hasselmann et al., 1976). Once f_p, n and α are known γ is the last parameter to define $F_{hf}(f)$. It was chosen as the value that produces the least square error between measured and fitted spectra.

The adjusted high frequency spectrum $F_{hf}(f)$ is subtracted from the measured spectrum yielding $F_{lf}(f)$ (4.5). The same process is repeated to obtain the parameters n, α and γ for the low frequency spectrum. These procedures outline the fitting of bimodal spectra.

The wave climate in Campos Basin is complex and spectra with 3 or more peaks are common, about one third as indicated by table 2.1 on page 15. The fitting procedures for

double-peaked wave spectra selects the two points of highest spectral ordinate. Many times however the wind sea spectra in Campos Basin were neglected to adjust the more energetic swell and young swell components. To avoid this limitation the fitting procedure was extended to model a third peak, but only if the two selected ones do not correspond to the wind sea (as defined in the next chapter). In addition the third peak must satisfy the three criteria previously outlined for the spectral selection. Therefore the wave spectrum generated by the local wind is always adjusted and a trimodal spectrum is given as

$$F(f) = F_{sea}(f) + F_{hf}(f) + F_{lf}(f). \tag{4.7}$$

In this situation the wind sea is represented by $F_{sea}(f)$, the young swell by $F_{hf}(f)$ and swell by $F_{lf}(f)$. In a bimodal spectrum (4.5) in general the wind sea will be $F_{hf}(f)$ and the young swell or swell will be represented by $F_{lf}(f)$.

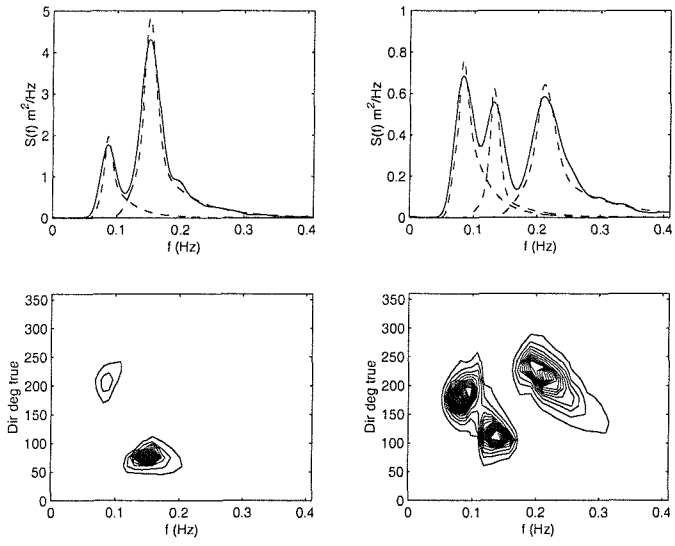

Figure 4.2: Examples of the adjusted wave spectrum. Top panels show the measured 1D spectrum (solid line) and the adjusted spectrum (dashed line) for a bimodal (left) and trimodal (right) case. Bottom panels show the respective directional spectra calculated using the Maximum Entropy Method.

Furthermore due to the response of the heave-pitch-roll buoy to the sea movements we have imposed a frequency band from 0.04 Hz to 0.35 Hz for the selection of the spectral peaks, but for the calculation of the high frequency decay paramenter n we have used all the data up to the Nyquist frequency cut-off, that is 0.5 Hz. Although the response of the buoy is not

reliable for the peak selection at higher frequencies due to noise its response is good enough for the determination of the high frequency decay n. The high frequency decay is a mean value calculated over several points, which diminishes the possibility of an erroneous value due to statistical variability. Additionally a quality parameter was also calculated, which basically is the ratio between the spectral energy measured by the buoy and the spectral energy yielded by the fitting procedure. Most of the values obtained range from 0.9 to 1.1, which means that in general the energy adjusted is within $\pm 10\%$ of the measured spectral energy. This implies that the value of significant wave height adjusted by the fitting procedure has a variability of $\pm 10\%$ around the value measured by the buoy. Other wave parameters such as wave period and wave direction are independent of this range since they are obtained directly from the buoy measurement. However the high frequency decay n and the parameters α and γ are dependent on the fitting procedure. Actually the values of n and the parameters α and γ vary in order to the area to be adjusted to get as close as possible to the measured area. Therefore it seems reasonable to assume that their variability is of the same order of the adjusted area, that is, around 10%.

Examples of bimodal and trimodal adjusts are presented in Figure 4.2. On the left the bimodal spectrum has a dominant high frequency peak from ENE at $0.1514\,Hz$ ($6.6\,s$) and an significant wave height (SWH) value of 1.83 m while the least energetic low frequency peak ($0.0859\,Hz$ or $11.6\,s$) from the south quadrant has SWH = 0.99 m. The more complicated trimodal spectrum on the right side presents wind sea, high and low frequency peaks of $0.2119\,Hz, 0.1318\,Hz$ and $0.0840\,Hz$ ($4.7\,s, 7.6\,s$ and $11.9\,s$) and SWH values of 0.83 m, 0.54 m and 0.69 m respectively. The directional information is used in the model for the adjustment of the 1D spectrum to select the wind sea. The accurate representation of the 2D spectrum is necessary as well to characterize the adjusted wave systems in terms of direction, energy and frequency which is of great interest in terms of offshore operations in Campos Basin.

Chapter 5

Buoy Observations of the Influence of Swell on Wind Waves Growth in the Open Ocean

The influence of longer (swell) on shorter, wind sea waves is examined using an extensive database of directional buoy measurements obtained from a heave-pitch-roll buoy moored in deep water in the South Atlantic. This data set is unique for such an investigation due to the ubiquitous presence of a young swell component propagating closely in direction and frequency with the wind sea, as well as a longer, opposing swell. Our results show, within the statistical limits of the regressions obtained from our analysis when compared to measurements in swell free environments, that there is no obvious influence of swell on wind sea growth. For operational purposes in ocean engineering that means that power-laws from fetch limited situations describing the wind sea growth can be applied in more realistic situations in the open sea when swell is present.

5.1 Introduction

Most of the studies that tried to address the problem of the growth of wind waves were carried out in laboratory tanks or coastal areas with well known fetches and without swell. The effect of longer waves on the evolution of wind sea is not well investigated in the open ocean where swell is ubiquitous. It is not clear whether or how its presence would change the mechanics of wave growth and to what extent.

The detailed processes that govern the shape and evolution of wind waves are still not completely well understood. It is however common knowledge that the growth of waves in deep water is a function of three dynamical processes called source terms, that is, the input of kinetic energy by the wind (S_{in}), energy dissipation due to wave breaking (S_{ds}) (also known as white capping) and nonlinear resonant wave interaction (S_{nl}). It is remarkable that wind waves spanning a variety of wind speed conditions present a similarity in their spectral shape, and although all three dynamical processes play an important role it is believed that the nonlinear interactions are mainly responsible for this 'shape stabilization' process. One of the main features of this universal shape of wave spectra is a high frequency tail decay proportional to a power law in the form $F(f) \propto f^n$ where $F(f)$ is the frequency (or one dimensional) spectrum, f is frequency and n is an exponent that determines the rate of decay.

The concept of equilibrium range was fundamental for the description of the evolution of waves under fetch limited conditions. Phillips (1958) using dimensional considerations suggested that in the frequency range between 1.5 to 3 times f_p (the peak frequency) due to wave steepness the spectral level is determined mainly by wave breaking. In this region the dynamical processes balance each other, that is $S_{in} + S_{ds} + S_{nl} = 0$ and the input of spectral energy equals the loss of energy yielding a saturation level. Phillips (1958) pointed out that the spectral tail that best describes this high frequency band is proportional to the minus fifth power ($n = -5$). Later on Phillips (1985) reanalyzed the equilibrium range theory and reported that an f^{-4} tail is more appropriate.

The evolution of the wave spectrum is determined by the sum of the dynamical terms S_{in}, S_{ds} and S_{nl} as represented by the energy transfer equation:

$$\frac{\partial F}{\partial t} + \mathbf{C_g} \cdot \nabla F = S_{in} + S_{ds} + S_{nl} \tag{5.1}$$

where $F = F(f, \theta)$ is the directional spectrum and $\mathbf{C_g}$ is the group velocity. The left hand side of (5.1) gives the advection of energy for each wave component whereas the right hand side describes the wave-wave interactions (S_{nl}), the wind input (S_{in}) and dissipative processes (S_{ds}). As a result of the dynamical processes the peak shifts to lower frequencies and broadens as the spectrum becomes more mature.

The study of the interaction of long and short wind waves is also relevant to understanding the processes involved in the modulation of radar backscatter at a shorter wave length scale.

Komen et al. (1984) solved (5.1) numerically to study the equilibrium range solution and the dynamics of wave generation and evolution, where they considered for computational reasons the range of frequencies around f_p. Moreover Komen (1988) points out that the evolution of short gravity waves can be described from consideration of the source terms and how they interact. For low wind speeds and at an early stage of development very short gravity waves are within the frequency range analyzed by Komen et al. (1984) and hence the source terms describe the physical processes involved in their evolution. The imaging of ocean waves by radar, for example the Synthetic Aperture Radar (SAR) imaging mechanism, is based on the interaction of these decimeter waves with longer waves through the process called Bragg resonant scattering. Most of the models of the tilting modulation transfer function assume a Phillips k^{-4} high wavenumber spectrum though it is not clear what is the best exponent for such models (see for instance Violante-Carvalho et al. (2002b) and the references in there). Although in the present study we are focusing on longer wind sea and swell waves (with wave lengths longer than 20 meters) the discussion might help to clarify how Bragg waves are hydrodynamically affected by longer waves.

Energy transfer among wave components due to nonlinear interactions has been considered an important aspect for determining the evolution of the wave directional spectrum since the pioneering JONSWAP experiment in the North Sea (see more on page 24). Its influence on the wind generated growth in laboratory experiments has also been determined (Donelan, 1987). Through numerical experiments, the importance of the spectral peaks for swell and wind sea to be nearly located within the frequency-direction space, has already been defined (Young et al., 1995; Masson, 1993).

More recently Lavrenov and Ocampo-Torres (1999), using the exact calculation for the energy transfer due to nonlinear interaction, studied the dependence on the directional spread. Non-zero values for energy transfer were calculated for waves traveling in opposite direction to the wind, specially for wide directional spreading within the spectra. Furthermore, for cases of similar directional spread, the relative nonlinear energy transfer was greater for wider frequency spectrum. Within this context, bimodal or trimodal spectra can be viewed as displaying rather wide directional spreading character. Therefore, this can be an obvious mechanism to influence wind wave growth under the presence of swell.

When performing strict calculations of energy transfer due to nonlinear interactions for bimodal spectra, a clear strengthening of interaction level is observed for cases when both wave fields (wind sea and swell) propagate in the same direction. Nevertheless, for cases when

both systems propagate in different directions the interaction still occurs at a lower strength (Lavrenov and Ocampo-Torres, 1999). Furthermore, non-zero values for energy transfer to directions opposite to the wind are always detected.

A number of experiments indicate that wind waves are attenuated in the presence of long waves but the mechanisms which cause the suppression of the wind waves are not clear although several theories have been proposed. Through numerical simulations Masson (1993) investigated the effect of nonlinear coupling due to resonant interactions in bimodal spectra in deep water waves. The nonlinear term S_{nl} has been shown to play an important role in the coupling between swell and wind sea causing the swell to grow at the expense of the wind sea in the frequency range just below the peak frequency of the wind sea. The magnitude of the coupling depends on the relative direction of propagation between swell and wind sea, where the coupling is maximum at about 40° (Masson, 1993). When the direction of propagation of swell moves away from the wind sea direction the nonlinear coupling decreases quickly. That work also considered the influence of swell on wind sea growth in relation to the separation between them in frequency space, where the coupling is not significant for ratios of swell and wind sea peak frequencies ($f_{p_{swell}}/f_{p_{sea}}$) less than about 0.6. Based on laboratory experiments Phillips and Banner (1974) suggested that the reduction in amplitude on wind waves is due to enhanced dissipation S_{ds} caused by modulation of the short waves by the long waves which then increases the surface drift at the crest of the mechanical waves and the premature breaking of the short waves. More recently Chen and Belcher (2000) developed a model to explain different results from wave tank experiments. They pointed out the important role of the wind input source term S_{in} and its coupling with the long waves. They supposed that the long wave absorbs momentum from the wind leaving a reduced amount of turbulent flux in the wind which causes a slower development of wind waves.

There is however a lack of evidence from measurements in the open ocean of the influence of swell on wind waves. This is caused partially by the difficulty to isolate wind sea from the swell contaminated spectra. Dobson et al. (1989) found no clear influence of opposing swell on wind sea in an experiment carried out in a fetch-limited coastal area. They concluded that the similarity of their results with those of Donelan et al. (1985) in a swell free environment was because of the short fetches involved in both experiments. The first attempt to investigate wind sea growth and dissipation in a swell dominated area in the open sea was carried out by Hanson and Phillips (1999) in the Gulf of Alaska. They computed 236 directional spectra where over a third of the cases were classified as without swell. In addition only 27% of the

swell cases (or less than 20% of the total spectra) were aligned with the wind sea direction whereas the great majority of the swell propagated non aligned with the wind sea. From their results they have found no clear effect of swell on wind sea growth regardless of the direction of swell propagation. They have not mentioned any sort of investigation of the relation between $f_{p_{swell}}/f_{p_{sea}}$ and its possible influence on wind sea growth. In an attempt to address the lack of measurements in the open ocean of the influence of longer waves on shorter waves we analyzed a data set that consists of over 5800 spectra from a heave-pitch-roll buoy deployed in deep water in the South Atlantic.

5.2 Data and Analysis

Campos Basin, located off the northern part of the state of Rio de Janeiro (see Figure 2.1 on page 10), is the most important offshore region in Brazil. In this basin are located tens of oil platforms responsible for around 75% of the oil and gas prospected in the country, besides the fact that this is a region of strong comercial and touristic activities. Several offshore operations take place daily in Campos Basin, such as underwater surveys, pipeline laying, platform maintenance, flexible riser inspections and so on. Its operationality depends on the most precise possible description of the sea state, in particular the surface waves, to ensure the safety of personnel and to avoid damage to equipment.

The South Atlantic Deep Water Program (PROCAP) was an experiment conducted by the Brazilian Oil Company (PETROBRAS) to study the development of the main meteorological and oceanographic features of the region and their temporal variability. This program consisted of mooring lines with several instruments for both near-surface and deep water measurements of currents, temperature, salinity, dissolved oxygen, pH and pressure. For wind and wave measurements a heave-pitch-roll buoy with meteorological sensors was deployed in the central region of Campos Basin nearly 150 km offshore. From March 1991 to March 1993 the buoy was moored at position $22°31' S$ and $39°58' W$ in a depth of 1250 m. The same buoy was redeployed from January 1994 to July 1995 at position $22°38' S$ and $40°12' W$ in 1050 m. Here we will describe briefly the wave data acquisition and analysis (more details about the wave and wind analysis on pages 9 and 13 respectively).

5.2.1 Wave Measurements

The heave-pitch-roll buoy, equipped with a Datawell Hippy 120 Sensor, was highly reliable for the most part of the campaign. However the present analysis is interested mainly in the spectral evolution of the wave field over time therefore we consider only the period when there were no, or very small, wave gaps. In this work the wave data comprise the months from February 1992 to January 1993 and from February 1994 to March 1995 totaling 26 months and over 5800 wave spectra.

The buoy acquired three time series, the vertical displacement and two slopes in the east and north directions, at a rate of 1 Hz during 20 minutes eight times a day every 3 hours. Records of 1024 points were segmented in 16 partitions of 64 points yielding 32 degrees of freedom and frequency resolution of 0.015625 Hz using the Welch Method to obtain the spectral estimators (see for example Marple Jr. (1987)). The classical Fast Fourier Transform (FFT) was applied to all three time series with a Hanning window and 50% overlap. The directional information was computed using the nonparametric Maximum Entropy Method (MEM) (Lygre and Krogstad, 1986).

The high frequency response of the instrument to the sea movement is critical for the analysis performed. The presence of noise generated for example by currents and the mooring system causes a limitation in the buoy frequency range. Furthermore the size of the buoy and its response to the sea displacement together with the accuracy of evaluation of the spectral estimators impose a frequency band from 0.04 Hz to 0.35 Hz (Tucker, 1989). Outside this range the buoy response is questionable and was not considered in the analysis.

5.2.2 The Spectral Fitting

A method for spectral fitting and selection of different wave systems of the 1D spectrum was developed and is comprehensively explained in Violante-Carvalho et al. (2002b) and on page 25. Here we will only give a brief description for completeness. Such a method is of great value for several applications since the wave spectrum is subdivided into a number of different wave systems which can be characterized by a small number of parameters like significant wave height, mean frequency, propagation direction and directional spread among others. Several works have attempted to address the problem of partitioning of the 1D wave spectrum, among them (Ochi and Hubble, 1976; Guedes Soares, 1984; McCarthy, 1989; Guedes Soares and Nolasco, 1992; Rodriguez and Guedes Soares, 1999a). Methods for the

partitioning of the directional (or 2D) spectrum have been introduced with the original work by Gerling (1992), and later modified by Hasselmann et al. (1996). We however prefer to use only the information yielded directly by the buoy (that is the 1D spectrum from the heave measurements) rather than applying a method for the estimation of the spreading function. We use the maximum entropy method rather than the classical Fast Fourier analysis to compute the direction of the wave systems adjusted by the spectral fitting method.

The main assumption in the method by Violante-Carvalho et al. (2002b) is to consider the 1D spectrum $F(f)$ as the sum of independent wave systems, hence a bimodal spectrum is characterized by a high frequency ($F_{hf}(f)$) and a low frequency ($F_{lf}(f)$) system yielding

$$F(f) = F_{hf}(f) + F_{lf}(f). \tag{5.2}$$

Each wave system $F_{hf}(f)$ and $F_{lf}(f)$ is adjusted using a spectral method based on the JONSWAP spectrum (Guedes Soares, 1984). The JONSWAP spectrum (Hasselmann et al., 1973) presents a rate of energy decay for the high frequency part which is inversely proportional to frequency to the fifth power ($F(f)^{-5}$). The high frequency tail that best describes the spectral decay is still subject to debate, although in many studies there is a clear evidence that its value lies between -3.5 and -5 (Toba, 1973; Mitsuyasu et al., 1975; Donelan et al., 1985; Banner, 1990; Prevosto et al., 1996; Rodriguez and Guedes Soares, 1999b; Young, 1998). Liu (1989) has reported for experiments in deep water a weak correlation of the high frequency decay at early wave growth stage with the total spectral energy, and for well developed or fully developed waves n seemed to be constant with values between -4 and -3. Young and Verhagen (1996) described the gradual decrease in magnitude of n as a function of the effects of finite depth in a shallow lake in Australia. In deep water they found that the exponent is approximately -5 and when the effects of the finite depth become more significant n approaches -3.

To investigate the behavior of the high frequency tail we employed a spectral form using a variable exponent n in the form $F(f)^{-n}$:

$$F(f) = (2\pi)\alpha g^2 (2\pi f)^{-n} \exp\left[-\frac{5}{4}\left(\frac{f}{f_p}\right)^{-4}\right] \gamma^{\exp\left[\frac{-(f-f_p)^2}{2\sigma^2 f_p^2}\right]}. \tag{5.3}$$

The exponent n is determined by logarithmic regression of the spectral points beyond 2 times the peak frequency f_p. The parameter α is the high frequency spectral level, γ is the

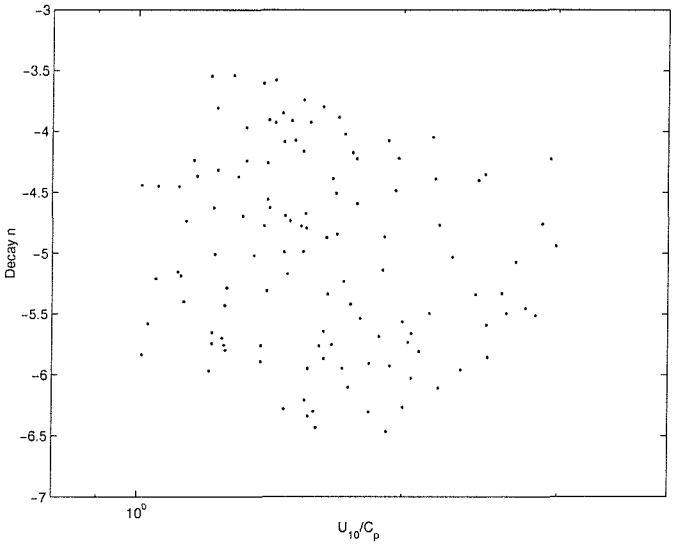

Figure 5.1: The exponent n for the cases selected as wind sea as a function of the inverse wave age U_{10}/C_p.

enhancement factor, σ is the spectral width in the peak region and g is the gravitational acceleration. It is worth noting that (5.3) reduces to the JONSWAP spectrum when n equals -5.

The high frequency decay n obtained from cases selected as wind sea (as defined later in this section) is highly variable although most of its values lie between -4 and -6. Figure 5.1 shows values of the exponent n for the cases selected as wind sea against the inverse wave age U_{10}/Cp. There is no clearly predominant decay that supports either $F(f)^{-5}$ or $F(f)^{-4}$, the forms normally encountered in the literature. The best representation of the high frequency tail of the spectrum, or even whether there is a unique value, remains an open question and perhaps a model with a variable exponent n as in (5.3) is a better approach. However using a constant value of n, either -4 or -5, would allow us to compare our results with previous works where a constant n was employed. We have found no clear dependency of n on other spectral parameters and its value presents a mean equal to -5.01 with a standard deviation equal to 0.78. For this reason we have set the value of n to -5 in (5.3) and hence we are adopting a JONSWAP model for the spectral fitting.

The first step in the fitting procedure is to select the points of highest spectral ordinate and to check whether they are in fact correlated to different geophysical processes or are a consequence of, for example, sampling variability. Spectra with 32 degrees of freedom and

50% overlap yielded a satisfactory relation between resolution and variance although further tests are necessary to ensure that a spectral maximum is in fact related to a wave system rather than to fluctuations arising from the spectral estimators (see more discussion about this in Pierson (1977)). We adopted three criteria that must all be satisfied for the selection of the spectral peaks:

- the peak must be separated 2 times the frequency resolution ($0.03Hz$) from its closest peak, a rather arbitrary value but which yielded satisfactory results.
- the ratio between the ordinate of the peak and of the adjacent one must be less than 15 to eliminate peaks that are below a background noise.
- the two peaks will be accepted if the ordinate of lower limit of the 90 percent confidence interval of the greater peak is higher than the ordinate of the upper limit of the 90 percent confidence interval of the trough between the peaks, which basically means that the valley between the peaks has to be sufficiently low.

The next step in the fitting procedure is to adjust $F_{hf}(f)$. The values of α and γ are chosen to produce the least-square error between measured and fitted spectra. The adjusted high frequency spectrum is then subtracted from the measured spectrum (5.2) and the same procedure is repeated to adjust the low frequency spectrum. These procedures outline the fitting of double peaked spectra.

The wave spectra encountered in Campos Basin are quite complex and over a third of the observations fitted using the above criteria present three or more spectral peaks. The fitting procedure for double peaked spectra selects the two most energetic peaks and hence may not select the wind sea system. The main goal of the present analysis is to investigate the influence of swell on the wind sea, therefore we must extend the fitting technique. To ensure that the wind sea is always fitted the above procedure was extended to model a third peak, but only if the two initially selected do not correspond to the wind sea. The third peak must also satisfy the three criteria for selection of wave systems. Therefore a trimodal spectrum is represented by

$$F(f) = F_{sea}(f) + F_{hf}(f) + F_{lf}(f) \tag{5.4}$$

where $F_{sea}(f)$ represents the wind sea system, $F_{hf}(f)$ may represent a young swell and $F_{lf}(f)$ is the swell at lower frequency.

We need reliable criteria to isolate the wind sea from the rest of the spectrum and the wind direction is used as a first condition for the selection. The high frequency peaks that remain within a $\pm 30°$ window of the wind direction measured by the buoy are selected as potential wind sea systems. However in the region of Campos Basin there is a strong presence of a young swell component which presents propagation directions close to the wind direction and lies in the high frequency part of the spectrum, although not related to the local wind (Violante-Carvalho, 1998). The equilibrium range theory is then applied as a second criterion for the selection of the wind sea component. Phillips (1958) suggested that in the high frequency part of the spectrum (from $1.5f_p$ to $3.0f_p$) the spectrum is proportional to frequency to a power -5 in the form

$$F(f) = \alpha g^2 (2\pi)^{-4} f^{-5}. \tag{5.5}$$

The high frequency level α is wind dependent and can be used as an indication of the stage of wave growth. This feature is exploited for the selection of the wind sea component of the spectrum. Examination of the data indicates that the wave components above $\alpha = 0.001$ are correlated to the wind energy transfer region and so were classified as wind sea. Figure 5.2 presents a typical trimodal spectrum from 1 May 1992 1600 UT with a swell peak at 0.0645 Hz (15.5 s), a young swell at 0.1266 Hz (7.9 s) and wind sea at 0.1887 Hz (5.3 s). The direction that the wind waves are coming from (not shown on the plot) are, respectively, 145° (SE), 44° (NE) and 33° (NE). Both peaks at higher frequencies lie on a band of active wind input and the wave directional information itself might not be enough for a correct isolation of the wind sea. The figure illustrates a case where the young swell system is just below the equilibrium level for a value of $\alpha = 0.001$. This threshold value is used in conjunction with the wave directional information for the selection of the wave system generated by the local wind.

5.3 The Influence of Swell on Wind Waves

Violante-Carvalho (1998) presented a comprehensive statistical description of the spectral evolution of different wave systems and their relation to the meteorological patterns encountered in Campos Basin (see more details on page 14). A distant swell propagating in the opposite direction to the wind sea and a young swell propagating close to the wind sea both

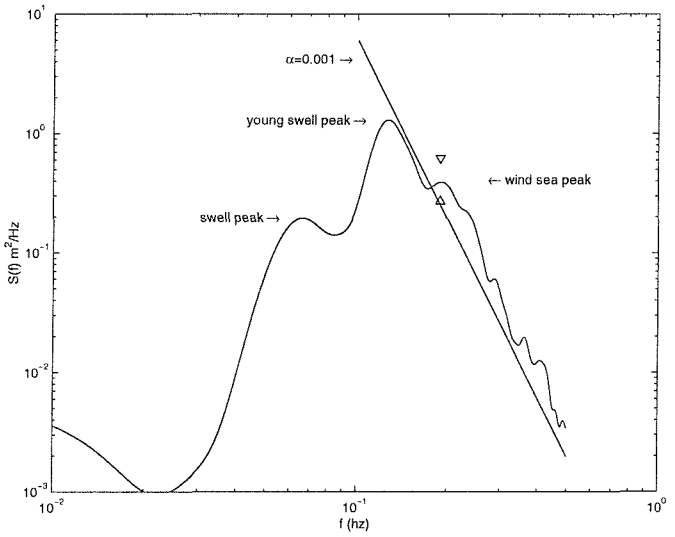

Figure 5.2: A trimodal spectrum with the equilibrium range $\alpha g^2(2\pi)^{-4}f^{-5}$ for $\alpha = 0.001$ included representing the separation between wind sea and young swell. Also appears on the plot the 90% confidence interval represented by the up and down triangles.

in direction and frequency is a common situation in Campos Basin. This is an ideal scenario for the investigation of the influence of swell propagation on wind sea growth.

Our analysis was limited to the cases of waves generated by winds whose direction remained relatively stable. The data set was prepared by selecting from 26 months of wind and wave observations the periods in which the wind direction remained within $\pm 20°$ of its mean for at least four days. Figure 5.3 illustrates one of the nine selected periods of relatively steady wind direction. The selection of steady wind conditions is of fundamental importance for the analysis since varying winds would increase the scatter in the data.

There is a level of uncertainty in our analysis in the band close to the Nyquist frequency associated with waves of small amplitudes. This is firstly due to the high frequency buoy response already pointed out and in second place to the method of spectral partitioning. The partitioning scheme using the one-dimensional spectrum rather than the full directional spectrum may compute an unknown amount of energy from high frequency components of swell propagating in directions other than the local wind. Hence, the fitting spectral method may overestimate the energy variance m_0 due to swell contamination of the wind sea spectrum. To mitigate this analysis limitation, and because of the uncertainty of the buoy response to high frequency waves, we eliminated the wave observations where the wind speed U_{10} is less than $7 m/s$. Furthermore Donelan et al. (1985) proposed that $U_{10}/c_p = 0.83$ corresponds

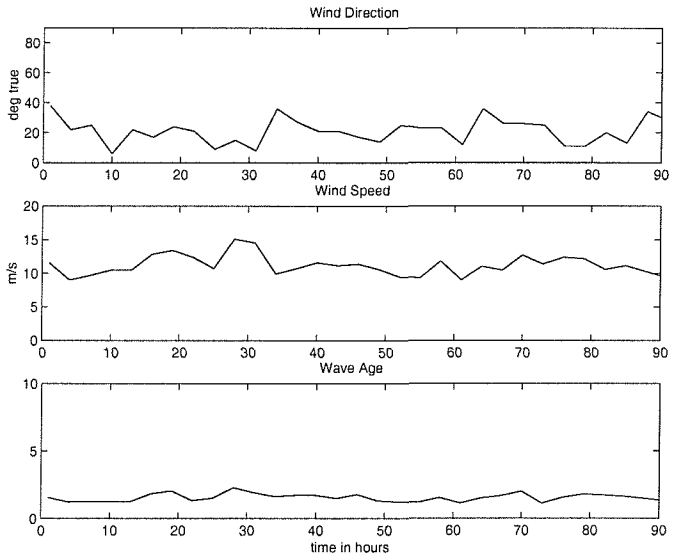

Figure 5.3: Respectively from top to bottom time history of wind direction, wind speed and wave age of the wind sea extracted from the model of spectral adjustment observed by the buoy during one of the selected periods of relatively steady wind direction.

to the value of the spectrum at full development, where the spectral components below this value are classified as swell and above as wind sea. Therefore we dropped the spectra for which $U_{10}/c_p < 0.83$, hence characterized as swell, because of the poorer correlation obtained which yields a total number of 119 ideal cases used in our analysis.

The values of the wind sea high frequency level α isolated by the method of spectral adjustment are plotted in Figure 5.4 against the reciprocal wave age U_{10}/c_p. Our results are in remarkable agreement to those obtained in idealized fetch limited conditions, despite the high scatter in the data as observed in similar studies. Due to the process of shape stabilization (see for example Komen et al. (1994) and Young (1999)) the spectral peak shifts to lower frequencies and α decreases due to its response to the wind input of energy. Therefore α has a geophysical meaning and can be used as an indication of the stage of wave development. The evidence that the value of α can be extracted from a multi-modal oceanic spectrum can be useful information for wave forecasting. Once the wind information is available, for example from a scatterometer on board a satellite, the value of α and therefore the stage of wave growth can be used to update wave models.

Table 5.1 presents the occurrence of directions of swell propagation relative to the wind sea direction. For the trimodal spectral cases swell is considered the closest wave system

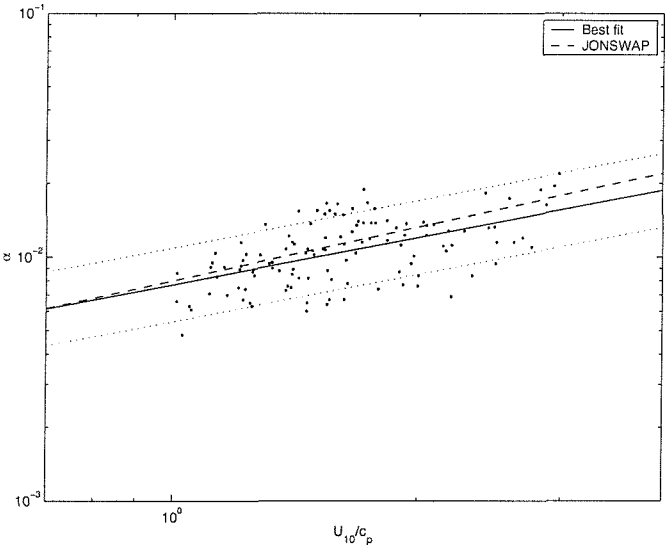

Figure 5.4: Values of the 119 cases of high frequency energy level α as a function of the reciprocal wave age U_{10}/c_p. The solid line is the best fit to our data $\alpha = 0.0077(U_{10}/c_p)^{0.64}$ with a correlation coefficient $r = 0.54$, whereas the 90% confidence interval is represented by the dotted lines. The dashed line is from JONSWAP, $\alpha = 0.0080(U_{10}/c_p)^{0.73}$.

to the wind sea in frequency space, regardless of whether it is the most energetic system or not. We classified as aligned swell those cases where the direction of propagation of swell is within a $\pm 45°$ window of the wind sea direction and all other cases are considered as non aligned swell. Moreover table 5.1 provides within brackets the number of cases where the ratio between the swell peak frequency and the wind sea peak frequency is less than 0.55 ($f_{p_{swell}}/f_{p_{sea}} < 0.55$). Hence considering bimodal spectra there are 13 cases out of 57 where the direction of propagation of the swell peak is aligned with the wind sea and the ratio $f_{p_{swell}}/f_{p_{sea}}$ is less than 0.55. Another information given in table 5.1 is that from the 37 cases of trimodal spectra there is only one where swell is not aligned with wind sea which is evidence of the strong presence of a young swell system in Campos Basin, whose peaks are close to the wind sea in terms of direction of propagation and in terms of frequency. Most of the time the second swell partition of the trimodal spectra propagates from the south quadrant at lower frequencies, usually with generation areas located at higher latitudes (Violante-Carvalho, 1998).

Donelan et al. (1992) carried out a detailed field experiment in Lake Saint Clair to explore the wave growth in a fetch-limited swell-free environment. They found a high correlation

Table 5.1: Occurrence of the direction of swell propagation relative to the wind sea direction in terms of the number of spectral peaks. Within brackets are the number of cases where the ratio between the swell peak frequency and the wind sea peak frequency is less than 0.55.

	aligned swell	non aligned swell	*num. obs.*
unimodal	-	-	3
bimodal	57 [13]	22 [12]	79
trimodal	36 [1]	1 [0]	37
total	93 [14]	23 [12]	119

between the reciprocal wave U_c/c_p and the dimensionless wave energy ϵ:

$$\epsilon = 0.0022\left(\frac{U_{10}}{c_p}\right)^{-3.3}. \tag{5.6}$$

In order to investigate whether the swell dominated environment of Campos Basin produces similar results we searched for the best regression to the data. We present in Figure 5.5 the variation of the dimensionless wave energy ϵ with U_{10}/c_p and the best-fit of the data expressed by

$$\epsilon = 0.0017\left(\frac{U_{10}}{c_p}\right)^{-3.21} \tag{5.7}$$

with a correlation $r = -0.82$.

The best fit to the data (5.7) is in close agreement with Donelan's relationship (5.6). Hanson and Phillips (1999) obtained similar results from their data in the Gulf of Alaska:

$$\epsilon = 0.0020\left(\frac{U_{10}}{c_p}\right)^{-3.22}. \tag{5.8}$$

Within the scatter in the data there is no clear evidence of the influence of swell on wind waves, with relations (5.6–5.8) being statistically identical. However both statistics carried out at open sea (5.7 and 5.8) seem to point to a small reduction on wave energy in the presence of swell in comparison to (5.6). The relation obtained at Campos Basin (5.7) seems to indicate a reduction of around 15% on the wind sea energy, whereas in the work by Hanson and Phillips (1999) (5.8) the reduction is less than 5%. It is worth noting that only 18% of spectra measured in the Gulf of Alaska presented swell propagating aligned with wind sea. In contrast over 78% of the spectra used in our analysis present swell propagating close both

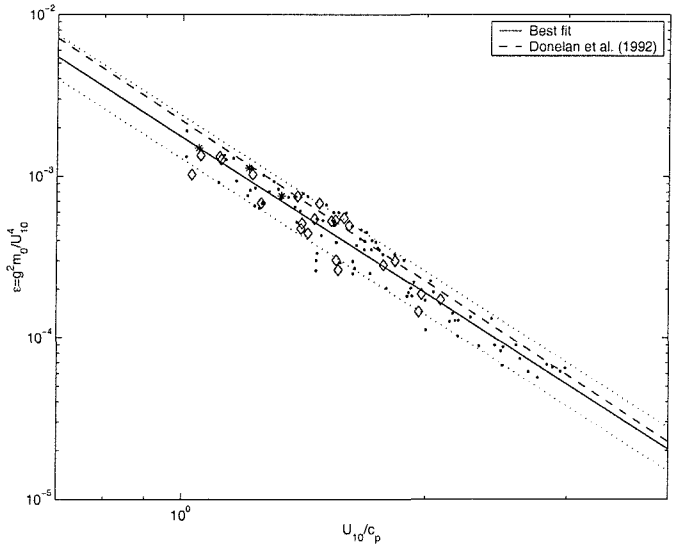

Figure 5.5: The dimensionless wind sea wave energy ϵ as a function of the reciprocal wave age U_{10}/c_p. The solid line is the best fit to the data $\epsilon = 0.0017(U_{10}/c_p)^{-3.21}$ and the dashed line is the power-law regression $\epsilon = 0.0022(U_{10}/c_p)^{-3.3}$ from Donelan et al. (1992). The diamonds are the 23 cases where swell is not aligned with wind sea, the stars are the 3 cases of unimodal spectra whereas the points are the 93 cases where swell is aligned with wind sea (see table 5.1). The 90% confidence interval is also shown as the dotted lines.

in frequency and in direction with the wind sea, where one would expect a stronger reduction on wind sea energy due to the presence of longer waves.

There is enough scatter in the plot to extend our analysis to investigate the influence of swell in terms of both direction of propagation and frequency. The best fit to our data considering non-aligned swell and aligned swell (with correlation coefficients r=-0.89 and r=-0.82) is given respectively by

$$\epsilon = 0.0018\left(\frac{U_{10}}{c_p}\right)^{-3.2} \tag{5.9}$$

and

$$\epsilon = 0.0016\left(\frac{U_{10}}{c_p}\right)^{-3.0}. \tag{5.10}$$

From Figure 5.5 it is not clear whether the direction of propagation of swell may affect the wave growth, although looking at (5.9) and (5.10) there seems to be a slight decrease in wave energy when swell propagates aligned with wind sea. Considering that most of the swell in Hanson and Phillips (1999) is propagating non aligned with wind sea, that could explain why

the relation obtained from their data presents a slightly higher value than ours.

Masson (1993) based on simulations concluded that the nonlinear coupling is negligible unless the two peaks are very close in frequency which can make the bimodal structure of the spectrum hard to identify. The data from Campos Basin provide ideal cases for validation of these assumptions. Just to illustrate an example a wind sea component at 0.189 Hz (5.3 s) and a young swell component at 0.127 Hz (7.9 s) propagating in close directions is a common situation. The spectrum in Figure 5.2 illustrates such a situation where the ratio between swell and wind sea peak frequencies is greater than 0.6. The spectral peaks are clearly separated in f space and the method adopted in the present work for the spectral adjustment is able to identify both systems. The regression obtained from the data considering the cases where the ratio $f_{p_{swell}}/f_{p_{sea}}$ is less than 0.55 is:

$$\epsilon = 0.0020\left(\frac{U_{10}}{c_p}\right)^{-3.3} \tag{5.11}$$

with a correlation coefficient r=-0.84. It is worth noting that (5.11) is closer to the relation obtained in a swell free environment (5.6). The regression of the 90 data points where $f_{p_{swell}}/f_{p_{sea}} \geq 0.55$ (with r=-0.82) is

$$\epsilon = 0.0017\left(\frac{U_{10}}{c_p}\right)^{-3.2} \tag{5.12}$$

which is the same as relation (5.7) when we consider the regression of all cases regardless of their direction of propagation or ratio $f_{p_{swell}}/f_{p_{sea}}$.

5.4 Discussion

We have examined the effect of long waves on the energy of wind sea considering different propagation directions and frequencies of swell. Based on Phillips' equilibrium range theory and applying a spectral method for the adjustment and partitioning we were able to isolate the wind sea from the swell contaminated spectra in a tropical open ocean region in the South Atlantic. From a data set of over 5800 buoy observations we selected cases where the direction of the wind remained stable in direction. The data obtained from the buoy in Campos Basin are unique for the investigation of the influence of swell on wind waves due to the ubiquitous presence of a young swell component propagating aligned with wind sea as

well as a longer, opposing swell.

The regression of the values of the high frequency energy level α against the inverse wave age is in very close agreement with similar studies from fetch limited areas. Such results obtained from multi-modal spectra in the open ocean are remarkable. There is a clear instrumental limitation from pitch-roll buoys in the band close to the Nyquist frequency although we have selected only cases of moderate to strong wind speeds to mitigate this problem. Furthermore we have imposed a representation of the high frequency exponential decay in the form $F(f)^{-5}$ although there is no clear indication from our data that a single, constant value should apply. The parameter α is very sensitive to the high frequency band of the spectrum which is a region where one would expect a strong influence of longer waves modulating the shorter, wind sea waves. A possible explanation for such close agreement could be the fact that oceanic waves are longer than those encountered in wave tanks. If the reduction of wind waves as observed in wave tanks is in fact mainly due to nonlinear coupling then longer waves with smaller wave slopes (less nonlinear and hence with weaker nonlinear interactions) would be less sensitive to the presence of swell. However we have found no clear dependency of the wave slope on the energy ratio between sea and swell (not presented here) with the scatter in the data showing no clear trend.

Our measurements demonstrate that there is no significant effect of swell on wind sea growth. The relation obtained from our observations is similar to the relation proposed by Donelan et al. (1992), which is striking due to the differences between the experiments, that is a lake without swell and an offshore region where swell is present and is responsible for most of the spectral energy. The relation between wind sea energy and inverse wave age from Campos Basin is statistically identical to the relation obtained in a swell free environment and to another experiment carried out in the open ocean. However there seems to be a small reduction in wave energy in both relations obtained from swell contaminated environments. The observation cases selected in our study when swell is aligned with the wind will exhibit a stronger nonlinear interaction, with the subsequent more active energy transfer. This mechanism will enhance energy distribution so as to reduce the wind sea spectral level. Although a subtle difference is obtained from our results, lower energy level for wind sea under the presence of swell seems to suggest that the nonlinear mechanism is an influencing factor. Further analysis seems to indicate that there is a slight reduction in wave growth when swell propagates close in direction to the wind sea. In addition the regression obtained from our data also seems to point to a minimal reduction on wave growth when swell and wind

sea components are close in frequency space, that is $f_{p_{swell}}/f_{p_{sea}} \geq 0.55$. Nevertheless all the regressions obtained lie within the 90% confidence interval limits which makes it difficult to make firm conclusions from these indications.

Our results are within the statistical limits of the regressions obtained in swell free environments, giving evidence that there is no strong effect of longer waves on wind waves in oceanic regions. If there is in fact any sort of influence of swell on wave growth it seems to us that it is relatively small and considering the present instrumental limitations in wave measurements such influence will be masked within the scatter in the data. For practical purposes that means that power-laws obtained from fetch limited situations can be applied in the open sea.

Chapter 6

On the Retrieval of Two Dimensional Directional Wave Spectra from Spaceborne Synthetic Aperture Radar (SAR) Images

In this chapter we revisit the main features of the SAR ocean wave imaging mechanisms together with a detailed description of the Max-Planck Institut (MPI) retrieval algorithm which runs operationally at the European Centre for Medium-Range Weather Forecasts (ECMWF). Some examples of retrieved spectra are compared against directional buoy measurements obtained in deep water in the South Atlantic and against WAM spectra. The main characteristics of the MPI retrieval scheme are discussed and some of its deficiencies and strengths are identified.

6.1 Introduction

Spaceborne Synthetic Aperture Radar (SAR) is to date the only source of two dimensional directional wave spectra with continuous and global coverage when operated in the so-called SAR Wave Mode (SWM). Since the launch in 1991 of the first European Remote Sensing Satellite ERS-1 and more recently with ENVISAT millions of SWM imagettes containing detailed spectral information are now available in quasi-real time. This huge amount of directional wave data has opened up many exciting possibilities for the improvement of our

knowledge of the dynamics of ocean waves.

The quality of the retrieval schemes compared against independent directional data has not yet been demonstrated. Bauer and Heimbach (1999) compared the significant wave height extracted from ERS-1 SAR using the MPI scheme against Topex altimeter data. They have found a good correlation between both measurements but the comparison of an integral parameter does not provide much insight about the spectral capabilities of the retrieval. The spectral performance of the MPI scheme was compared against three years of WAM wave model spectra (Heimbach et al., 1998) which were used themselves as first guess for the inversion. Although the overall agreement was quite promising it was clear that an assessment against independent data, for example spectra from a directional buoy, would be more likely to point to any deficiencies of the method.

The performance of the retrieval schemes has been indirectly assessed as well through data assimilation exercises. The assimilation of spectral SAR data retrieved from the MPI scheme (Hasselmann et al., 1997; Dunlap et al., 1998) and from the scheme by Krogstad et al. (1994) (Breivik et al., 1998) has shown no clear positive impact on the wave forecast. It is not clear from these assimilation experiments if the lack of improvement in the forecasting is due to the SAR data and its retrieval or due to the assimilation schemes. The nonlinear SAR imaging process has a degree of uncertainty due to the complex mechanisms involved. Thus a comparison of the retrieved spectra—meaning hereafter the final product to distinguish from the intermediate spectra obtained in the course of the inversion—against, for instance, directional buoy spectra has twofold importance. On the one hand such a comparison would allow us to clearly pinpoint deficiencies in the retrieval scheme. On the other hand the linearly mapped low frequency band of the SAR image could give insights about the swell measured by the buoy.

The main goal of the present chapter is to supply a detailed investigation of the possibilities/limitations of mapping wind waves with a spaceborne SAR instrument using the MPI retrieval algorithm. The MPI scheme runs operationally at ECMWF and is the most broadly used algorithm to date implemented in several institutions around the world. However very little is known about its performance assessed against independent measurements. We are comparing SAR wave spectra extracted from the MPI scheme against directional buoy spectra measured in the open ocean in the South Atlantic and against WAM spectra used as first guess to the inversion. The main characteristics of the MPI retrieval scheme are presented together with a comprehensive review of the SAR modulation transfer functions. The struc-

ture of the chapter is the following. In section 2 the SAR imaging mechanisms are described in some detail while the MPI retrieval scheme is discussed in Section 3. Collocation criteria are presented in section 4 and finally results of the comparison and discussions are illustrated in sections 5 and 6.

6.2 SAR Ocean Wave Imaging Mechanisms

It is quite remarkable that an instrument like SAR that emits microwave pulses able to penetrate no further than the very top skin layer of the ocean is capable of capturing in its back scattered pulse information about several oceanic features such as internal waves, shallow water bathymetry, current boundaries and surface gravity waves among others. In the explanation for what is, at first sight, a surprising response lie the principles of the SAR ocean wave imaging mechanism.

The ERS-1 satellite was launched in July 1991 into a sun-synchronous, polar, near-circular orbit operating at an altitude of about 785 km. Its payload consisted of an Active Microwave Instrument comprising a SAR (image and wave modes), a Wind Scatterometer, a Radar Altimeter and an Along Track Scanning Radiometer. In SAR image mode the instrument acquires 100 x 100 km images but due mainly to onboard data storage limitations it can be operated only in the vicinity of a ground station. The SAR Wave Mode was introduced to yield global coverage of directional wave spectra since the much smaller images acquired in this mode are stored onboard and transmitted once per orbit to ground stations. Figure 6.1 shows the several thousand of SAR Wave Mode imagettes acquired by ERS-1 during the period of one month over the South Atlantic. The resolution of the SAR Wave Mode imagette is similar to the SAR image mode, around 30 x 30 m. The spectrum consists of 12 x 12 polar wavenumber coordinates ranging from approximately 100 to 1000 m in wavelength (wave periods from 8 s to 25 s) and covering a 180° sector and so with directional resolution of 15°.

The ERS-1 SAR is a right side looking imaging radar operating at C-band (frequency of 5.3 GHz). A SAR is an active all weather sensor transmitting its own radiation and receiving back part of the energy that was back scattered from the sea surface. The fraction of incident energy reflected back is called the radar cross section and the radar modulation transfer function (MTF) is used to define the relation between the surface wave height and the amplitude of the variabilities of the radar cross section. At the typical incidence angles used in SAR onboard satellites (23° from vertical for ERS-1) the electromagnetic waves emitted

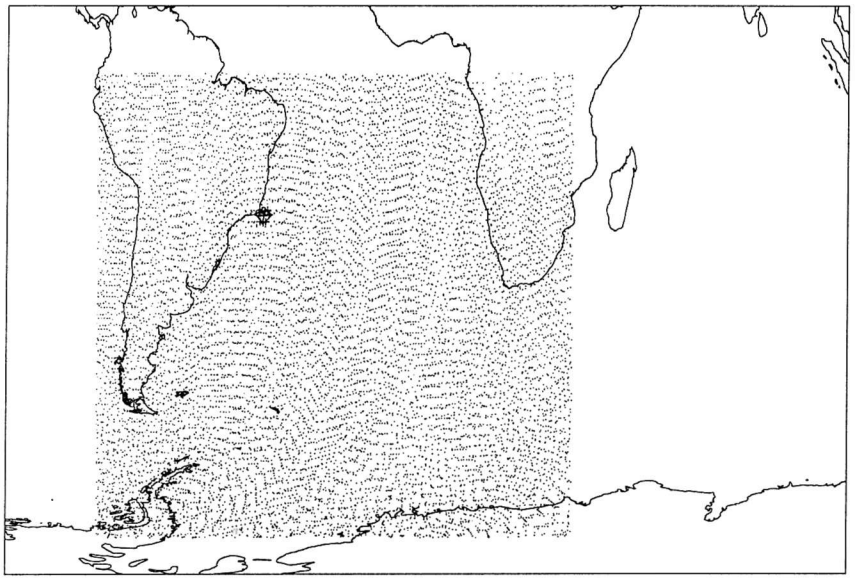

Figure 6.1: The selected area covers the South Atlantic from the Equator line to 72° S and from 74° W to 30° E which is the lat-lon grid used for the wave model. Every dot represents a SAR Wave Mode imagette and the $*$ are those closer than 150 km from the buoy in Campos Basin during October in 1994.

by SAR interact with short ocean surface waves in a process called the Bragg resonant scattering process (see for example Robinson, 1985, chapter 12). The back scattered signal is proportional to the amplitude of these decimetric ocean waves denominated Bragg surface ripples. For ERS-1 the Bragg ripples have a wavelength of approximately 8 cm. These short waves are modulated by longer waves, for example a swell propagating on the surface or even internal waves propagating several meters in depth, which causes the longer waves to be visible on SAR images.

The imaging of ocean surface waves by SAR is based on a two-scale model (see for instance Komen et al., 1994) consisting of the short waves whose wavelength is approximately half as long as the incident radar wavelength and the longer swell waves. The back scattered signal is affected by the slope of the long waves that changes the angle of view that the ripples present to the radar, the tilt modulation. In addition the amplitude of the short waves is modulated by the long waves in a process called hydrodynamic modulation, which increases the energy of the Bragg waves near the swell crests and reduces the energy near the troughs. The linear Real Aperture Radar (RAR) modulation is composed by the hydrodynamic and

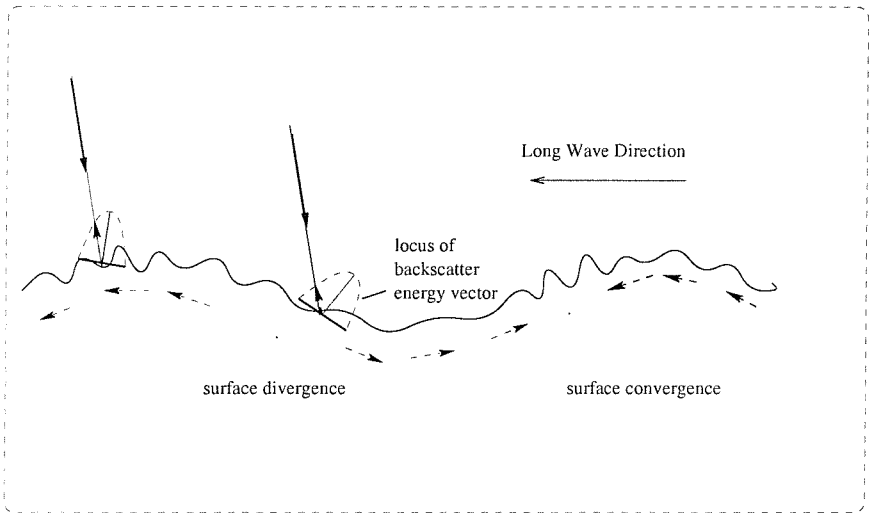

Figure 6.2: Representation of the tilt and hydrodynamic modulation processes. The dashed arrows indicate the component of the long wave orbital velocity creating convergent and divergent patterns at the sea surface—the hydrodynamic modulation. The locus of backscatter energy vector illustrates the radar backscatter being strongest from the slope of the wave facing towards the radar and weakest facing away—the tilt modulation. Adapted from Robinson (1985).

tilt modulation and assumes that the target is stationary (see Figure 6.2). SAR imaging is sensitive as well to the vertical movement of the sea surface caused by the orbital motion of the waves. An azimuthal displacement occurs due to the Doppler effect of a moving target—the velocity bunching mechanism—causing image smearing. If the azimuth image shift becomes comparable with the length of the long waves the image modulation becomes nonlinear causing loss of information beyond the azimuthal cut-off wavenumber and limiting the SAR resolution in the azimuth direction. It is still not clear which one of the three imaging mechanisms is the dominant one (see a comprehensive review in Hasselmann et al., 1985) and in the following we will extend a bit further the discussion of each one of the modulation transfer functions.

The amount of energy reflected back to the sensor by the ripples which scatter the radar will be a function of the inclination of the longer (swell) wave on which they ride (Figure 6.2). The tilt modulation represents the change in cross section relative to the change in the incidence angle due to slope variations. Basically the amount of energy reflected back will be greater for the target plane (facet) facing towards the radar, while for the slope of the wave facing away the cross section will be smaller. This mechanism is primarily sensitive to range

(perpendicular to the direction of satellite flight) travelling waves. Models of the Tilt MTF assume a Phillips k^{-4} (or f^{-5}) slope although the best representation for this high frequency decay exponent is still open to debate (see for instance Violante-Carvalho et al., 2002a). The Tilt MTF is represented by

$$T_t = -k_r \frac{4\cot\theta}{1 \pm \sin^2\theta} e^{\frac{i\pi}{2}} \tag{6.1}$$

where k_r is the component of the wavenumber vector in the range direction and θ is the radar incidence angle. The $\pm$ sign represents vertical and horizontal polarization respectively and hence the tilt MTF is strongest for horizontal polarization. The maximum cross section occurs on the face of the long wave—$\pi/2$ from the wave crest—as described by the phase in (6.1).

The amplitude of the Bragg waves is modulated by the phase of the longer swell wave in a process called hydrodynamic modulation. The currents induced by the orbital velocity field under the crest of the longer wave advect the Bragg waves resulting in a convergent field which causes an increase in the amplitude of the ripples on the surface near the swell crest. Near the trough there is a corresponding reduction in ripple amplitude generating a pattern of increase and decrease of ripple amplitude connected to swell phase (Figure 6.2). There are several equations to represent the hydrodynamic modulation, here we follow the form proposed in Hasselmann and Hasselmann (1991)

$$T_h = \frac{\omega - i\mu}{\omega^2 + \mu^2}(4.5)k\omega \left(\frac{k_r^2}{k^2} + Y_r + iY_i\right). \tag{6.2}$$

The feedback coefficients Y_r and Y_i depend on the wind speed, μ is a damping factor and $\omega = 2\pi f$ where f is frequency. The best representation for the hydrodynamic modulation, the less well understood of the MTFs, is an issue under dispute. There is no phase dependence in (6.2), which implies that the maximum cross section is on the crest of the long wave. The above equation expresses that the radar cross section depends on the local wind speed and on the long wave spectrum and, like the tilt modulation, can not image azimuth travelling waves. Due to the less well understood representation of the hydrodynamic modulation the incidence angle for the ERS-1 SAR was deliberately chosen to minimize the importance of this term in comparison with the better understood tilt modulation. Monaldo and Beal (1998), using a simplified version of (6.2), found a ratio between T_t/T_h equal to 6.1 for an incidence angle of 23°.

Therefore long waves travelling in the range direction are detected by SAR because of their

effect on decimetric Bragg waves through the tilt and hydrodynamic modulations. However long waves travelling in the azimuth direction can not be detected in this way. The mechanism for the imaging of azimuth travelling waves is closely tied to the aperture synthesis process used to achieve a finer resolution in the azimuth direction. The along track resolution for an antenna of 10 m (like the one onboard ERS-1) without using the principle of aperture synthesis would be in the order of 5 km. Alternatively for an azimuth resolution of 25 m an antenna of length 4 km would be necessary. The concept of aperture synthesis is used to improve the resolution without the need for augmenting the antenna's dimensions. The basic idea is to take advantage of the forward motion of the satellite using many returns of the target's reflection to build up a signal equivalent to that from a much larger antenna. Since the satellite's velocity is always changing in relation to the target the instrument uses the time dependent Doppler shift in frequency of the returned pulse to resolve the different target's position when performing the aperture synthesis.

Nevertheless the sea surface is not a stationary target. The orbital velocity of the long ocean waves produces a vertical displacement of the location of the facets of small resonant waves. This vertical movement modifies the Doppler shift of the target, providing its own Doppler offset, implying that its apparent azimuthal position is displaced on the SAR image. The spatial mispositioning depends on the orbital velocity of the long waves which is directly proportional to their mean frequency and significant wave height, and therefore sea state dependent. For ERS-1 a wave of mean frequency of say 0.1 Hz—wavelength of 156 m—and significant wave height of 5 m would be displaced by more than 170 m in both azimuthal directions. The rising face of the wave is displaced in the positive azimuth direction whereas the falling face shifts in the negative azimuth direction. If this displacement, called velocity bunching, is small when compared to the wavelength of the long wave the effect is approximately linear. But if the displacement is of the same order as (or larger than) the wavelength of the long waves, which is the case for waves as in the previous example, the velocity bunching mechanism is strongly nonlinear. These nonlinearities cause smearing of the image and an azimuthal fall-off with a high wavenumber azimuthal cut-off beyond which waves are not mapped into the SAR image plane. The azimuthal cut-off is sea state dependent and hence varies, but in general SAR can not detect waves shorter than 150–200 m propagating in the azimuth direction. Therefore the SAR imaging process can be thought of as a low-pass filter damping out the high wavenumber part of the spectrum.

The linear velocity bunching MTF is represented as

$$T_{vb} = \frac{R}{V} k_a \omega \left(\sin^2\theta \sin^2\phi + \cos^2\theta\right)^{1/2} \tag{6.3}$$

where R is the distance between the radar and the ocean surface (slant range), V is the satellite ground track velocity, k_a is the component of the wavenumber vector in the azimuth direction and ϕ is the wave propagation angle with the satellite track ($\sin\phi = \frac{k_r}{|\mathbf{k}|}$). The phase of (6.3) depends on the sign of k_a; for positive values, or waves propagating in the same direction as the satellite, the maximum cross section occurs at the wave crest. For negative values of k_a, or waves propagating antiparallel to the satellite, the minimum cross section occurs at the wave crest. Reducing the ratio R/V, for instance with SAR on a lower altitude satellite, brings down the azimuth degradation caused by orbital motion and as a result the linear behavior of the velocity bunching mechanism applies over a larger wavenumber band.

The mapping of a wave spectrum into a SAR image spectrum (and its inversion) has to take into account all the imaging mechanisms and the nonlinearities encountered at least in part of the spectrum. Hasselmann and Hasselmann (1991) developed a closed nonlinear integral transform for treating this problem which combines additional information, in general from wave models, with the incomplete information yielded by SAR images. The main feature of this integral transform is an exponential term that describes the azimuthal fall-off. The characteristics of the integral transform, together with a discussion of the MPI retrieval scheme, are presented in the next section.

6.3 The MPI Retrieval Scheme

Hasselmann and Hasselmann noted that since the imaging mechanisms are quite well understood the forward mapping of an ocean wave spectrum into a SAR image spectrum can be computed numerically. However the wave spectrum provided by SAR images is an incomplete spectrum. First of all this is due to the directional ambiguity. Secondly the nonlinearities caused by orbital motions result in an azimuthal high wavenumber cut-off and therefore waves shorter than 150–200 m propagating parallel to the satellite path are not imaged. In addition due to spatial resolution and storage limitations waves shorter than approximately 70 m (period of approximately 7 s) propagating even in the range direction are not mapped onto the SAR image either. These constraints impose the use of a first guess to augment the

spectral information. Hasselmann and Hasselmann recognized that because of this lack of information in the high wavenumber part of the spectrum not only a forward mapping was necessary but a method for inverting this mapping relation must be devised which extends the missing spectral information with the use of a first guess wave spectrum.

The retrieval algorithm used in this work is the improved MPI scheme presented by Hasselmann et al. (1996). The mapping of an ocean wave spectrum $F(\mathbf{k})$ into a SAR image spectrum $P(\mathbf{k})$ (Hasselmann and Hasselmann, 1991) is a closed integral transform in the form

$$P(\mathbf{k}) = exp(-k_a^2 \xi'^2) \sum_{n=1}^{\infty} \sum_{m=2n-2}^{2n} (k_a \beta)^m P_{nm}(\mathbf{k}) \tag{6.4}$$

where $exp(-k_a^2 \xi'^2)$ describes an exponential fall-off of the spectrum beyond an azimuthal cut-off wavenumber. This term can be thought of as a low-pass filter where the information beyond the cut-off is suppressed. The root mean square (rms) azimuthal displacement (ξ') is given by $\xi' = u_r \beta$ where β is the ratio of the slant range to the platform velocity R/V and u_r is the orbital velocity. P_{nm} represents the Fourier transform of the auto and cross-covariance functions of the Real Aperture Radar image intensity and the orbital velocity. The indexes m and n indicate the order of nonlinearity with respect to the velocity bunching mechanism and to the input wave spectrum, respectively.

The full nonlinear mapping relation may be approximated by a quasi-linear mapping relation truncating (6.4) at $n = 1$ which is

$$P(\mathbf{k}) \sim \exp(-k_a^2 \xi'^2) P_1(\mathbf{k}). \tag{6.5}$$

In the quasi-linear approximation the representation of the azimuthal cut-off term is retained but the nonlinearities in the mapping are not taking into account. The nonlinearities in the mapping mechanism cause transfer of energy from high to low azimuth wavenumbers, which are ignored using (6.5).

The MPI retrieval is performed in two steps. The first step or inner loop is the inversion of the mapping relation. An improved estimate of a given first guess wave spectrum is constructed through the minimization of a cost function. The second step or outer loop is meant to reduce the spectral gap in the azimuthal cut-off. After the minimization of the cost function the wave spectra of both the first guess and the observed SAR are partitioned into different wave systems and cross-assigned. The first guess wave systems are modified to

conform to the observed SAR wave spectrum. In the following we discuss in more detail the two steps performed in the retrieval scheme.

The main idea behind the MPI retrieval scheme is to create a simulated SAR image spectrum from a first guess wave spectrum through the mapping relation $P(\mathbf{k}) = \Phi(F(\mathbf{k}))$ (as specified by equation 6.4). This first guess spectrum is compared to the observed SAR spectrum and the differences between both spectra are minimized through the following cost function

$$\begin{aligned} J &= \int [P(\mathbf{k}) - \hat{P}(\mathbf{k})]^2 \hat{P}(\mathbf{k}) d\mathbf{k} + \\ & \mu \int \frac{[F(\mathbf{k}) - \hat{F}(\mathbf{k})]^2}{\{B + min[F(\mathbf{k}), \hat{F}(\mathbf{k})]\}^2} d\mathbf{k} + \\ & \eta \frac{(\alpha \lambda_{cl}^2 - \hat{\lambda}_{cl}^2)^2}{max\{\lambda_{cl}^4, \hat{\lambda}_{cl}^4\}}. \end{aligned} \tag{6.6}$$

The first error term is a function of the deviation between the observed SAR spectrum $\hat{P}(\mathbf{k})$ and the fitted SAR spectrum $P(\mathbf{k})$. The second term, expressing the deviations between the first-guess wave spectrum $\hat{F}(\mathbf{k})$ and the optimal fit wave spectrum $F(\mathbf{k})$, is necessary to solve the 180° directional ambiguity and to extend the information at high wavenumbers beyond the azimuthal cut-off. The factor μ is set in order that the first-guess wave spectrum has a small influence in the part of the spectrum where SAR information is available but is great enough to solve the directional ambiguity ($\mu = 10^{-3}\hat{P}_{max}^3$) and B is a constant to prevent the denominator from vanishing. The third term in equation (6.6) penalizes the differences between the clutter cut-off length scale from the observed and simulated SAR spectrum represented by $\hat{\lambda}_{cl}$ and λ_{cl}. The value of the weighting factor η is chosen to make the third error term of the same order of magnitude as the first term. To correct the errors in the cut-off the scale parameter α is applied to the whole spectrum and not only to the low wavenumber part where there is SAR information. Hence α also modifies the high wavenumber components that contribute to the rms orbital velocities and consequently to the rms azimuthal displacement $\xi\prime$. Since λ_{cl} is determined by $\xi\prime$ (both are proportional), α then affects λ_{cl} reducing then the error between the observed and simulated cut-off.

The performance of the MPI scheme is evaluated in terms of the reduction of the cost function J through a quality control flag called *jqual* (Hasselmann et al., 1998). When the cost is reduced to less than 10% of its value ($jqual = 0$) the inversion is considered

excellent, whereas for $jqual = 1$ (cost reduced to $10-50\%$) the result is considered acceptable. Inversions with cost reductions lower than 50% ($jqual = 2$) are considered questionable. For $jqual = 3$ the inversion was performed without convergence and $jqual = 4$ indicates that no azimuthal cut-off adjustment was achieved. In general the inversions are accepted when $jqual$ equals 0 or 1.

Hence the MPI scheme finds a retrieved wave spectrum by minimizing a cost function which depends on the wave spectrum, the SAR spectrum and the azimuthal cut-off wavenumber. The full nonlinear mapping relation (6.4) is used to calculate the SAR image spectrum from a first guess wave spectrum. However the quasi-linear approximation (6.5) is applied to yield the direction of minimization of the gradient of the cost function (6.6). The inversion is performed by the minimization of the cost function J, which is achieved when the difference between two iterations is smaller than a specific value, in general after 6–10 iteration steps. The form of the spectrum is modified only up to the point where there is SAR spectral information and beyond the cut-off wavenumber it retains the information from the first-guess wave spectrum. At this point an improved estimation of the first guess wave spectrum is constructed which is used in the next step.

The second step or outer loop replaces at every iteration the input spectrum by the wave spectrum derived in the previous cycle. So the first-guess wave spectrum from the model is used only in the 0-th cycle, and after the first cycle of the outer loop its information is modified by new information based on the SAR image. The main reason for this additional loop is to resolve the discontinuities in the vicinity of the cut-off wavenumber once the inversion modifies the spectrum up to this point. In addition the second loop decouples the retrieval from the WAM first guess wave spectrum implying that the retrieval (in a sense) is independent of the first guess.

The input two dimensional spectrum is partitioned in different wave systems, that is swell, wind sea, old wind sea, each one represented by some wave parameters: significant wave height, mean frequency, spread width and direction. The shape of the wave systems does not change and only the wave height, mean frequency and direction are adjusted. Thus the input spectrum maintains the characteristics of the original one, but the scales and directions are adjusted to conform to the observed spectrum. The program cycles five times around the outer loop and the updated spectrum from the previous loop is used as the input spectrum for the inversion in the next cycle.

Figure 6.3 shows one example of the retrieval operation. Panel (a) is the observed SAR

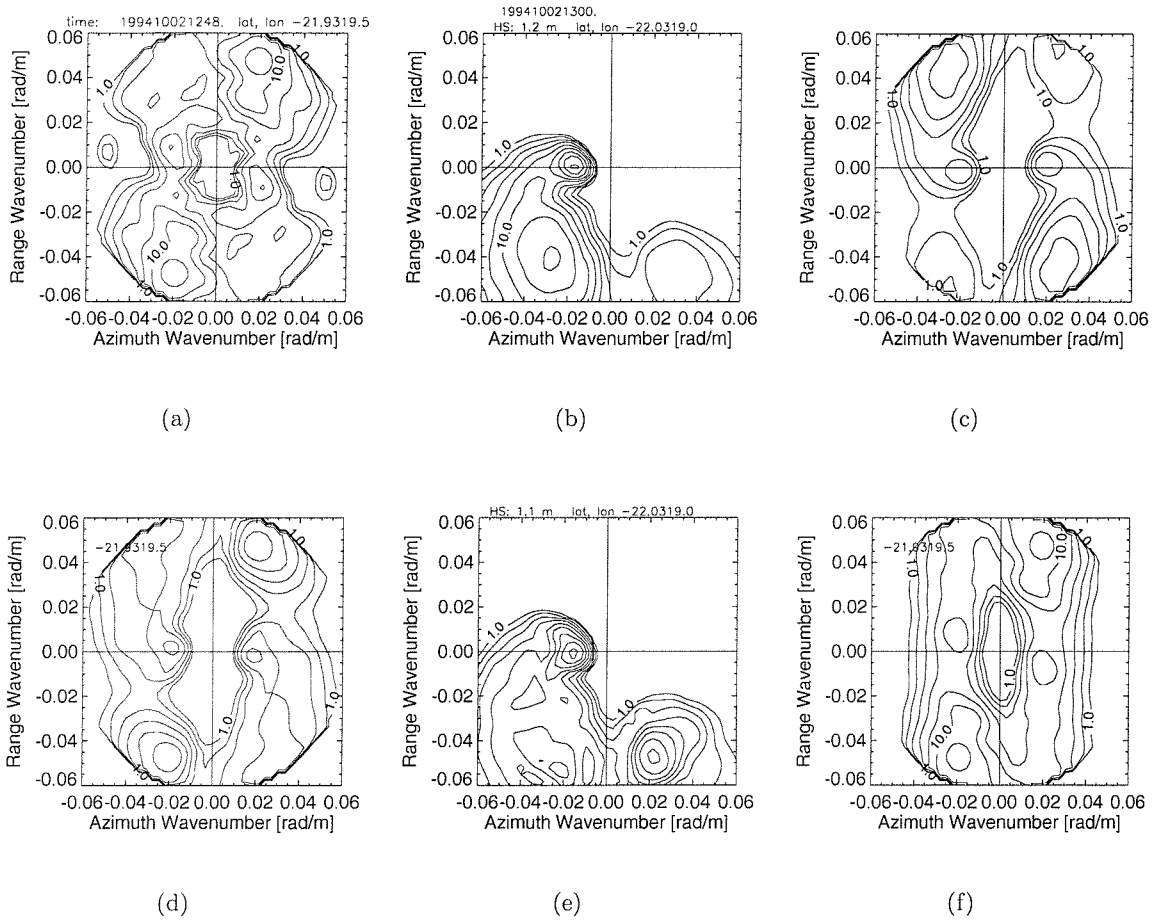

Figure 6.3: Example of the retrieval operation using the MPI scheme from 2 October 1994 1248 UT. Panel (a) is the observed SAR image, (b) is the a priori WAM wave spectrum, (c) is the first simulated SAR, (d) is the best simulated SAR of the iteration, (e) is the inverted wave spectrum of the iteration and finally (f) is the retrieved SAR spectrum. All spectra in wavenumber domain with the x axis indicating azimuth direction whereas y axis indicates range direction.

image spectrum whereas panel (b) is the a priori WAM wave spectrum which is used as first guess in the 0-th iteration. Panel (c) is the first simulated SAR spectrum using the mapping relation $P(\mathbf{k}) = \Phi(F(\mathbf{k})$ of the first guess wave spectrum (panel (b)). Panels (d) and (e) are respectively the best simulated SAR spectrum of the 0-th iteration and its inverted wave spectrum. The best inverted wave spectrum (e) is used as input spectrum for the next iteration and so on. Panel (f) is the retrieved SAR image spectrum from the iteration which yielded the smallest error between the observed spectrum and the input spectrum.

The MPI retrieval scheme is a complicated algorithm. The best way to identify its skill deficiencies and strengths is through comparisons against independent data.

6.4 Collocated Data Set

All SAR image spectra were collocated in space and time with WAM spectra at a maximum distance of 50 km (approximately half a WAM grid increment) and maximum time separation of 30 minutes (half a WAM time increment). To validate the SAR inversions we have chosen a maximum time difference of 1.5 hour and a maximum distance of 150 km between buoy and SAR measurements. We are not using the quality control parameter from the MPI scheme to reject inversion results. The buoy is located around 150 km offshore in a depth over 1000 meters. We have chosen these collocation criteria due to the relative temporal invariance and spatial homogeneity expected to be encountered in deep ocean areas.

6.5 Comparisons of Retrieved ERS-1 SAR Spectra Against Directional Buoy Data

For the present comparison of wave spectra extracted from ERS-1 SAR against directional buoy measurements and against WAM wave spectra we selected some cases in the month of October 1994. The wave climate in Campos Basin can be explained on the grounds of the meteorological conditions encountered in the region (Violante-Carvalho, 1998) (see more details about the wave climate in Campos Basin on page 14).

Figure 6.4 is an example of retrieved spectra. Figure 6.4a shows the observed SAR image spectrum with the azimuthal cut-off wavenumber around 0.045 rad/m (or around 9.5 s). Two wave systems are clearly observed, a low wavenumber swell system propagating in azimuth direction and a partially observed wind sea system propagating in range direction. Figure 6.4b is the the WAM first guess wave spectrum and the retrieved SAR spectrum (6.4c) is in good agreement with the observed SAR spectrum. A typical scenario of good weather conditions measured by the buoy is presented in 6.4d, that is a swell system propagating northward and a wind sea propagating southwestward. The swell wave systems of the WAM first guess spectrum (6.4e) and of the retrieved SAR spectrum (6.4f) differ significantly, which demonstrates that the first guess is used only to solve the directional ambiguity. The wind sea system is clearly overestimated both in 6.4e and 6.4f due to an overestimation of the wind

speed yielded by the ECMWF model compared to the wind measured by the buoy. However there is reasonably good agreement between the low frequency components measured by the buoy and retrieved using the MPI scheme, which is the part of the spectrum directly measured by SAR.

Only the wave components in the low frequency part of the spectrum are visible on SAR images whereas the high frequency information yielded by the retrieval is derived from the wave model. Therefore only the swell systems are directly measured by SAR. Another example of good agreement between swell components measured by the buoy and retrieved by the MPI scheme is illustrated in Figure 6.5. Figure 6.5d is the directional spectrum measured by the buoy with a swell component propagating northward, a wind sea component propagating towards WSW and a young swell component propagating close to the wind sea both in direction and frequency (westward and 0.116 Hz). Although the wind sea component of the WAM spectrum (6.5e) is in good agreement with its counterpart in the buoy spectrum the two spectra differ substantially in the low frequency components. The northward swell in 6.5d is barely detectable in 6.5e, whereas the direction of propagation of the young swell components differ by more than 30° probably due to a mispositioning of the South Atlantic high pressure center in the meteorological model. The retrieved spectrum (6.5f) shows clearly the northward swell component in very good agreement with the buoy observations in terms of direction of propagation, frequency and energy. The young swell component, which is located beyond the instrument cut-off and not mapped directly by SAR, still remains in disagreement with the buoy spectrum.

Figure 6.6 and 6.7 are examples of spectral intercomparisons that show a poor agreement in the high frequency band between the buoy measurement on one side and the WAM estimates and SAR retrievals on the other side. Due to the passage of a cold front over the buoy the wind direction turns quickly from eastnortheastern to southeastern in Figure 6.6. The time averaged wind input from the ECMWF model is not able to describe such fast variations properly, which reflects in a poor representation of the high frequency band estimated by the wave model and hence retrieved from the MPI scheme. Figure 6.7 presents a case of an underprediction of the wind speed from the ECMWF model and consequentely a poor representation of the retrieved wind sea system. However the low frequency swell components are fairly well described in both examples.

These examples illustrate how the retrieved spectrum may yield useful information on the low frequency spectral components, but show as well indications that the wind sea part of

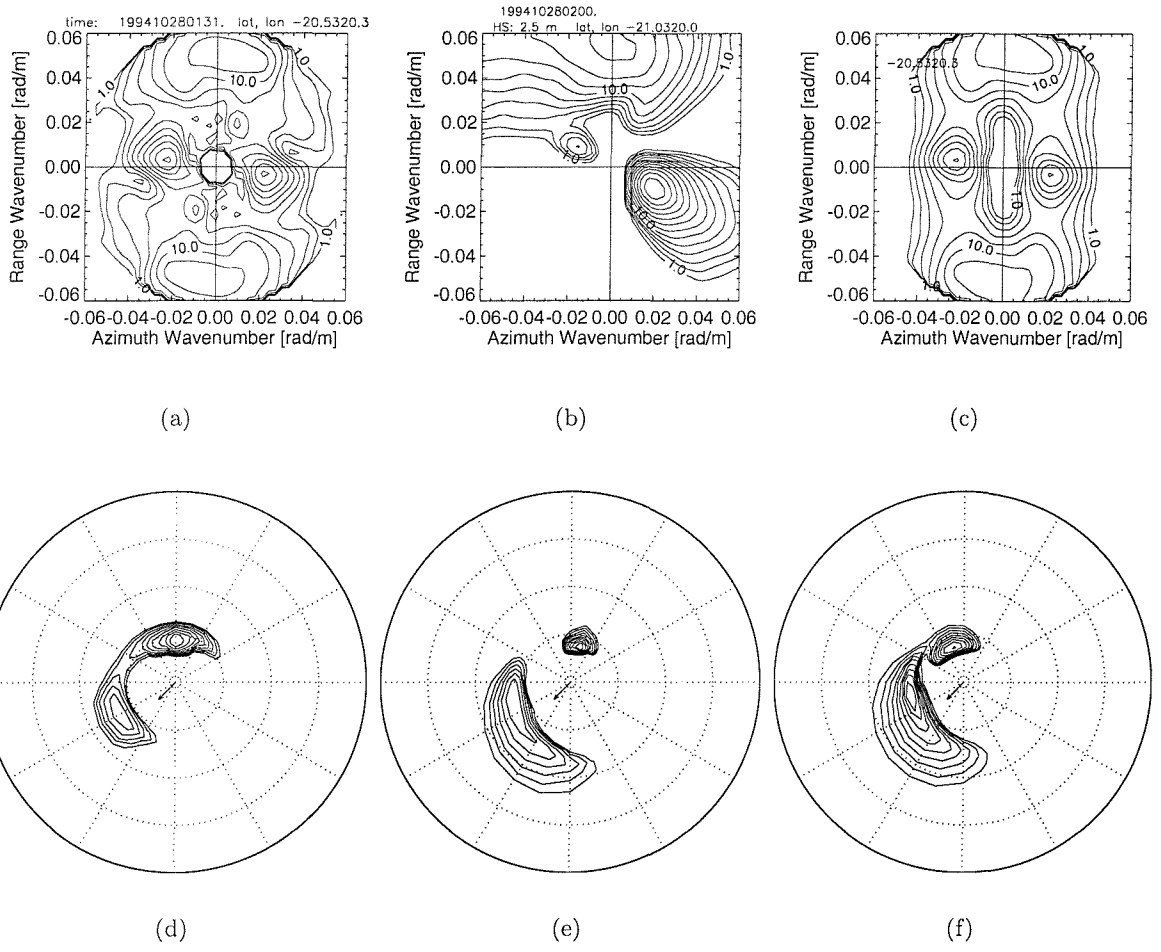

Figure 6.4: Example of the retrieval from 28 October 1994 0131 UT. Top row: panel (a) is the observed SAR image, (b) is the first guess WAM wave spectrum, (c) is the retrieved SAR spectrum. Spectra in wavenumber domain with the x axis indicating azimuth direction whereas y axis indicates range direction. Bottom row: panel (d) is the buoy directional spectrum, (e) is the WAM first guess spectrum and (f) is the retrieved SAR spectrum. Spectra in polar frequency-directional plots with the wind direction represented by the arrow in the center. Circles denote frequency at 0.1 Hz interval from 0.1 Hz (inner circle) till 0.4 Hz (outer circle). Isolines are logarithmically spaced relative to the maximum value of the spectral energy density. Wind data: measured by the buoy (speed and direction of 3.94 m/s and 220° and from the ECMWF model (speed and direction of 11.07 m/s and 202°).

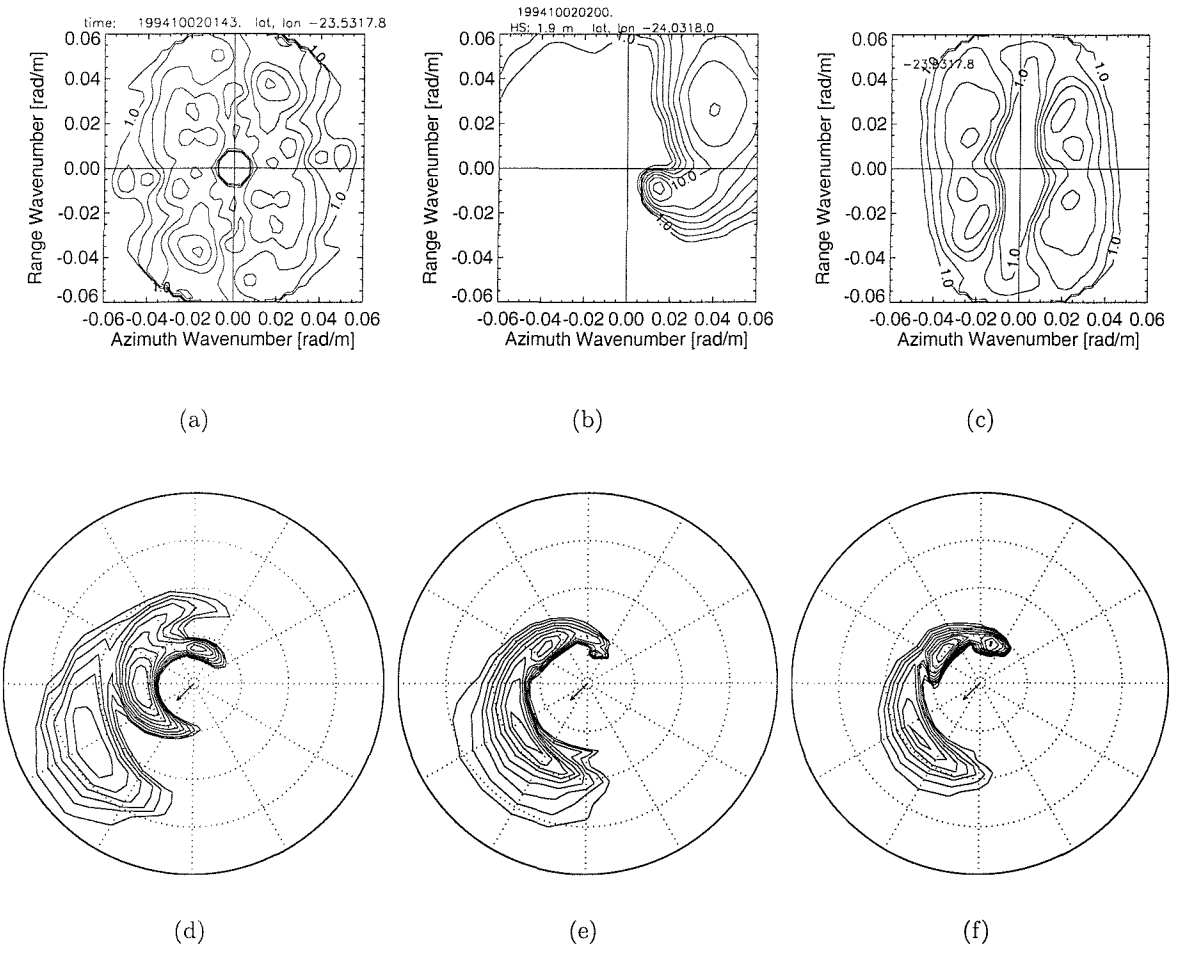

Figure 6.5: Example of the retrieval from 2 October 1994 0143 UT. Top row: panel (a) is the observed SAR image, (b) is the first guess WAM wave spectrum, (c) is the retrieved SAR spectrum. Spectra in wavenumber domain with the x axis indicating azimuth direction whereas y axis indicates range direction. Bottom row: panel (d) is the buoy directional spectrum, (e) is the WAM first guess spectrum and (f) is the retrieved SAR spectrum. Spectra in polar frequency-directional plots with the wind direction represented by the arrow in the center. Circles denote frequency at 0.1 Hz interval from 0.1 Hz (inner circle) till 0.4 Hz (outer circle). Isolines are logarithmically spaced relative to the maximum value of the spectral energy density. Wind data: measured by the buoy (speed and direction of 7.66 m/s and 226° and from the ECMWF model (speed and direction of 11.12 m/s and 223°).

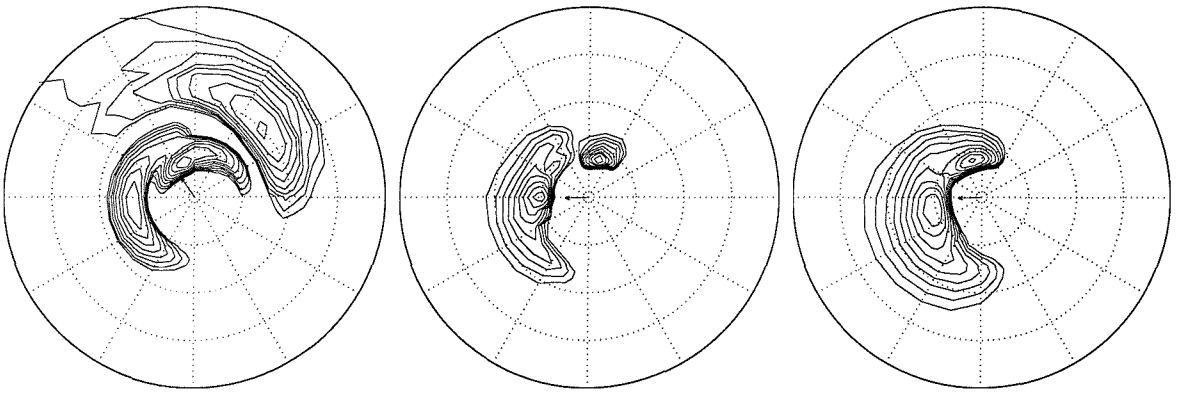

(a) (b) (c)

Figure 6.6: Example of the retrieval from 5 October 1994 0138 UT. Panel (a) is the buoy directional spectrum, (b) is the WAM first guess spectrum and (c) is the retrieved SAR spectrum. Spectra in polar frequency-directional plots with the wind direction represented by the arrow in the center. Circles denote frequency at 0.1 Hz interval from 0.1 Hz (inner circle) till 0.4 Hz (outer circle). Isolines are logarithmically spaced relative to the maximum value of the spectral energy density. Wind data: measured by the buoy (speed and direction of 4.51 m/s and 325° and from the ECMWF model (speed and direction of 2.37 m/s and 268°).

the spectrum is not very well retrieved by the MPI scheme. It is worth mentioning however that selected cases such as those previously shown are important to illustrate strengths and deficiencies of the retrieval but are not representative in a statistical sense. The MPI algorithm is quite complex and a more extensive validation with in situ data are necessary, which will be presented in the next chapter. Preliminary results show that for periods longer than 12 seconds (the part of the spectrum observed by SAR) the MPI method performs as well as (and for same frequency bands even better than) the WAM model for values of SWH, mean direction of propagation and for values of mean frequency. However, for periods shorter than 12 seconds its performance is worse, even considering the fact that the model is used as first guess to the MPI scheme.

6.6 Discussion

The MPI scheme was the first ever proposed and most widely used algorithm to retrieve directional wave spectra from SAR images. When operated in the SAR Wave Mode thousands

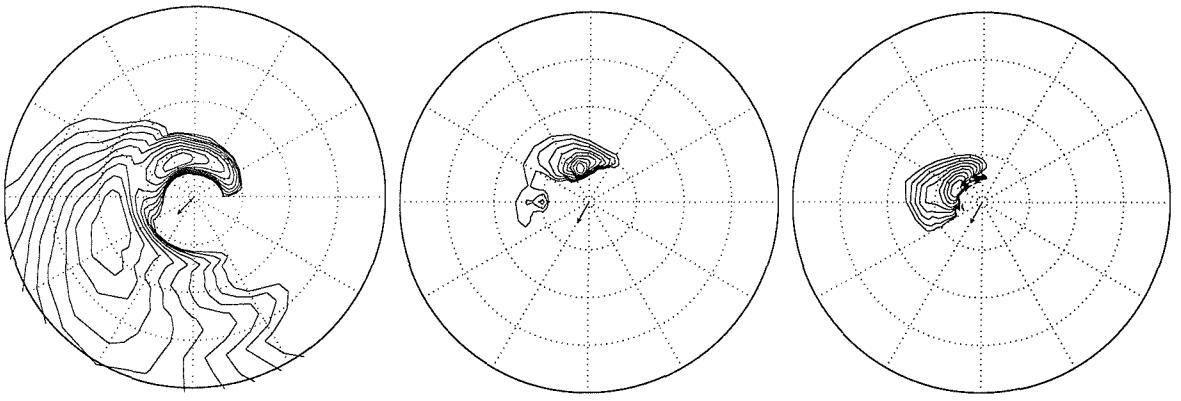

Figure 6.7: Example of the retrieval from 16 October 1994 1257 UT. Panel (a) is the buoy directional spectrum, (b) is the WAM first guess spectrum and (c) is the retrieved SAR spectrum. Spectra in polar frequency-directional plots with the wind direction represented by the arrow in the center. Circles denote frequency at 0.1 Hz interval from 0.1 Hz (inner circle) till 0.4 Hz (outer circle). Isolines are logarithmically spaced relative to the maximum value of the spectral energy density. Wind data: measured by the buoy (speed and direction of 13.29 m/s and 224° and from the ECMWF model (speed and direction of 5.70 m/s and 209°).

of imagettes are available daily in quasi-real time with global and continuous coverage. This is a unique data set far beyond the capabilities of any other operational wave measurement system, both in terms of spatial and temporal coverage. We discuss in this paper the main strengths and weakness of the retrieval scheme together with a review of the ocean wave-radar modulation transfer functions.

The retrieval of wave spectra from SAR images requires a first guess wave spectrum to solve the directional ambiguity inherent of frozen images and to extend the spectral information beyond the high wavenumber cut-off caused by nonlinearities in the imaging process. Some examples of spectra retrieved with the MPI scheme are compared against directional buoy data and against the model spectra used as first guess to the inversion. These examples highlight the strengths of the retrieval scheme, that is the performance of the retrieval is better than the performance of the model for long (swell) components both in terms of direction of propagation and in terms of mean frequency.

This is exactly the compromise that must be achieved, or in other words to stress the strength of one to compensate the deficiency of the other. Third generation wave models

such as WAM are known to describe very well the wind sea part of the spectrum, where there is no information mapped onto SAR images. On the other hand the low frequency part is comparatively less well described by wave models, partially due to a poor understanding of the dissipation processes. The low wavenumber part of the spectrum is mapped quasi-linearly onto SAR images and hence the wave components are measured directly with additional information used only to solve the direction of propagation.

SAR data are valuable information but must be considered with care because the retrieval schemes need to improve the performance of the wind sea retrieval. The three schemes proposed so far require a better representation of the high wavenumber part of the spectrum to fill in the spectral gap beyond the cut-off. However, as demonstrated in this paper, SAR does in fact yield useful information in the low frequency part of the spectrum.

Chapter 7

Assessment of ERS Synthetic Aperture Radar through Intercomparisons of One Year of Directional Buoy Measurements

One year of directional buoy measurements comprising the period from May, 1994 to April, 1995 acquired in deep ocean waters by an offshore heave-pitch-roll buoy are used for the assessment of the directional wave spectra retrieved from the Max-Planck Institut (MPI) scheme. Detailed validations of the main wave parameters, that is SWH, mean direction of propagation, mean wave length and directional spreading are performed. We demonstrate that the MPI scheme deteriorates the input first guess increasing the bias and the error of the retrieved spectra. For longer waves in the part of the spectrum observed by SAR, on the other hand, the algorithm performs better than (or at least as well as) the third generation WAM wave model. In addition to the limitations of the MPI scheme in extending the spectral information beyond the high wavenumber cut-off, the use of the quasi-linear model to map the SAR image spectrum back to the wave spectrum causes the scheme to interpret wind sea energy as swell.

7.1 Introduction

Since the advent of spaceborne Synthetic Aperture Radar (SAR) in the early nineties all weather ocean wave spectra are now available on a global basis and in quasi-real time. SAR is the only instrument so far deployed from satellites that is capable of measuring the two dimensional directional wave spectrum and hence allowing the complete characterization of a sea state. When operated in the SAR Wave Mode (SWM), the Advanced Microwave Instruments (AMI) on the European Remote Sensing satellites ERS-1 and ERS-2 acquire 10 x 5 km imagettes every 30 seconds yielding an along track resolution of 200 km and a cross track resolution of 1000–2000 km. The 1500 imagettes that are collected daily bring enormous new possibilities for the study of wind generated waves providing global data with high temporal and spatial coverage.

From the practical point of view this huge amount of spectral data has applications such as in optimization of ship routing, wave climate atlases, offshore operations and coastal management. But this kind of information is also valuable for several scientific investigations. Improving the understanding of the dynamics of surface ocean waves is important for a better knowledge of, for example, the climate dynamics (Janssen and Viterbo, 1996), the transfer of momentum from the wind (Donelan, 1990) and the exchange of gases through the air-sea interface (Csanady, 2001). The information extracted from SAR images has opened up new and exciting possibilities for wave modelers to assimilate observations of directional spectra into third generation wave models, an approach that has been hindered by the sparseness of directional wave measurements.

However to retrieve the two dimensional spectrum from SAR images is not a simple exercise. There are two main limitations in the images observed by SAR which demands great care in the process to derive the wave spectrum—as already discussed in chapter 6. In the first place there is a 180° directional ambiguity inherent in frozen images. This problem has been overcome with the launch of ENVISAT carrying the Advanced Synthetic Aperture Radar (ASAR) which uses successive images to solve the direction of propagation. In addition the SAR imaging mechanism is strongly nonlinear due to distortions induced by the orbital wave motions (the velocity bunching mechanism) causing degradation of the azimuthal (parallel to the satellite flight) resolution. The result of this distortion is that there is a loss of information beyond a cut-off wavenumber and waves with wavelengths shorter than 150–200 m propagating in the azimuthal direction are not mapped onto the SAR image directly.

Therefore to extract the wave spectrum from a SAR image spectrum requires additional information to solve the directional ambiguity and to recover the spectral information at the higher wavenumber band corresponding in general to the wind sea part of the spectrum. This problem has been tackled by three different methods for which the basic difference in their strategies lies in how they address the problem of reconstructing the directional spectrum beyond the high wavenumber azimuthal cut-off and hence filling in the spectral gap in the wind sea part of the spectrum.

The first retrieval algorithm was developed at the Max-Planck Institut (MPI) by Hasselmann and Hasselmann (1991) and an improved version was published later by Hasselmann et al. (1996). They derived a closed expression for the mapping of a wave spectrum onto a SAR image spectrum, the forward mapping relation, together with a computationally efficient technique to invert the mapping relation. This algorithm has been described in detail in chapter 6. The main idea behind the MPI scheme is to use a first guess wave spectrum, in general from a wave model, and iteratively change its inverted SAR image spectrum to match the observed SAR image spectrum. They claim that the retrieval is independent of the first-guess which is used just to solve the directional ambiguity and to augment the spectrum beyond the azimuthal cut-off.

The second retrieval scheme to be proposed is a simplified version of the MPI scheme. Krogstad et al. (1994) applied a very similar approach but they use a quasi-linear approximation of Hasselmann and Hasselamann's full nonlinear forward mapping relation. The nonlinearities in the mapping mechanism cause transfer of energy from the short wave components to the long wave components. Ignoring such nonlinearities applying a quasi-linear approximation might cause spurious swell peaks when the SAR image spectrum is mapped back into the wave spectrum (see Hasselmann et al., 1985).

The Semi-Parametric Retrieval Algorithm (SPRA), the third retrieval scheme, was proposed by Mastenbroek and de Valk (2000) who employ additionally the wind information from the scatterometer that is operating simultaneously with the SAR. In this approach there is no need for a first guess wave spectrum since they apply a parameterized wind sea spectrum and estimate its direction of propagation from the wind measurements. The drawback of this methodology is that the direction of propagation of swell is not determined and in general there is a spectral gap in the vicinity of the azimuthal cut-off, the delimitation between the part of the spectrum observed and not observed by SAR. In addition if there is a swell shorter than 150–200 m its spectral component will not be detected by the retrieval scheme. The

authors argue that their scheme is able to retrieve the wave components observed by SAR, which in the end is the information that is meant to be recovered. However the most precise possible characterization of the full two dimensional spectrum is extremely desirable for two main reasons. First of all it is much more convenient for practical purposes to handle the full spectrum rather than just its low frequency part. In second place the SAR mapping of the low frequency components is influenced by the shorter (high frequency) waves through the nonlinear transformation. Therefore a better retrieval ought to be directly linked to a better representation of the high frequency components of the spectrum.

Voorrips et al. (2001) (hereafter referred to as VMH01) compared the MPI and the SPRA schemes against several non directional buoys deployed mostly off the North American coast. In that work it became clear that both schemes have room for improvement, and that their main deficiencies lie in how to augment the spectral information beyond the azimuthal cut-off. However one of the most striking characteristics of SAR data, its directional spectral information, was not considered. The main problem for such a comparison is a lack of available directional buoy data in deep water. The few directional buoys available to VMH01 were not included in their analysis because they are moored in relatively shallow coastal waters, where one would expect a greater spatial variation of the wave parameters when compared to the more spatially homogeneous situations in the open sea.

7.2 Collocated Data Set

A data set was constructed which matches the SAR wave mode acquisitions with the corresponding data available from the wave buoy in Campos Basin, which was described in chapter 2. The collocation criteria applied to match the data from each source are those listed on page 61, that is the maximum distance between the SWM imagette and the WAM spectrum used as first guess was 50 km and a maximum time separation of 30 minutes. For the comparison between retrieved wave spectra and buoy measurements the maximum allowed distance and time difference was 150 km and 90 minutes respectively, yielding a total of 105 matched spectra evenly spaced over the one year period considered. The mean SWH (H_{S_t}) measured by the buoy is 1.88 m with ratio between the mean wave energy of components longer than 12 seconds ($H_{S_{12}}$) and mean SWH ($H_{S_{12}}/H_{S_t}$) equal to 33%, which means that on average around one third of the wave energy is at the low frequency part of the spectrum. In relation to the satellite track both paths were equally selected, with 49% of the

cases consisting of descending orbit.

7.3 Statistical Validation of ERS-1 SAR Retrievals and WAM Estimates against Buoy Measurements of Significant Wave Height, Propagation Direction and Mean Frequency

7.3.1 Methodology

In Hasselmann et al. (1996) a partitioning method based on the original idea proposed by Gerling (1992) was introduced into the MPI retrieval scheme (Hasselmann and Hasselmann, 1991) in an additional iteration loop. In this improved version of the retrieval scheme after the minimization of the cost function the two dimensional wave spectrum is divided into different wave systems. Each one of them is represented by a set of mean parameters, that is significant wave height, propagation direction and mean frequency. Wave systems from the observed SAR wave spectrum are cross assigned with wave systems from a first guess and the later ones are modified to match the mean parameters of the observed wave systems. The result is that the retrieved SAR wave spectrum is smoother in the high wavenumber cut-off, the region between the observed and non-observed part of the SAR spectrum. In addition the reduction of the number of spectral values, from 600 bins of 25 frequencies and 24 directions into a number of wave systems each one represented by some mean parameters suits very well the requirements of wave data assimilation into models. In the present work the wave systems extracted using the partitioning scheme proposed in Hasselmann et al. (1996) are used for the intercomparison.

Different wave systems of different spectra are cross assigned to each other (SAR x Buoy and WAM x Buoy) based on the following criteria:

1. The coordinates of the two partitions must be within some critical distance to each other in $\mathbf{k}$ space. A wave system of a spectrum A with wave numbers (k_x^a, k_y^a) is cross assigned with a wave system of a spectrum B with wave numbers (k_x^b, k_y^b) if their normalized squared distance in $\mathbf{k}$ space is less than some arbitrary value, thus reading

$$\frac{(k_x^a - k_x^b)^2 + (k_y^a - k_y^b)^2}{(k_x^{a\,2} + k_x^{b\,2}) + (k_y^{a\,2} + k_y^{b\,2})} \leq 0.75.$$

The arbitrary value of 0.75, the same as suggested by Hasselmann et al. (1996), suits well as a first constraint. However, by itself, this criterion is not enough to ensure a reliable match.

2. In Hasselmann et al. (1996) four different classes of wave systems are proposed based on the wave age—wind sea, old wind sea, mixed wind sea–swell and swell. In the present work different wave systems are cross assigned if they are of the same type, that is if both wave systems are pure wind sea (we are not considering old wind sea and mixed wind sea–swell) or both wave systems are swell.

3. To eliminate spurious partitions the peaks must be above an arbitrary frequency dependent energy threshold value

$$e_{min} = \frac{20 \cdot 10^{-6}}{f_p^4 + 3 \cdot 10^{-3}}$$

where f_p is the peak frequency of the wave system.

4. If more than one partition fulfills the previous conditions the closest one is chosen.

Each partition is considered to be an independent wave system generated by different meteorological events and is fully characterized by its significant wave height, mean direction of propagation and mean frequency. As described by Hasselmann et al. (1996) each wave system is defined by an inverted catchment area consisting of spectral points with ascents running into a local peak. Therefore mean parameters can be determined integrating over the spectral interval (f, θ) that the partition belongs to as:

- Significant Wave Height (SWH) is $4\sqrt{E_t}$ where E_t is the total energy of a wave system

$$E_t = \int S(f,\theta) df\, d\theta \tag{7.1}$$

- Mean direction

$$\arctan\left(\frac{\int S(f,\theta)\sin\theta df\, d\theta}{\int S(f,\theta)\cos\theta df\, d\theta}\right) \tag{7.2}$$

- Mean Frequency

$$\frac{E_t}{\int S(f,\theta) f^{-1} df\, d\theta}. \tag{7.3}$$

However the intercomparison of mean parameters based on the cross assignment of different wave systems, each one a component of the full two-dimensional spectrum $S(f,\theta)$, has two drawbacks. In the first place there is a limitation in the retrieval of the directional spectrum from buoy measurements. From spectral analysis of the three time series acquired by the buoy, that is the elevation and two orthogonal inclinations in the east and north directions, one can recover the one dimensional spectrum $S(f)$ and the first four Fourier coefficients—obtained for example from the relations presented in Long (1980). The limitation in the number of coefficients that can be determined is due to the fact that there are only three time series available. The expansion of the spreading function $D(f,\theta)$ as a Fourier series as proposed by Longuet-Higgins et al. (1963) is truncated after the second harmonic causing negative lobes, which is not suitable since $D(f,\theta)$ is always positive definite. Other different approaches have been proposed for the representation of the spreading function—and therefore for the reconstruction of the directional spectrum—which can be divided in two main groups, parametric and nonparametric methods. In parametric methods such as the ones proposed by Longuet-Higgins et al. (1963) and Donelan et al. (1985), $D(f,\theta)$ has a prescribed form and a controlling parameter which depends on the peak frequency. However, these methods are not consistent when wind sea and swell co-exist in the same frequency band since they tend to fit a single peak in between both wave directions (Young, 1994). In contrast to parametric methods, nonparametric methods such as the Maximum Entropy (Lygre and Krogstad, 1986) do not impose any analytical form for the representation of $D(f,\theta)$. In these methods a particular solution from the feasible set of all solutions consistent with the data is selected by minimizing a cost function. But again due to the limitation in the number of Fourier components yielded by a heave-pitch-roll buoy the directional distribution is underdetermined implying that the directional spectrum retrieved from buoys have a degree of uncertainty.

In addition to the limitation of single point measurements such as wave buoys to reconstruct the directional spectrum, the use of mean parameters for the intercomparison based only on the cross assignment of wave systems has a second drawback. One of the main difficulties in the cross assignment is the association of a wave system in one spectrum with its counterpart in another spectrum, for example to intercompare the two-dimensional spectrum retrieved from the buoy against the two-dimensional wave spectrum from the model or from SAR. Quite often the SAR wave spectra contain more partitions than the WAM spectra and than the buoy spectra, possibly due to noise or to limitations in the retrieval scheme (Hassel-

mann et al., 1996). Although the criteria listed above seem to be rigorous enough to guarantee the right selection, the cross assignment procedure may select nonassociated wave systems. Therefore we also apply a second approach where rather than the two-dimensional spectrum the one-dimensional spectrum is used for the intercomparison. From the first Fourier components that are directly measured by the buoy one can reliably retrieve the one-dimensional energy density spectrum $S(f)$ and some other mean parameters. The main advantage of such an approach is that no sort of directional distribution is imposed and the mean parameters, including direction of propagation and directional spread, are determined directly by the first Fourier coefficients. Moreover in the second approach the intercomparison is performed using specific frequency bands rather than individual wave systems which will assure that only related information will be intercompared.

In the second approach used in our study the two-dimensional directional spectra (retrieved from SAR and computed by the WAM) are integrated to provide the frequency spectrum $S(f)$ in addition to the directional distribution and then the first Fourier coefficients $a_1(f)$ and $b_1(f)$ are obtained (see similar approaches in, for instance, Voorrips et al., 1997; Wyatt et al., 1999). Comparisons are made of parameters over specific frequency bands—4s to 6s, 6s to 8s and so on till 16s to 18s. The mean parameters over specific frequency bands are calculated as follows (using the method presented in Kuik et al., 1988):

- SWH is $4\sqrt{e_t}$ where e_t is the total energy over the frequency band from f_{min} till f_{max}

$$e_t = \int_{f_{min}}^{f_{max}} S(f)df \tag{7.4}$$

- Mean direction

$$\arctan\left(\frac{b_1(f)}{a_1(f)}\right) \tag{7.5}$$

- Mean Frequency

$$\frac{e_t}{\int_{f_{min}}^{f_{max}} S(f)f^{-1}df}. \tag{7.6}$$

Naturally f_{max} and f_{min} delimit the frequency band interval and the Fourier coefficients $a_1(f)$ and $b_1(f)$ are also calculated over the same interval.

Although the intercomparison of the one-dimensional spectra over specific frequency bands seems to be more rigorous than the cross assignment of partitioned wave systems, both approaches will be presented and discussed in the following. The use of wave systems

from the partitioning scheme have been used so far in some assimilation exercises (Hasselmann et al., 1997; Dunlap et al., 1998) and in another intercomparison study (Heimbach et al., 1998). For assimilation purposes the use of individual partitions seems to be the most operationally feasible solution. However, as commented earlier, the cross assignment of wave systems is subject to a degree of uncertainty that, at best, needs to be investigated. There is a trade off between being sufficiently rigorous to ensure the correct selection and the need to avoid imposing excessive constraints and therefore unreasonably reducing the number of matches.

7.3.2 Significant Wave Height

In order to validate the performance of the MPI retrieval scheme and the WAM model against buoy measurements we calculate the energy of all wave components integrating over the whole frequency domain, as in

$$H_{S_t} = 4\left\{\int S(f)df\right\}^{1/2}. \tag{7.7}$$

The scatter plots of significant wave height of SAR and WAM against buoy measurements are shown in Figure 7.1. The performance of the wave model is superior than the SAR, in terms of bias, standard deviation and normalized RMS error. Although the MPI scheme uses the WAM spectra as first guess to the inversion the results of SWH retrieved from SAR are worse. The scatter in the WAM is about 25% lower than the scatter in the SAR retrievals with the MPI scheme adding its own error. The same was observed in VMH01 but in that work the correlation between both WAM-Buoy and SAR-Buoy was higher, probably because they have selected a narrower collocation window (maximum time and distance of 30 min and 80 km between SAR and buoy measurements) and due to the fact that altimeter data have been assimilated into the ECMWF WAM model used in their comparison. However the values of normalized RMS error that we find are very similar to the ones obtained by VMH01. In our results the mean value of SWH retrieved by the MPI scheme is 9.6% higher than the mean value of SWH computed by the WAM, which is in accordance with the results reported by Dunlap et al. (1998).

In the imaging of wind waves by SAR the vertical movement of the sea surface caused by the orbital motions of the waves results in an azimuthal displacement due to the Doppler effect of a moving target. As a consequence there is a loss of information in the azimuth direction beyond a high wavenumber cut-off. This cut-off wavenumber is sea state dependent

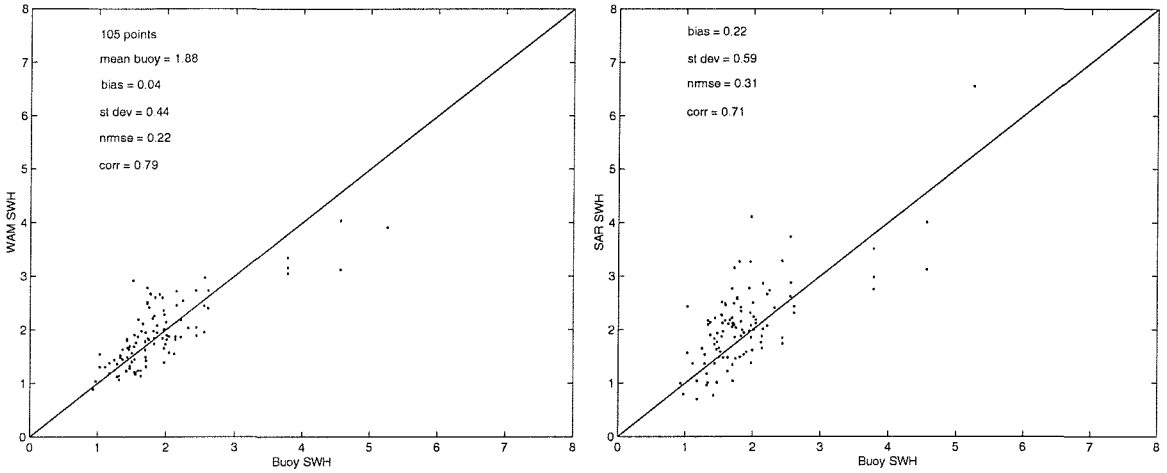

Figure 7.1: Scatter plots of Significant Wave Height (SWH) calculated using (7.7) and their statistics, respectively bias, standard deviation (st dev), RMS error normalized with the RMS buoy wave height (nrmse) and correlation (corr). On the left plot SWH computed by the WAM model against buoy measurements and on the right plot SWH retrieved from SAR against buoy measurements. The line of slope unity is also shown.

but in general waves shorter than 150/200 m propagating parallel to the satellite track are not mapped directly by SAR. In the MPI scheme in general a wave model is used as a first guess to augment the spectral information beyond the cut-off and to resolve the directional ambiguity inherent in frozen images. Therefore to investigate the performance of the MPI scheme in the low wavenumber band where waves are mapped directly onto the SAR image we calculate the energy of the wave components longer than 225 m (or periods longer than 12 s in deep water):

$$H_{S_{12}} = 4\left\{\int_{f_1}^{f_2} S(f)df\right\}^{1/2} \tag{7.8}$$

where $f_1 = 0$ and $f_2 = 1/12$ Hz.

The scatter plots of the low wavenumber wave heights using (7.8) are shown in Figure 7.2. In contrast to the results presented in Figure 7.1 the performance of the MPI retrieval scheme is as good as the WAM model for values of significant wave height in the low frequency band of the spectrum. Apart from the fact that the WAM results are virtually bias free, the MPI retrievals have a standard deviation and a normalized RMS error of the same order as the WAM. These results are in contrast with those presented in VMH01, where the WAM results compare slightly better with buoy measurements than the MPI retrievals, even considering

only the low frequency part of the spectrum.

There are two main differences between our comparisons and the ones presented by VMH01, the collocation criteria and the wave model used as first guess to the inversion. In VMH01 a narrower collocation window, both in time and space was imposed which to some extent would explain their greater correlation when considering the energy of the spectrum over the whole frequency interval using (7.7). In VMH01 most of the buoys are located in relatively shallow waters where one would expect a greater variability of the wave parameters when compared to the more spatially homogeneous situations encountered by the deep water buoy in Campos Basin. However, when considering the frequency band directly mapped onto SAR images (7.8), our results are very similar to the ones presented in VMH01 which indicates that our coarser collocation criteria is not the cause for the discrepancy.

The second main difference between the present study and VMH01 is that although both works are using the spectra calculated by the WAM model as first guess to the inversion, in their work altimeter data have been assimilated into the ECMWF WAM version. In this paper no sort of modification was imposed to the model output and the spectra computed by the WAM are the direct result of the physics behind the model. If assimilation of altimeter data is in fact the reason for the somewhat better performance of the WAM results than the MPI retrievals in the low frequency part of the spectrum as presented in VMH01 then this fact raises an interesting point. The main conclusion in the work by VMH01 is that the MPI retrieval scheme deteriorates the quality of the first guess used to the inversion. This seems to be corroborated by our results shown in Figure 7.1, at least when the high wavenumber band where the model is used to augment the spectral information beyond the cut-off is considered in the calculation of SWH. However looking at Figure 7.2 in the low wavenumber part of the spectrum the MPI retrievals match the buoy measurements as well as the WAM results. Thus, in opposition to the conclusions presented by VMH01, we have found that the low wavenumber SWH retrieved from the MPI scheme does not make the low wavenumber SWH estimated by the model and used as first guess any worse.

One of the main characteristics of the MPI retrieval scheme as has already been pointed out is a partitioning method to isolate and to cross assign different wave systems from the inverted SAR wave spectrum and the WAM first guess spectrum. As a result at the end of the retrieval not only the directional SAR wave spectrum has been recovered but each wave system is defined by a number of mean parameters as well. The reduction of the number of degrees of freedom of the wave spectrum is a very desirable feature that has been exploited in

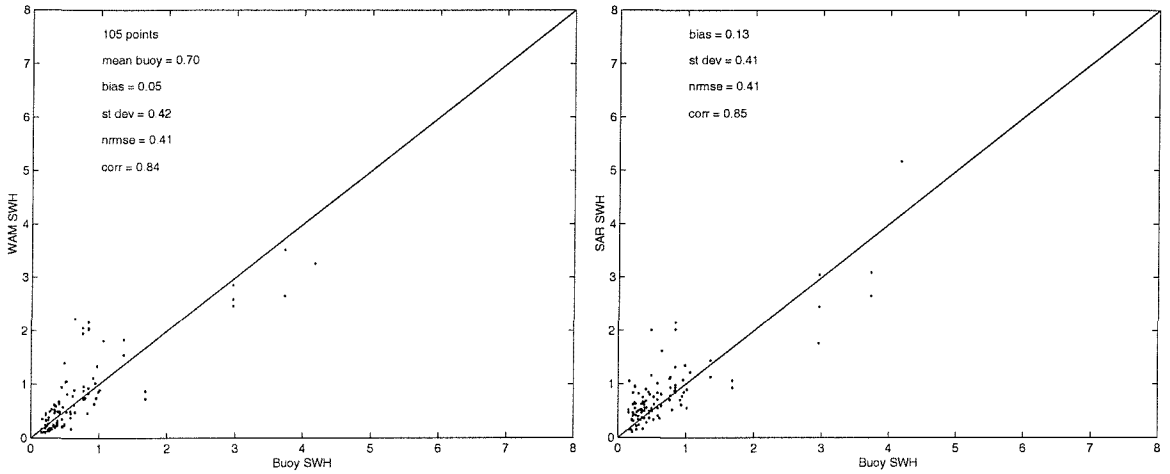

Figure 7.2: Same as Figure 7.1 but for values of $H_{S_{12}}$ (7.8).

data assimilation studies. Figure 7.3 shows the scatter plots of SWH of the cross assignment of partitions using (7.1). The reason why the number of partitions that were cross assigned differ among plots (and are different from the number of spectra in Figures 7.1 and 7.2) is that more than one partition per spectrum might be selected. The statistics shown in Figure 7.3 are similar to those in Figure 7.1 which is an indication that the criteria for the cross assignment listed at the beginning of this section are rigorous enough to ensure that only related partitions will be selected.

The statistics of the wave systems whose mean wave length are greater than 225 m would give us insights about the performance of the retrieval of long waves. However the low number of points that resulted from applying this constraint, 29 and 26 respectively for SAR and WAM, yielded high correlation coefficients for SWH (ranging from 81% to 90%) but very low correlations for mean frequency and mean direction of propagation (values ranging for both frequency and direction from 42% to 53%). As the number of points is low any sort of conclusion should be considered with caution and the results presented in Figures 7.4, 7.6 and 7.9 are more statiscaly meaningful, as all the points are employed in these calculations.

To analyze the SWH retrieved from SAR and estimated by the model in more spectral detail we calculate the energy of the wave components over specific frequency bands using (7.4) (Figure 7.4). The WAM estimates are virtually bias free whereas the MPI retrievals show a positive bias over the whole spectral range. It is worth mentioning however that for periods smaller than approximately 12 s the information retrieved from the MPI scheme is yielded

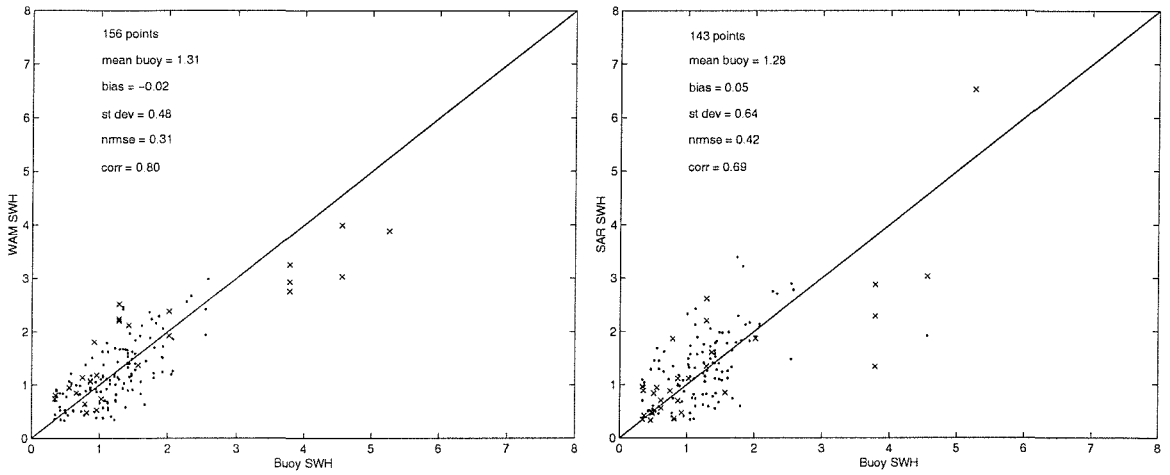

Figure 7.3: Scatter plots of SWH for every partition calculated using (7.1) and their statistics as in Figure 7.1 with the line of slope unity drawn passing through the origin. On the left plot SWH computed by the WAM model against buoy measurements and on the right plot SWH retrieved from SAR against buoy measurements. The crosses are the partitions whose mean wavelength are greater than 225 m—periods greater than 12 s.

from the WAM model and therefore the retrieval is adding its own error increasing the bias. But in the part of the spectrum directly observed by SAR (periods greater than 12s) the bias of the MPI scheme slowly decreases with wave period and for very long waves (periods longer than 16 s) it performs better than the model with a smaller bias. The standard deviation and the normalized RMS error of both MPI retrievals and model estimates show a trend to increase with period with the MPI scheme presenting greater errors for waves with periods smaller than 12 s. Likewise the error of the MPI scheme in the low wavenumber part of the spectrum is of the same order as (and for longer wavelengths even smaller than) the WAM results.

7.3.3 Propagation Direction

The waves measured by the buoy have basically two main characteristic features: relatively short waves with a westward component and a northward long swell generated far away from Campos Basin (see page 14 for more details about the wave climate in Campos Basin). Since the ERS-1 satellite had a polar orbit the long northward swell is propagating in the azimuth direction and the shorter westward waves in the range direction. In Figure 7.5 we present a comparison of the histograms of the direction of propagation of the wave systems calculated

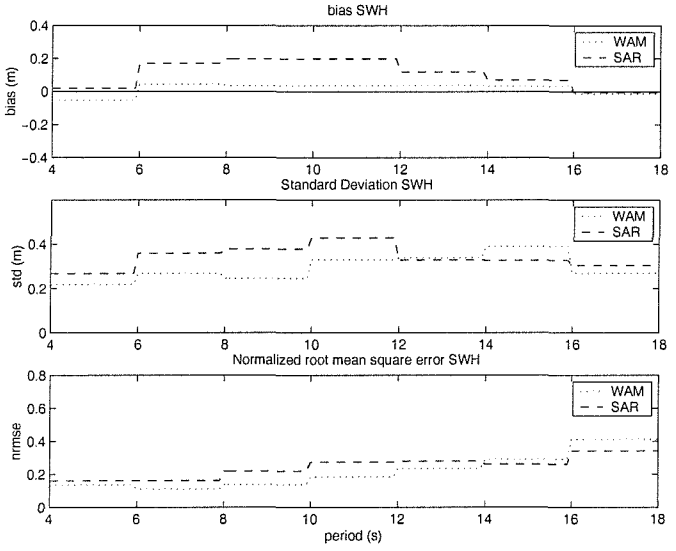

Figure 7.4: Statistics of SWH compared with buoy measurements over frequency bands using (7.4).

Table 7.1: Statistics of the comparisons against buoy measurements of the direction of propagation of the wave systems calculated using (7.2)—bias and standard deviation in degrees.

	points	bias	st dev	nrmse	corr
WAM	156	0.93	33.50	0.37	0.88
SAR	143	4.84	53.10	0.60	0.72

using (7.2) with the statistics of the point by point comparisons presented in table 7.1. The overall statistics of the WAM-Buoy comparison appears to be better than the SAR-Buoy with smaller errors and a greater correlation. However the agreement of the SAR-Buoy comparison is much better in the northward and northwestward direction of propagation, that is the results of the MPI retrievals compare better with the buoy data for long swell.

In Figure 7.6 we calculate the propagation direction using (7.5). The WAM results present a very small bias for waves with periods shorter than 10 s but for longer waves the bias has a trend to increase with wave period. In the part of the spectrum observed by SAR (waves with periods longer than 12 s) the MPI retrievals have a slightly smaller bias than WAM. Both WAM estimates and the MPI retrievals have a directional resolution of 15° which is of the same order as the maximum bias found. The standard deviation and the normalized RMS error of both WAM and MPI increase with wave period.

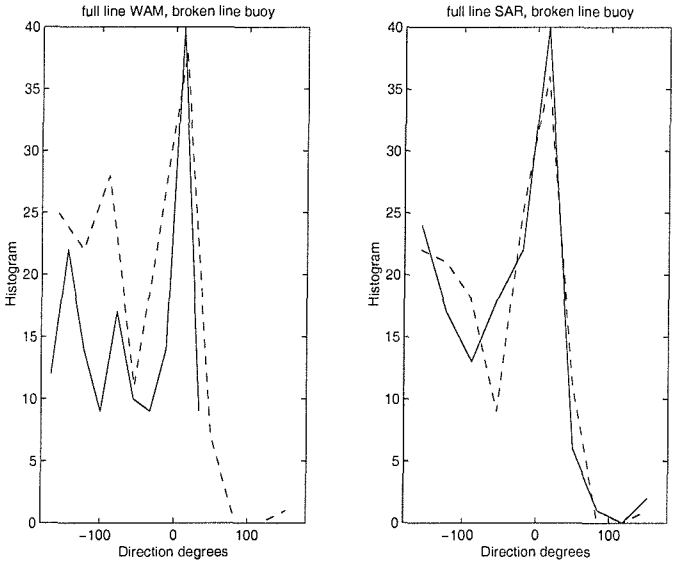

Figure 7.5: Histograms of the mean direction of propagation (direction waves go to) of the WAM estimates and buoy measurements (on the left) and the MPI retrievals and buoy measurements (on the right). Buoy measurements are represented by the broken lines whereas the MPI and WAM by the full lines.

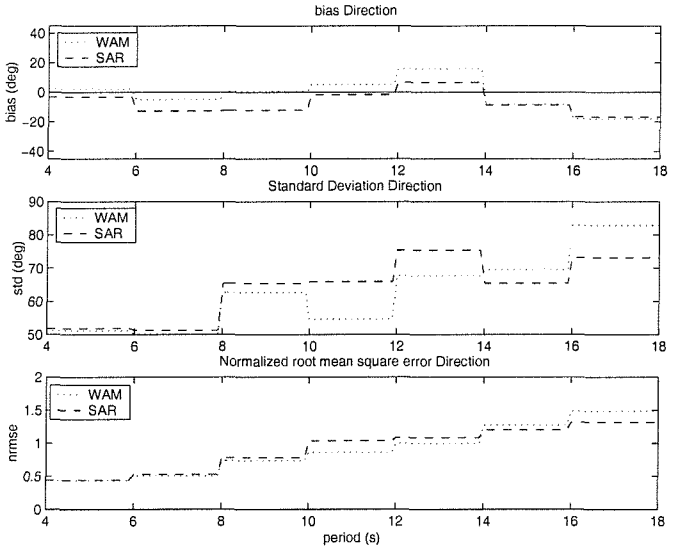

Figure 7.6: Values of direction of propagation over frequency bands using (7.5).

In Figure 7.7 we show the scatter plots of propagation direction for the low wavenumber

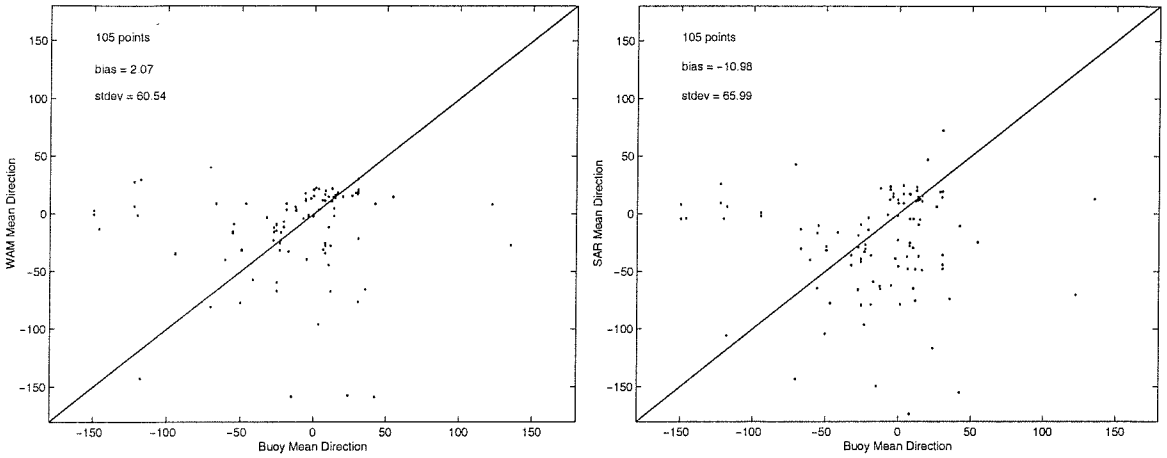

Figure 7.7: Scatter plots of mean propagation direction for the low wavenumber components (longer than 225 m or periods greater than 12 s) and their statistics using (7.9). On the left plot propagation direction computed by the WAM model against buoy measurements and on the right plot propagation direction retrieved from SAR against buoy measurements. The line of slope unity is also shown.

components using

$$\arctan\left(\frac{\int_{f_1}^{f_2} S(f,\theta)\sin\theta df d\theta}{\int_{f_1}^{f_2} S(f,\theta)\cos\theta df d\theta}\right) \tag{7.9}$$

where $f_1 = 0$ and $f_2 = 1/12$ Hz. Although the correlation coefficients of both plots is quite low (less than 15%) they show some interesting aspects of the data analyzed. They show a cluster of points near the northward direction which is typical of swell generated further south from Campos Basin, whereas the values of standard deviation and bias are in agreement with Figure 7.6. The point by point comparisons show a very poor agreement among plots, both for SARxBuoy and WAMxBuoy comparisons, implying that the performance of mean directions of WAM and SAR for long waves are not particularly good.

7.3.4 Mean Frequency

We present in Figure 7.8 histograms of mean frequency of retrieved SAR and WAM estimates against buoy measurements with the statistics presented in table 7.2. Similar to the results of propagation direction the overall statistics of the wave model is superior to the SAR results although once again the plots should be examined with care in terms of spectral detail. The comparison of WAM results against buoy data shows two distinct patterns, the high frequency

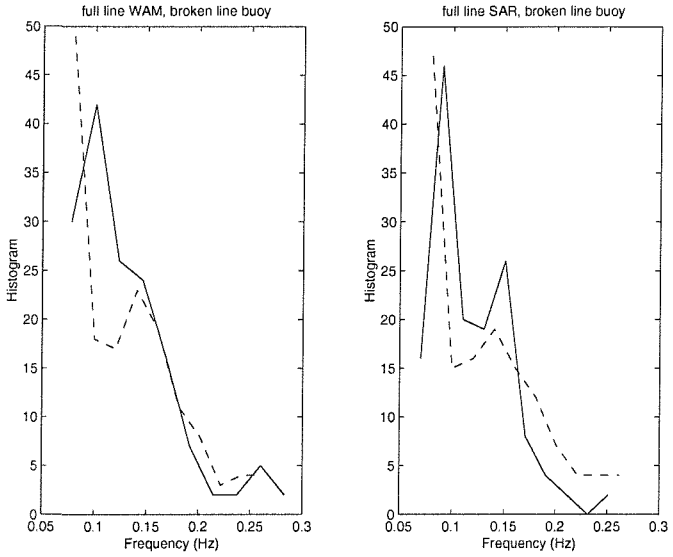

Figure 7.8: Histograms of the mean frequency of the WAM estimates and buoy measurements (on the left) and the MPI retrievals and buoy measurements (on the right). Buoy measurements are represented by the broken lines whereas the MPI and WAM by the full lines. Mean frequency is calculated using (7.3).

Table 7.2: Statistics of the comparisons against buoy measurements of the mean frequencies of the wave systems calculated using (7.3)—bias and standard deviation in Hertz.

	points	bias	st dev	nrmse	corr
WAM	156	-0.0017	0.0299	0.21	0.82
SAR	143	-0.0131	0.0354	0.27	0.73

band with a much better agreement than the low frequency part of the spectrum. This is in contrast with the SAR-Buoy comparison where the MPI retrievals compare better with buoy measurements than the model results for longer waves.

Figure 7.9 shows that both the MPI scheme and the WAM model tend to underestimate the mean frequency of short waves. Both WAM and SAR show a negative bias in frequency for periods shorter than 12 s with a trend to decrease with wave period whereas for longer waves the bias show the opposite trend. Standard deviation and normalized RMS for both WAM and SAR decrease with wave period with the standard deviation in the band of periods from 4 to 8 s being 5 times larger than for periods greater than 16 s. Both in terms of bias and error the MPI retrievals perform better than WAM estimates for waves with periods longer than 12 s.

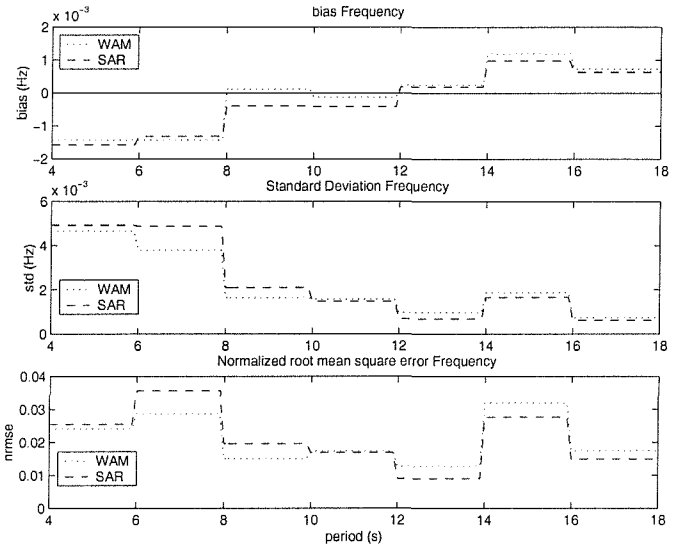

Figure 7.9: Values of the mean frequency over frequency bands using (7.6).

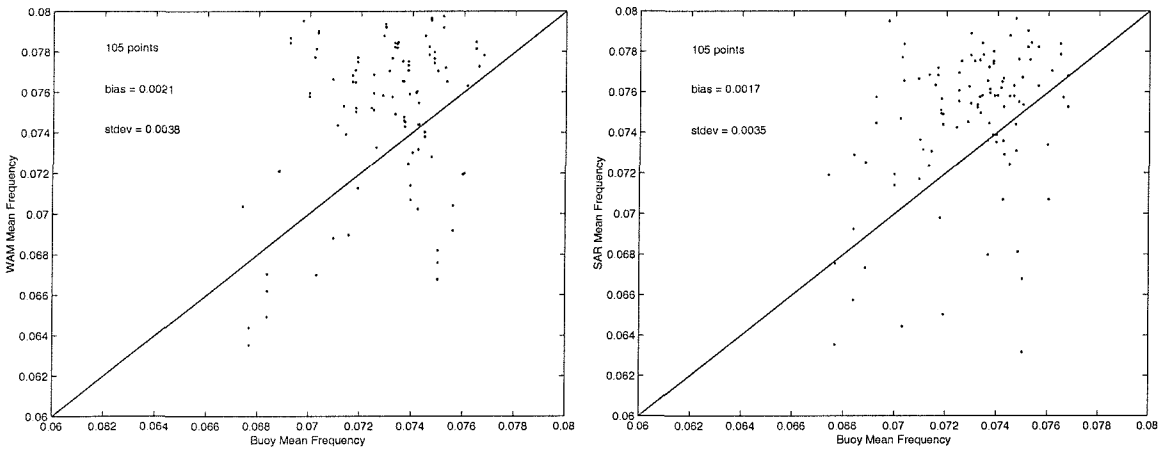

Figure 7.10: Scatter plots of mean frequency for low wavenumber components (longer than 225 m or periods greater than 12 s) and their statistics using (7.10). On the left plot mean frequency computed by the WAM model against buoy measurements and on the right plot mean frequency retrieved from SAR against buoy measurements. The line of slope unity is also shown.

Figure 7.10 shows the scatter plots of mean frequency for low wavenumber components using

$$\frac{E_t}{\int_{f_1}^{f_2} S(f,\theta) f^{-1} df d\theta} \tag{7.10}$$

where $f_1 = 0$ and $f_2 = 1/12$ Hz. They show that most of the long wave energy is in the 12-14 second band (frequency from 0.071 Hz to 0.083 Hz) which needs to be taken into consideration in the analysis of Figures 7.6 and 7.9. Therefore the results in the longer wave period bands are not particularly relevant due to the fewer points in longer 2 second bands. Both plots in Figure 7.10 present low correlation cofficients (lower than 15%) and the 12-14 second band seems to express a reasonable picture of the performance of WAM and SAR for long waves. Figures 7.7 and 7.10 show that mean frequency and mean directions are not particularly good in either case.

7.4 Underestimation of the Mean Frequency of Short Waves by the WAM Model

The larger errors encountered in the band of short wave components in Figure 7.9 could be explained by a wrong wind input used by the WAM where the negative bias would be related to an overestimation of modeled wind speeds. Figure 7.11 is a point by point comparison of the wind speeds measured by the buoy and the wind speeds calculated by the ECMWF atmospheric model. The bias of the model wind speed is low, about 6% of the mean value measured by the buoy, and its negative value represents an underestimation of the modeled wind speed. Consequently it seems that the wind input is not the cause for the poorer agreement in the high frequency band.

The underestimation of the mean frequencies calculated by the WAM could be related to the spectral discretization employed. One of the main features of second generation wave models is that to ensure a stable spectral evolution some sort of parameterization is imposed, in general with some prescribed spectral form being applied to the wind sea (SWAMP Group, 1985). A third generation wave model such as WAM, on the other hand, computes the wave spectrum integrating the energy balance equation without any restriction on the spectral shape (Komen et al., 1994; Young, 1999). The fundamental role of the nonlinear interactions in the growth of wind waves became clear during the JONSWAP experiment (Hasselmann et al., 1973). In the initial growth phases of fetch or duration limited wind seas a peak normally starts to develop at high frequencies just after the wind begins to blow. The nonlinear interactions cause a migration of energy from higher frequencies to frequencies near the spectral peak. The nonlinear interactions are also responsible for a spectral shape stabilization forcing the high frequency portion of the spectrum to decay in a manner inversely propor-

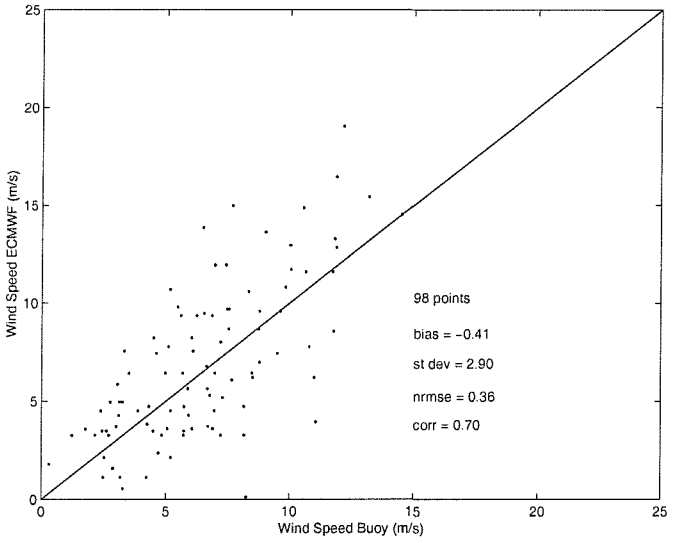

Figure 7.11: Statistics and scatter plot of the wind speed measured by the buoy and estimated by the ECMWF model (in m/s for a reference height of 10 m). The mean wind speed measured by the buoy is 6.5 m/s.

tional to frequency (Young and van Vledder, 1993). The result is that as the wind continues to blow the spectrum broadens and the peak shifts to lower frequencies with increasing fetch up to the point where it attains full development.

Hence the proper estimation of the wave spectrum by a third generation model in the initial phases of growth is closely connected to the frequency discretization used in high frequency. Beyond the maximum high frequency used in the model the wind sea growth cannot be simulated properly since the transfer of energy from higher frequencies through nonlinear interactions will be neglected. Around the cut-off frequency the wind sea peak starts to grow slowly only because of the direct input of energy by the wind and only after it attains a higher spectral level the nonlinear interactions then begin to act and the peak gradually migrates to lower frequencies. Thus the choice of the highest discrete frequency is fundamental for the modeling of the wind wave development since it will impose the initial position of the peak in frequency space and in addition will be responsible for a time gap necessary for the nonlinear interactions to become effective.

The spectral discretization used in the present version of the WAM cycle 4 is 24 directions and 25 logarithmicaly spaced frequencies from 0.042 Hz to 0.41 Hz (WAMDI Group, 1988). Tolman (1992) has investigated numerical errors in third generation wave models and their influence on the initial stages of growth. Considering scaling laws, that work discusses the

effect of the frequency range for different wind speeds. He concludes that the frequency discretization used in the WAM results in good scaling behavior for wind speeds spanning from 15 to 25 m/s whereas for lower winds the mean wave energy is overestimated and the mean frequency is underestimated (see Figure 2 in Tolman, 1992). This optimal wind speed range is high, specially considering tropical regions where lower wind speeds are much more common. Using 10 years of wind measurements acquired on an oil platform in Campos Basin, Violante-Carvalho et al. (1997) describe typical meteorological situations encountered in the study area, where 97% of the wind speeds observed during this period are below 15 m/s and 74% are below 9 m/s. Thus clearly the mean wind speeds in Campos Basin are lower than the optimal range for what the model frequency discretization best applies.

The underestimation of the mean frequency by the WAM in the early stages of wave growth as observed in Figure 7.9 could be related to the diagnostic tail added beyond a high frequency cut-off. The wave spectrum estimated by the model comprehends a prognostic part which extends up to 2.5 times the mean frequency (or maximally up to 0.41 Hz) and beyond this point a diagnostic part represented by an f^{-4} tail. Therefore beyond 0.41 Hz the model cannot simulate properly the initial growth of the wind sea with the modeled waves developing near the cut-off only due to the wind input rather than by nonlinear transfer of energy from higher frequencies. Since the nonlinear transfer is only triggered after a certain level this results in a delay in the development of the wind sea peak which is in addition located at lower frequencies.

Tolman (1992) also shows the effect of the extension of the high frequency cut-off to a much higher value of 0.97 Hz (his Figure 4) and as a result the reduction of the discrepancies with wave energies and mean frequencies closer to nondimensional growth curves. This underestimation of the mean frequency of the wind sea in early stages of development is more easily detectable through detailed spectral comparisons like the one presented in Figure 7.9. When the mean frequency is calculated over the whole spectral domain or comparisons are performed on a global scale—as most of the validation tests of the WAM have been so far—this limitation of the model in the initial generation phases are less likely to be found.

7.5 Comparisons of Directional Wave Spectra

7.5.1 The Directional Spreading Retrieved from the MPI Scheme

The overall performance of the MPI retrievals is best measured by quantitative results such as those obtained above, although direct comparisons of the directional spectra are interesting to enable a clearer understanding of the differences through qualitative validations. We are, however, comparing spectra obtained in rather different ways. Remote sensing instruments like ERS-1 SAR measure the wavenumber spectrum whereas the wave model WAM estimates the frequency spectrum. The buoy, on the other hand, yielded the frequency spectrum $S(f)$ from the heave series and the first Fourier coefficients with the directional distribution being reconstructed using the Maximum Entropy Method (Lygre and Krogstad, 1986). One way to assess the differences among spectra is to determine the Fourier coefficients by integrating the directional spectra and to compare them with the coefficients measured directly by the buoy.

In the MPI scheme the WAM first guess wave systems are rotated and scaled in order to adjust to the wave systems of the inverted SAR wave spectrum. However their spectral forms are not allowed to vary which means that the spectral widths of the wave systems retrieved from the MPI scheme are the same as those from the first guess wave model. The importance of the nonlinear term S_{nl} in determining the directional spreading has been pointed out by Donelan et al. (1985) and later confirmed by numerical simulations in Banner and Young (1994) and evidence from measurements (Young et al., 1995). In third generation wave models the directional spreading is computed from the integration of the source terms where S_{nl} forces the spectrum to a typical shape with a relatively narrow spread around the peak that slowly broadens at higher and lower frequencies (Young and van Vledder, 1993). The directional distribution predicted by the model used by Banner and Young (1994), however, employed the full solution of the nonlinear source term called Exact-NL. In the WAM model the complex wave-wave nonlinear interactions S_{nl} is approximated by a non-exact solution called the DIA (Discrete Interaction Approximation) for computational efficiency. Although the SWH computed from the WAM model has been exhaustively tested against measurements the impact of the DIA on the spreading has not yet been quantitatively demonstrated.

In order to assess the performance of the MPI scheme in estimating the directional spreading we present in Figure 7.12 a swell component propagating in the azimuth direction with its frequency spectrum and directional spreading shown in Figure 7.13. The spreading is

calculated using the expression proposed by Kuik et al. (1988) that reads

$$\sigma(f) = \left(2\left(1 - \sqrt{a_1^2(f) + b_1^2(f)}\right)\right)^{\frac{1}{2}} \tag{7.11}$$

where $a_1(f)$ and $b_1(f)$ are the first Fourier coefficients. The overall agreement of the directional spectra is good (Figure 7.12d, Figure 7.12e and Figure 7.13a) with the model overestimating the wind sea component in range direction. In Figure 7.13b the input wave spectrum from the WAM slightly underestimates the value of SWH measured by the buoy with a somewhat broader angular distribution. As shown in VMH01 since the MPI scheme is not allowed to narrow the spectrum width it has no choice rather than increasing the energy level.

The values of $\sigma(f)$ are presented in Figure 7.13c, where the directional spectra of the SAR retrievals and WAM estimates are integrated to provide the Fourier coefficients. The values of $\sigma(f)$ computed from the coefficients directly measured by the heave-pitch-roll buoy (Buoy Coef in Figure 7.13c) are also shown, with the typical shape of a narrow distribution around the peak that broadens at both higher and lower frequencies. The directional spreading computed by the model and retrieved from SAR present much the same value of directional spread at the peak of the spectrum, which is narrower than the one calculated from the Fourier coefficients measured by the buoy.

Another case of a very long and energetic swell component generated far away from Campos Basin with SWH measured by the buoy of 8.9 m is illustrated in Figure 7.14 and 7.15. Once again the agreement between spectra is good (Figure 7.14d, Figure 7.14e and Figure 7.15a) both in terms of frequency, direction, spreading and energy. In Figure 7.15c the same behavior of the spreading as in the previous case is observed. From the two examples shown, a northward swell and a much longer and more energetic case, the spreading computed from the model (and therefore imposed on the spectrum retrieved by the MPI scheme) seems to represent fairly well the spreading directly computed from the buoy data. Although the value at the peak is slightly narrower, the overall shape of the directional spread retrieved by the MPI scheme describes very well the same trend measured by the buoy in the cases selected above.

7.5.2 Nonlinearities in the SAR Imaging Mechanism

Nonlinear SAR degradation of azimuth waves causes energy of high wavenumber waves to be transferred to low azimuthal wavenumbers. In the MPI scheme for computational reasons

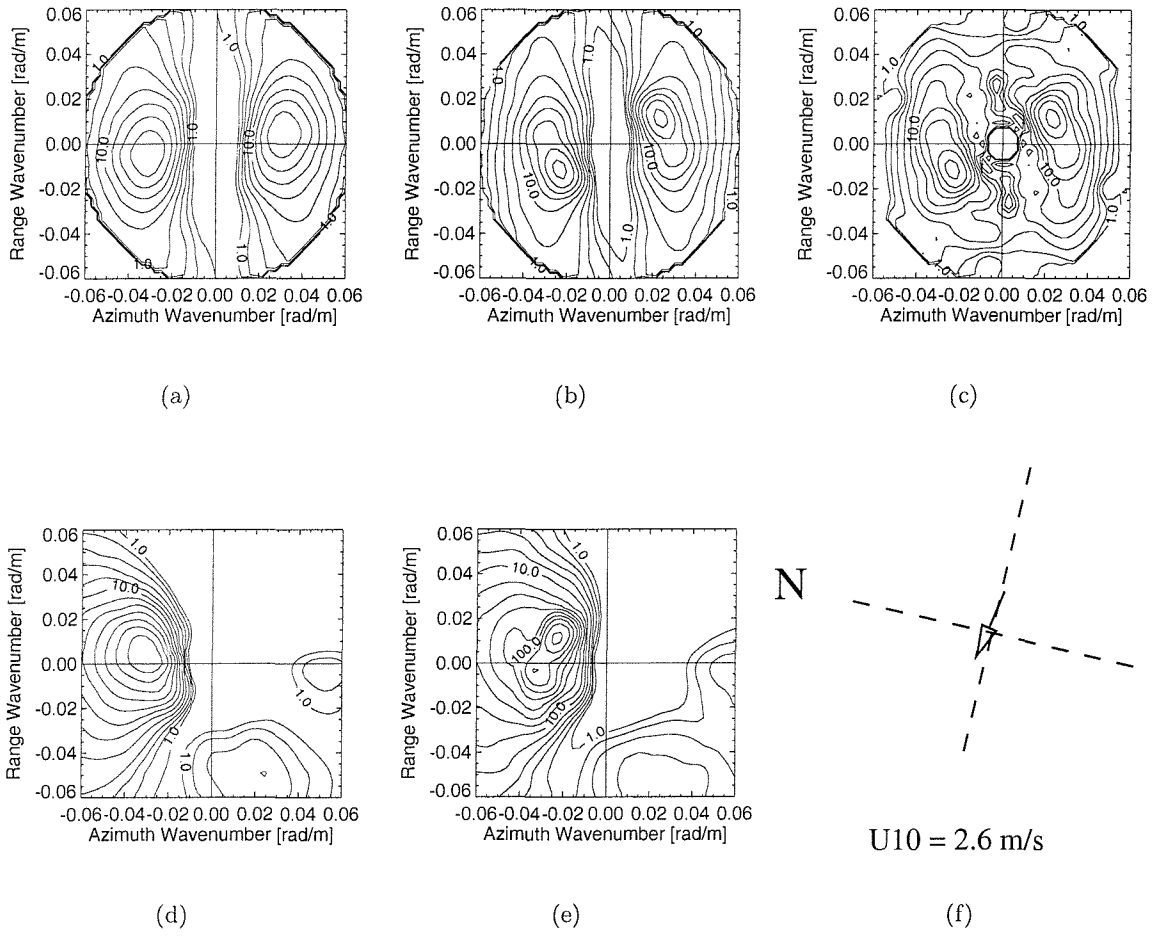

Figure 7.12: Example of a 195 m swell on August 29 1994, 1243 UT. The upper row shows SAR image spectra and the second row shows wave spectra (with exception to the third panel). Panels a to c are respectively the WAM image spectrum, the image spectrum retrieved by the MPI scheme and the observed SAR spectrum. Panels d and e are the WAM wave spectrum and the wave spectrum retrieved by the MPI scheme. In panel f the arrow indicates the wind speed estimated by the model (no wind information available from the buoy).

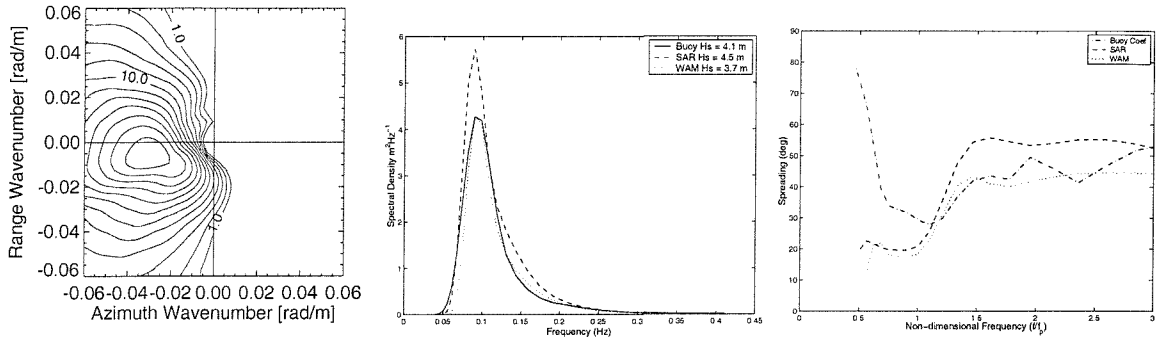

(a) (b) (c)

Figure 7.13: Panel a is the wave spectrum measured by the buoy for the case in Figure 7.12. The frequency spectrum with the values of significant wave height is shown in panel b. Panel c is the spreading function calculated using (7.11) directly calculated from the Fourier coefficients (Buoy Coef), and from the SAR and WAM.

the SAR spectrum is mapped back to the wave spectrum using a quasi-linear approximation to the mapping relations, in contrast to the forward mapping that uses the full nonlinear transform (Hasselmann and Hasselmann, 1991). The quasi-linear term is an approximation to the full nonlinear transform obtained by terminating the expansion after the first linear terms where the azimuthal cut-off is retained but nonlinearities in the mapping are not taking into account. Mastenbroek and de Valk (2000) and Voorrips et al. (2001) have already discussed the implications in neglecting the transfer of energy when the quasi-linear approximation is employed with the generation of spurious swell peaks in azimuth direction.

Figures 7.16 and 7.17 show the case of a swell peak erroneously enhanced due to the way that the MPI scheme deals with the nonlinearities in the SAR mapping mechanism. The frequency spectra (Figure 7.17b) illustrates a poor first guess where the wind sea component is underestimated by the WAM model probably because of an underestimation of the wind input by the ECMWF model (Figure 7.16f). The energy that this wind sea creates in low azimuth wavenumber caused by the nonlinearities in the SAR mapping mechanisms is erroneously interpreted by the MPI scheme as swell, which was already overestimated by the WAM model. The result is a swell peak that is 10 times larger than the one measured by the buoy. It is worth noting that although the value of SWH computed by the model is exactly the same as the one measured by the buoy, the frequency spectra differ enormously which

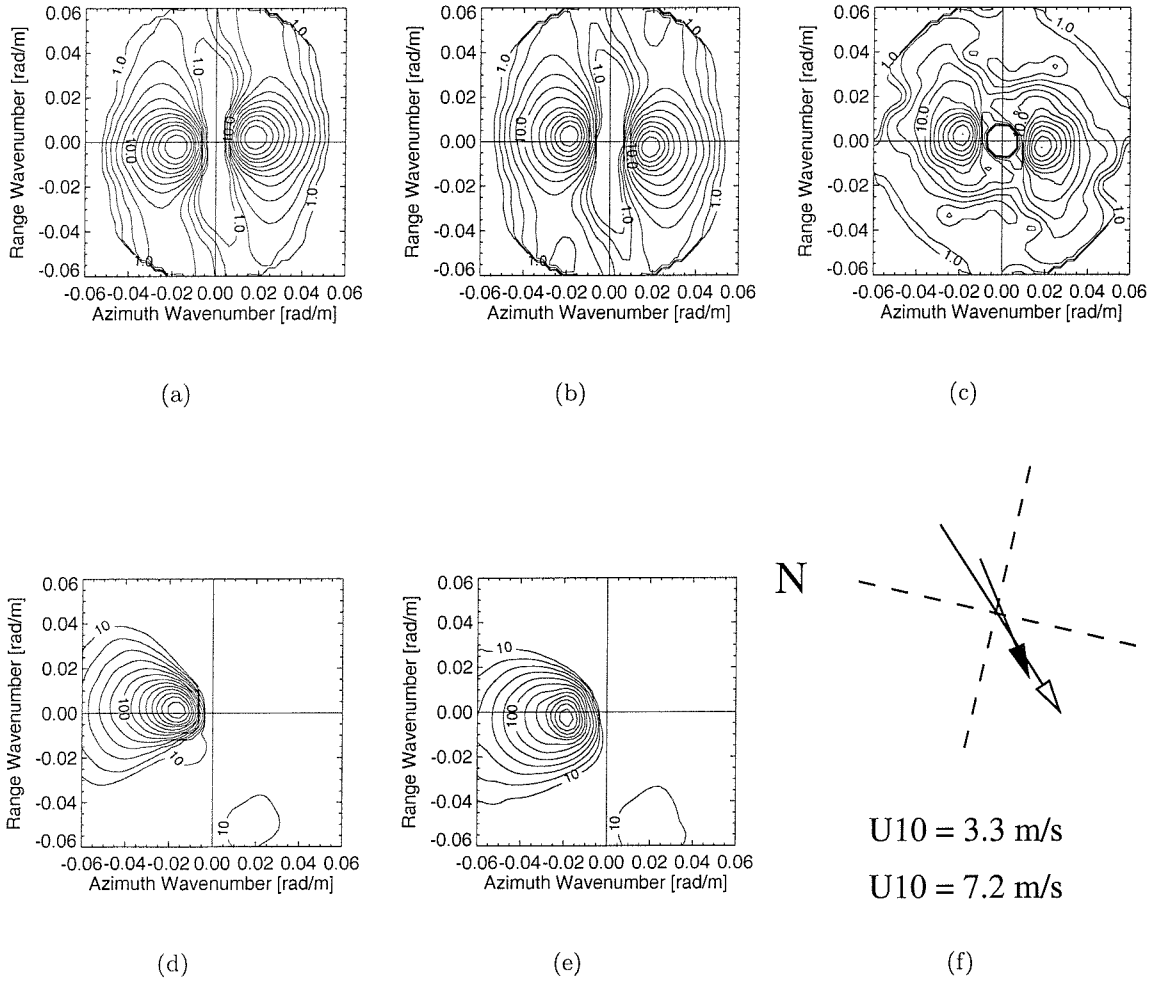

Figure 7.14: Example of a 345 m swell propagating northward (in azimuth direction) on June 30 1994, 1250 UT. See the caption in Figure 7.12. The wind speed measured by the buoy is indicated by the black arrow (first value of U10 on top) and the wind speed estimated by the ECMWF model is indicated by the open arrow (second value of U10).

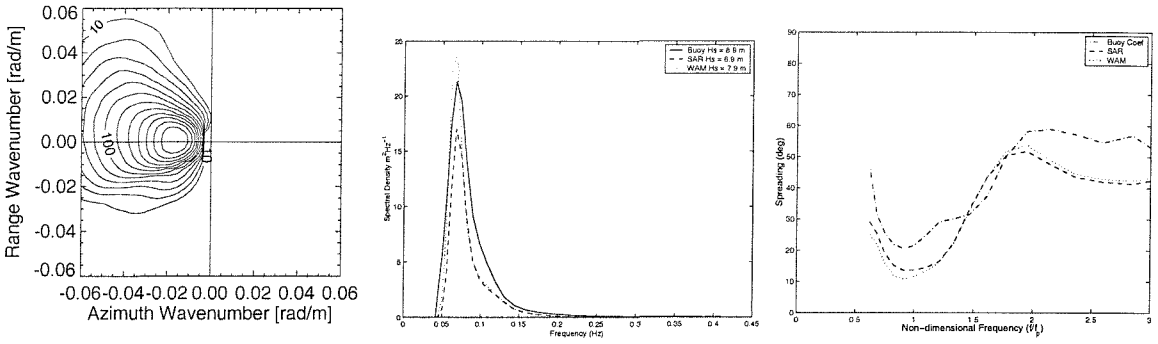

(a) (b) (c)

Figure 7.15: Directional spectrum measured by the buoy, frequency spectrum and spreading for the same case in Figure 7.14.

demonstrates the need for detailed spectral information in assimilation exercises.

The directional spectrum measured by the buoy in the case illustrated in Figure 7.16 is used as first guess to the inversion and the retrieved wave spectrum is presented in Figure 7.17c. The spurious peak at low frequency has disappeared and although the wind sea is somewhat underestimated the swell component is well retrieved both in terms of direction, frequency, energy and directional spread (Figures 7.16d and e). This case demonstrates how the nonlinearities in the SAR imaging mechanisms may be erroneously interpreted by the MPI scheme causing wind sea energy to be transferred to low azimuth wavenumbers.

7.6 Discussion

In a previous validation exercise where only SWH was taken into account, Voorrips et al. (2001) concluded that the MPI scheme increases the bias and the error of the WAM spectra used as first guess, even considering only the low wavenumber part of the spectrum directly mapped onto SAR images. Similar comparisons were performed in the present work but in contrast to the findings presented in Voorrips et al. (2001) we have found that the performance of the MPI scheme, when only the low wavenumber part of the spectrum is included in the computation of SWH, is as good as than the wave model. The main difference between both works is the WAM model employed. The ECMWF WAM version used in their study has assimilated SWH from altimeter data whereas our first guess wave spectra were estimated

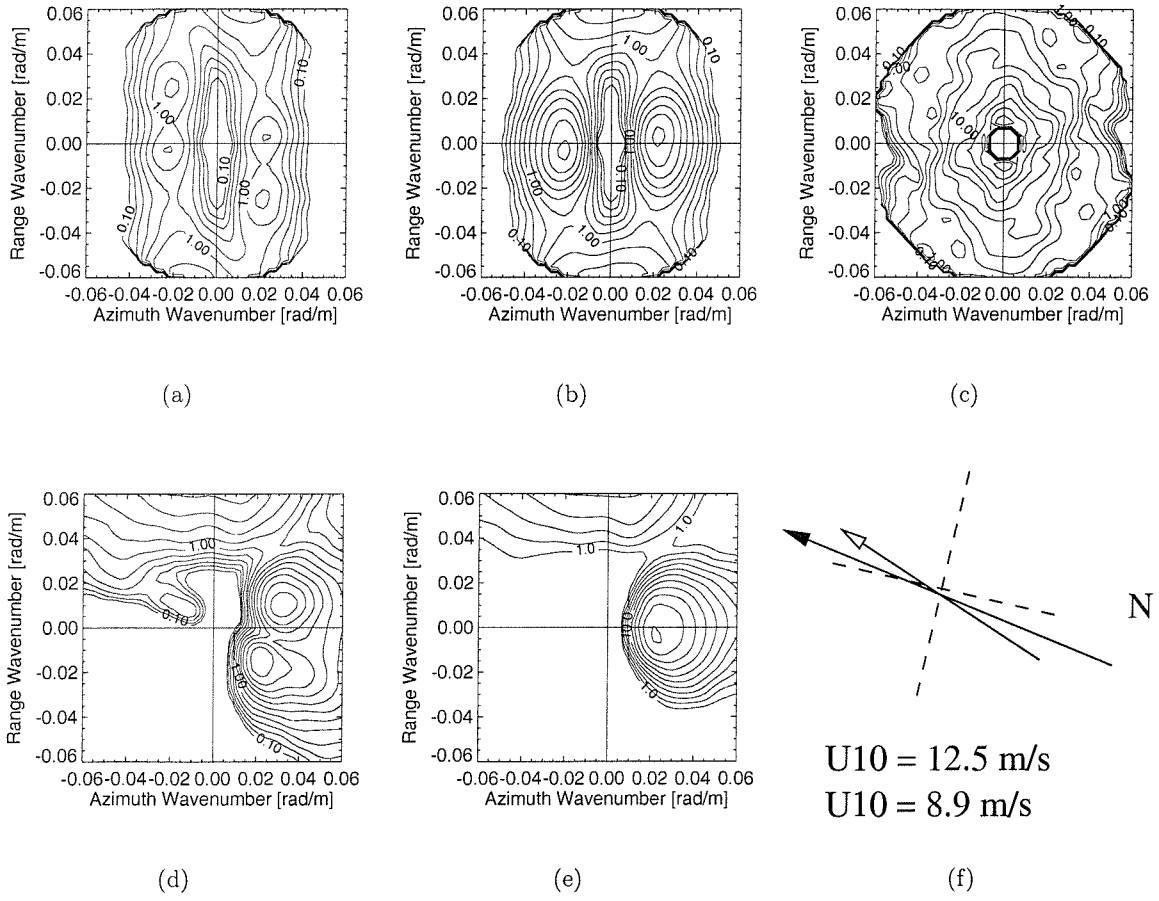

Figure 7.16: An erroneously enhanced swell peak due to a poor first guess on November 28 1994, 0141 UT (see Figure eg2cont too). See the caption in Figure 7.12. The wind speed measured by the buoy is indicated by the black arrow (first value on top) and the wind speed estimated by the ECMWF model is indicated by the open arrow (second value of U10).

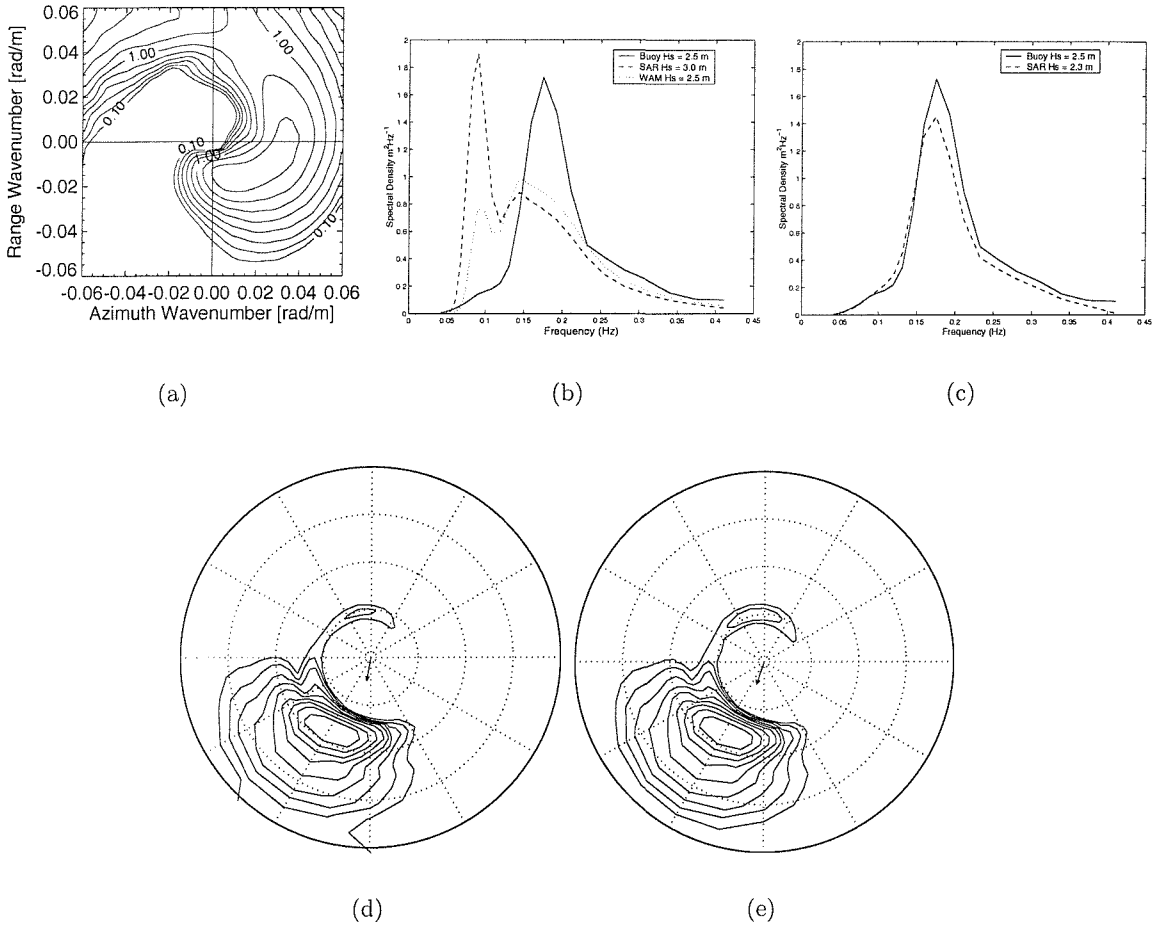

Figure 7.17: Directional spectrum measured by the buoy (a) and frequency spectrum (b) for the same case in Figure 7.16. Panel c is the frequency spectrum retrieved using the directional spectrum measured by the buoy as first guess to the inversion. Panels d and e are respectively the directional spectrum of the buoy measurement and the retrieved SAR wave spectrum correspondent to panel c with both spectra in polar frequency-directional plots with the wind direction represented by the arrow in the center. Circles denote frequency at 0.1 Hz interval from 0.1 Hz (inner circle) till 0.4 Hz (outer circle). Isolines are logarithmicaly spaced relative to the maximum value of the spectral energy density.

without any sort of assimilation procedure.

As well as the assessment of SWH, directional wave parameters were also considered in our analysis. For short waves the MPI scheme also deteriorates the retrievals of mean direction of propagation and mean frequency, where the model spectra used as first guess compare better to the buoy spectra than the retrievals. However for waves longer than 225 m, directly measured by SAR, the performance of the MPI scheme is at least as good as the WAM model. However most of the long wave energy is in the 12-14 second band so any conclusions drawn need to bear in mind that the results in the wave period bands longer than 14 s are not particularly relevant. In addition to the shortcomings of the algorithm to extend the spectral information beyond the high wavenumber cut-off, another constraint is the way that the MPI scheme deals with the nonlinearities in the SAR imaging mechanism. The use of the quasi-linear model to map the SAR image spectrum back to the wave spectrum might cause the algorithm to interpret a transfer of wind sea energy to low azimuth wavenumber components as swell.

In summary, the MPI scheme indeed degenerates the high wavenumber part of the first guess spectrum increasing the bias and the error of the wave parameters considered in the present work, that is SWH, mean direction of propagation and mean frequency. However for longer swell components it does not make the input spectrum any worse, on the contrary its performance is at least as good as—and even slightly better at some frequency bands—than the WAM wave model. However due to the fewer points in bands longer than 14 s these results should be considered with care.

Chapter 8

Conclusions and Perspectives

This work has investigated the use of Synthetic Aperture Radar for the observation of wind waves. The interaction between short and long waves and its importance in the modulation transfer functions has been discussed. A data set consisting of over four years of directional buoy measurements has been employed to study the influence of swell on wind sea growth, where their direction of propagation and separation in terms of frequency is analyzed. Additionally the widely used SAR retrieval scheme developed at the Max-Planck Institut has for the first time been evaluated through statistical intercomparisons against one year of in situ directional measurements and the WAM wave model data. The main conclusions of the analysis are summarized in the following:

- for practical purposes there is no clear effect of swell on wind sea growth and power laws from fetch limited situations apply to the open sea,
- the k^{-4} high wavenumber spectrum suits well to models of the Tilt modulation,
- our measurements point to a dependence of the long-short wave modulation on the wind speed and in the present representation of the Hydrodynamic modulation this dependency is neglected,
- for wave data assimilation exercises the proposed criteria for the cross assignment of wave systems are appropriate yielding satisfactory results,
- the frequency discretization employed by the WAM is not appropriate resulting in an underestimation of the mean frequency of the short waves,

- for short waves the MPI scheme deteriorates the first guess increasing the bias and error of the retrievals of SWH, mean direction and mean frequency,
- for waves longer than 225 m or periods longer than 12 s—the part of the spectrum observed by SAR—the performance of the MPI scheme is worse than WAM,
- the directional spreading of the MPI retrievals is in close agreement with the values obtained from the coefficients directly measured by the heave-pitch-roll buoy,
- the use of the quasi-linear model to map the SAR image spectrum back to the wave spectrum ignoring the nonlinearities might cause wind sea energy to be interpreted as swell.

In the rest of this chapter these conclusions and their implications are developed in more detail.

8.1 The Modulation of Wind Waves by Swell

Our understanding of the dynamics of wave generation and growth have improved substantially over the last few decades but there are still many unknowns in the fundamental processes which have been left to be elucidated. The main characteristics of wave evolution in controlled environments such as wave tanks or in sheltered areas without the presence of swell and in well defined fetches have been extensively documented and investigated. However observations of the wave growth in more common situations encountered in the open sea, that is in the presence of swell, are scarce. Therefore the question of how, and to what extent, long waves interact with shorter wind waves in the real ocean has not yet been properly investigated.

This question has attracted the attention of many researchers due to the increasing interest that this topic has aroused lately. Decimetric gravity waves (ripples) play a key role in the exchange processes through the air-sea interface and are hence associated with the transfer of momentum, heat, gases and mass. In addition—as so-called Bragg waves—they are involved in the modulation of radar backscatter and thus in the imaging of, for example, ocean surface waves. In the present work the energy balance of the wind waves propagating in the presence of longer waves was investigated. We have analyzed an extensive data set obtained from a directional buoy in tropical deep ocean waters where the influence of swell on wind waves was

examined, both in terms of their direction of propagation and their separation in frequency space. Although the wind sea waves observed in our analysis are two orders of magnitude longer than the Bragg waves responsible for the radar backscatter, the approach presented by Komen et al. (1984) where the dynamics of the wind waves are described by the source terms, can be applied to the decimetric waves according to the justifications presented in Komen (1988).

Together with a lack of long term wave measurements in the open sea, the main reason why the investigation of the influence of long waves on short waves has been delayed is the need for proper spectral methods for the partitioning between wind sea and swell. Although the partitioning scheme of the directional spectrum described by Hasselmann et al. (1996) was available we have opted to develop a new approach where the frequency spectrum is adjusted instead. The high frequency spectral tail, which is one of the main points in our investigation, is very sensitive to the spectral width of the two-dimensional spectrum (Banner and Young, 1994). The directional spectrum retrieved from buoys is subject to a certain degree of uncertainty due to the limited number of time series available and therefore the partitioning of the one dimensional spectrum, obtained directly from the heave measurement, yields more robust results.

The partitioning scheme developed in this work is based on a modified version of the JONSWAP spectrum where the exponent of the high frequency decay is estimated from the measured spectra. Spectral parameters such as for instance SWH, mean direction of propagation, mean frequency and wave age among others in addition to the JONSWAP parameters α and γ are calculated. Parameters estimated from the spectral adjustment are in close agreement with growth laws obtained in swell free environments, a result which has twofold importance. Firstly, for practical purposes, the presence of swell has no significant influence on wave growth and power laws obtained in fetch limited situations apply to the open sea where swell is ubiquitous. In the second place these results demonstrate that the spectral scheme for the partitioning of the frequency spectrum has ability to recover properly the wave parameters.

The Modulation Transfer Functions (MTFs) define the relation between the surface Bragg wave heights and the amplitude of the variabilities of the amount of energy that is reflected back to remote sensing sensors. In the specific case of Synthetic Aperture Radars imaging surface waves, swell travelling in the range direction is detected because of its effect on the decimetric Bragg waves through the Tilt and Hydrodynamic MTFs, both composing the

linear Real Aperture Radar (RAR) modulation. In contrast to the well known mechanism of imaging of azimuth travelling waves, the velocity bunching, the environment-dependent RAR modulations are poorly understood. For spaceborne SARs at high altitude, the velocity bunching mechanism surpasses the other modulation mechanisms. In addition, for the low incidence angles that have been deliberately chosen, the importance of the Hydrodynamic MTF, the less well understood of the modulation processes, is minimized in comparison with the Tilt MTF. However, for range travelling waves, the Hydrodynamic MTF becomes of the same order as the other MTFs.

Several laboratory experiments have demonstrated that the amplitude of short waves decreases in the presence of longer waves, although there is no clear consensus on what is the mechanism or mechanisms which cause this suppression. The relation between the wind sea energy ϵ and the inverse wave age U_{10}/c_p obtained from our measurements in the open ocean is statistically identical to the same relation from an experiment carried out in a lake without swell (Figure 5.5 on page 45). However, within the scatter in our data, the reduction in wind sea energy is more strongly observed for younger waves (larger values of inverse wave age), which might point to a dependence of the long wave-short wave modulation on the wind speed. This indication might lead to development of a more physically meaningful representation of the Hydrodynamic MTF, which describes how the amplitude of the Bragg waves are modulated by the phase of the swell waves. The damping factor μ in the Hydrodynamic MTF represents the rate at which the perturbed short waves tend to relax back to equilibrium. In the MPI scheme μ is represented by a constant relaxation time, which perhaps could be better described by a wind speed dependent term. The development of an improved Hydrodynamic MTF is beyond the scope of the present work and due to the scatter within the data these findings should be considered with care, although there are other evidences that suggest that μ is in fact wind speed dependent (Wright et al., 1980).

Our observations that the relation between ϵ and U_{10}/c_p is statistically identical to an experiment in a swell free environment may not be in disagreement with laboratory results as pointed out by Hanson and Phillips (1999). Chu et al. (1992) performing an experiment in a wave tank observed the reduction in amplitude of the short waves by breaking near the crest of the long wave accompanied by a shortening of the wind waves due to straining caused by the currents induced by the orbital velocities of the swell component. These effects combined compensate each other since the reduction of the energy of the short waves due to wave breaking comes along with an increase of the inverse wave age due to a decrease of the

phase velocity c_p—since c_p is directly proportional to the wave length.

The tilting modulation of the sea surface represents the change in the radar cross section due to variations in the incidence angle relative to the slope of the swell wave. The better known Tilt MTF assumes that the Bragg waves are represented by a high wavenumber spectrum in the form $F(k) = \alpha k^{-4}$, which corresponds to an f^{-5} spectrum. From our data no clear single representation for the high frequency decay of the spectrum in the frequency band between 1.37 and 2 times the peak frequency was observed, which together with several other experiments suggest that the assumption of a unique slope model might not be appropriate. The relation between the high frequency energy level α adjusted from the partitioning method against the inverse wage age, on the other hand, shows a remarkable agreement with data obtained in a swell free experiment (Figure 5.4 on page 43). This is an indication of the shape stabilization effect of the nonlinear interactions S_{nl} which forces the spectrum to a universal shape, even in the presence of swell as shown from our measurements. This fact demonstrates that although the imposition of a single high frequency decay to the Tilt MTF may not be the ideal option, the JONSWAP parametric spectral form fits our data well which is an indication of its applicability even in situations where one would expect strong modulations of the wind waves.

8.2 Assessment of ERS SAR Retrievals and WAM Estimates Against Directional Buoy Measurements

One year of measurements acquired in tropical deep waters in the South Atlantic is employed to perform intercomparisons of wave spectra retrieved by the MPI scheme and estimated by the WAM model. For the first time a scheme for the retrieval of wave spectra from ERS SAR images was statistically validated against directional buoy observations. Two different approaches were applied. In the first one, wave systems extracted from a partitioning method of the directional spectrum are cross assigned and their main parameters, that is SWH, mean direction, mean frequency and directional spread, are intervalidated. The comparison of wave systems, each one a constituent of the directional spectrum, is of interest for being an operationally feasible option for wave data assimilation studies. For the second approach, in contrast, the directional spectra retrieved from SAR images and estimated by the model are integrated to provide the frequency spectrum. The comparisons of the main wave parameters are made over specific frequency bands which assures that only related information is being

assessed. The statistics of SWH obtained using both approaches are very similar which is indicative of the suitability of the criteria employed for the cross assignment.

Due to the sparseness of observations, specially at sea, the deficiencies of meteorological models in computing the wind in the Southern Hemisphere are well known. The selection of about one hundred cases of wind measurements acquired by the offshore buoy, distributed over the whole year of analysis, yielded a good opportunity to also validate the wind fields estimated by the ECMWF model. The overall agreement is good with a correlation coefficient of 0.70 and normalized root mean squared (rms) error of 36%. The model presents a small negative bias that correspondes to about 6% of the mean speed measured by the buoy, although the spread is relatively high with a standard deviation of the order of 50% of the mean buoy wind speed.

Heimbach et al. (1998) comparing WAM estimates against SAR retrievals that used the wave model results themself as first guess have found a systematic underprediction of the energy of the swell components and an overprediction of the wind sea, whereas from our measurements this trend was not observed with the model being virtually bias free over the whole spectral range. Confirming the findings of Voorrips et al. (2001), we have observed that the MPI scheme deteriorates the values of SWH used as first guess for the inversion. The scatter in the WAM-Buoy point by point comparisons of SWH is 25% lower than the SAR-Buoy scatter indicating that the MPI scheme adds its own error. The mean value of SWH retrieved by the MPI scheme is about 10% higher than the mean value of SWH estimated by the model, which is in accordance to the results presented by Dunlap et al. (1998). The performance of the MPI scheme is shown to be worse than the wave model for values of SWH computed considering only the low wavenumber part of the spectrum—waves longer than 225 m.

The overall agreement between the propagation direction estimated by the WAM and from the buoy measurements is quite good with a correlation coefficient of 0.88. The model estimates present very small bias for waves with periods shorter than 10 s with a trend to increase its value for longer waves, although both WAM and SAR retrievals present maximum bias of the order of 15° which is their directional resolution. The performance of the MPI scheme for propagation direction is worse than the wave model with an increase of the standard deviation and normalized rms error with wave period.

Some discrepancies have been identified between the mean frequency of short waves estimated by the model and measured by the buoy. The underestimation of the computed

mean frequencies may be explained by an inadequate spectral discretization employed by the model, which appears to cause a delay in the development of the wind sea peak. WAM and SAR retrievals perform better for longer waves, with both bias and error decreasing slowly with wave period.

The retrieval of the directional spreading was assessed through some selected qualitative validations. In the MPI scheme the spectral shape of the retrieved wave systems are the same as their counterparts in the WAM first guess wave spectrum. The spreading computed by a third generation wave model depends on the integration of the source terms, whereas the nonlinear interactions S_{nl} play a key role in this process as has already been demonstrated by simulations and in situ measurements (Donelan et al., 1985; Young and van Vledder, 1993; Banner and Young, 1994). The impact on the directional spread of the non exact approximation of the calculation of S_{nl}, called discrete interaction approximation (DIA), has not yet been quantitatively demonstrated. However there is considerable uncertainty associated with the spread retrieved from heave-pitch-roll buoys due to the limitation in the number of time series acquired by the instrument, which means that the buoy in this case is not a reliable reference for the other observations. Hence a cross-validation exercise was performed, where the spread retrieved by the MPI scheme (and therefore estimated by the model) and computed from the Fourier Coefficients directly measured by the buoy were compared. The MPI and WAM results are very close to the value computed from the Fourier coefficients. However a statistical validation of the retrieved spreading against the values obtained by the heave-pitch-roll buoy has not been performed yet. One of the main reasons for such a lack of this sort of statistical validation is the complicated shape of the directional spreading when peaks lie close in frequency space. A possible way forward for investigating the spreading could be a spectral approach based on the partitioning of the directional spectrum, where different wave systems are classified in accordance with their mean direction, energy, frequency and spreading. Once different wave systems are isolated their respective Fourier coefficients could yield valuable information about the spreading characteristics of different waves systems, an approach that should be pursued as a future work.

In addition to the deficiency of the MPI scheme in extending the spectral information beyond the cut-off, another shortcoming was observed. The SAR image spectrum is mapped back to the wave spectrum using a simplification of the full nonlinear mapping relation, the so-called quasi-linear approximation. We presented a case where an underestimation of the wind sea used as first guess resulted in an overestimation of the retrieved swell peak due to the

way that the algorithm interprets the nonlinearities in the SAR spectrum. The nonlinearities in the quasi-linear approximation are ignored and the energy created by the wind sea in the low azimuth wavenumber was interpreted as swell energy.

8.3 Future Directions

The aim of data assimilation is to take advantage of the available observations by introducing them into modeling procedures, in such a way that the forcing or the initial conditions are improved giving better predictions with the model (a broader description of wave data assimilation techniques is presented in the Appendix). Data assimilation methods have been used for over four decades in meteorological models with the objective of improving the forecasting by making use of the widely available network of meteo-stations all over the world. Wave modelers, in contrast, have put off such an approach mainly due to the sparseness of wave observations. However after the advent of satellite oceanography this picture has changed and, in the particular case of wind waves, since the 1990's measurements of significant wave heights from altimeters became available and have been assimilated by several weather centers. Nevertheless the exercise of distributing the energy averaged over frequency and direction from wave height measurements over the whole two-dimensional spectrum requires several assumptions to be made, specially about the separation of wind sea and swell (Thomas, 1988; Janssen and Bidlot, 2001). But with the advent of SAR measurements and with the better understanding of the imaging processes, retrieval algorithms have been proposed and the full directional spectra extracted from SAR images are now available in quasi-real time with global coverage. It is recognized that the assimilation of wave observations can improve both the present sea state and, in the case of swell, the forecast of the models (see for example Lionello et al., 1995; Voorrips et al., 1997; Breivik et al., 1998; Dunlap et al., 1998).

However, as demonstrated in this work, the assimilation of the directional spectra retrieved from SAR images using the MPI scheme must be performed with great care. The MPI retrieval algorithm performs worse than the WAM wave model, therefore a more consistent procedure to extract the spectral information from SAR images should be pursued. Even the part of the spectrum directly mapped onto SAR images seems to performe worse than the WAM wave model which might be the explanation for the poor performance of the forecasting when the MPI scheme was applied in assimilation experiments.

The combination of measurements and numerical estimations can be translated into bet-

ter and more physically consistent model parameterizations. Inverse modeling techniques consist of estimating optimal parameters that minimize a function describing the difference between observed and estimated conditions, therefore improving the model parameters. Such approaches in oceanography have been already pursued (see the examples listed in Wunsch, 1996), although its application in wave modeling is in its infancy (de las Heras et al., 1994; Hersbach, 1998). Modeling of inverse problems of wind waves depends on good quality observational networks, therefore global measurements of the directional spectrum from the SAR wave mode are fundamental in this context.

The present work discussed many of the potentialities of using Synthetic Aperture Radar onboard satellites for the study of surface gravity waves. A scheme to retrieve wave spectra from SAR image spectra was investigated in detail through comprehensive statistical analyses of the main wave parameters and direct comparisons of the directional spectra. However further investigations are necessary for the improvement of the present retrieval schemes. Over ten years of measurements which yielded a few million of SAR wave mode imagettes represent a unique data set for the investigation of the wind wave dynamics. These figures will increase with the recently launched ENVISAT providing more global observations of the directional spectrum for the years to come.

Appendix A

A Review of the Techniques for the Assimilation of the Two-Dimensional Directional Spectrum into Wave Models

Several meteorological centers are investigating methods on how to use the new information retrieved from spaceborn SAR measurements in order to improve the wave forecasting. With this picture in mind, and focusing mainly on the problem of the full directional spectrum, the theory of wave data assimilation techniques is reviewed. The present chapter aims as well to describe in some detail the three techniques used so far in the assimilation of the two dimensional spectrum, that is the Optimal Interpolation Scheme, the Adjoint Technique and the Green's Function Method.

A.1 Introduction

The aim of data assimilation is to improve the forecasting introducing available observations into the modeling procedures in order to minimize the differences between model estimates and measurements. Both model and data are assumed to contain errors, which must be taken into consideration during the assimilation procedure. The assimilation of scatterometer, altimeter and Synthetic Aperture Radar (SAR) data can be applied in a combined wind and wave data assimilation procedure to improve the modeled data, and its difference from the

observed data should be smaller than before. As the number of observations to be assimilated is inevitably less than the model grid the data inserted at one grid point must be distributed over neighboring points. To avoid discontinuities the information should be interpolated using either sequential or variational methods.

Sequential methods (also known as kinematic) are time independent assimilations because they make corrections only at the time when an observation is available, in general over a synoptic interval of 6 hours. The strategy is to run the model forward in time, stopping at intervals to assimilate the available observations and then continuing the model run with the corrected state. Threfore winds are updated only locally, although waves in a particular grid point are the result of winds acting in a large area over a large period of time. These methods are computationally cheaper than variational methods, which make them particularly fit for operational use. Some examples of Sequential methods are the Optimal Interpolation (Lionello et al., 1992; Hasselmann et al., 1997; Voorrips et al., 1997), the Kalman filter (Voorrips et al., 1999) and Successive Corrections (Breivik et al., 1998).

The Optimal Interpolation method (OI) is the most commonly used sequential method and is implemented operationally at several weather forecast centers in the world, using so far only significant wave heights (SWH) derived from altimeters. In the assimilation of altimeter wave heights some *ad hoc* assumptions are imposed on the distribution of the energy between wind sea and swell, which are treated separately as in second-generation wave models. Thus one of the most powerful features of third-generation wave models such as WAM is neglected, that is the spectrum has no prescribed form and is free to respond to the source functions. This problem arises because a single point wave height measurement has to be distributed over the whole two-dimensional spectrum, a restriction that no longer applies to the assimilation of retrieved SAR wave spectra.

Variational (or dynamical) are time dependent methods which take the model dynamics into account but have a much higher computational cost compared to Sequential methods. A best estimation is obtained through the minimization of a cost function which is dependent on some control variables, generally the wind input. Observations over different time levels are considered in contrast to the single time level scheme used in Sequential methods. Hence it is possible to correct the wind field that generated a wave component at a time preceding the available observations. A swell generated by a distant storm acts over a large area and the method needs to compute the dynamical regime to track its position back in space and time. So the best model solution not only fits the data available but also is consistent with the

constraints of the model. Examples of applications in wave data assimilation are the Adjoint Model (de las Heras, 1994; Hersbach, 1998) and the Green's Function Method (Bauer et al., 1996; 1997).

More information about assimilation of altimeter wave heights is described in Komen et al. (1994, chap. 6). A comprehensive description of assimilation schemes is also presented in de las Heras (1994), while the main purpose of the present work is to review the state of the art of techniques for assimilation of the two dimensional wave spectrum, for instance extracted from SAR images or from buoy measurements. The structure of the paper is as follows. In section 2 the main aspects of the theory of wave data assimilation are presented. Sections 3, 4 and 5 discuss in more details, respectively, the three most applied wave data assimilation techniques: Optimal Interpolation, Adjoint Model and Green's Function. The final remarks are presented in section 6.

A.2 Theoretical Basis of Wave Data Assimilation

The evolution of wave energy as a function of frequency, direction, position and time $E(f, \theta, \mathbf{r}, t)$ is represented by the energy balance equation (Komen et al., 1994) which for deep water reads

$$\frac{D}{Dt}E = \frac{\partial E}{\partial t} + \mathbf{c_g} \cdot \bigtriangledown E = S_{in} + S_{nl} + S_{ds} \tag{A.1}$$

where $\mathbf{c_g}$ is the group velocity and the right hand side of (A.1) represents the source and sink terms due, respectively, to wind input, nonlinear interactions and white-capping dissipation. However it is more convenient for data assimilation purposes to rewrite (A.1) in a matrix form where a set of state variables is forced by a set of control variables:

$$\mathbf{x_{t+1}} = F(\mathbf{x}_t + \mathbf{u}_t) \tag{A.2}$$

where a state vector $\mathbf{x}_t$ is the wave energy E at each direction, frequency and grid point at time t and a control vector $\mathbf{u}_t$, in general the wind speed, is also defined over each point at time t (Wunsch, 1996). The nonlinear functional F represents the physics of the wave model and must be linearized in order to describe how a perturbation in the control vector is dynamically represented by a perturbation in the state vector. Hence performing a Taylor expansion of (A.2) and retaining only the terms up to the first-order the wave energy balance

equation can be represented as

$$\mathbf{x}_{t+1} = \mathbf{x}_t + \left[\frac{\partial F}{\partial \mathbf{x}_t}\right] \delta \mathbf{x}_t + \left[\frac{\partial F}{\partial \mathbf{u}_t}\right] \delta \mathbf{u}_t. \tag{A.3}$$

Therefore the nonlinear energy balance equation (A.1) is rewritten in matrix form (A.2) and its linear representation (A.3) describes how perturbations in the state vector (the wave energy E) are determined by perturbations in the wind field, which is the way that variational methods can track back a swell component both in time and in space.

Deviations between observations and model data are used to obtain the best estimate of the wave model. In order to minimize such differences, the wave model output is modified by adjusting its control variables—the initial conditions or the wind field. The best solution is the one which minimizes a *cost function* that consists basically of quadratic differences between observed and modeled data (respectively $\mathbf{d}^o$ and $\mathbf{d}$). Considering the probability distribution $P(\mathbf{d} - \mathbf{d^o}; \mathbf{c})$ given a set of control variables $\mathbf{c}$ and assuming that the distribution of the data error representing the model is Gaussian around its maximum (which is reasonable using the Central Limit Theorem) it follows that:

$$P(\mathbf{d} - \mathbf{d^o}) \simeq \exp(-\frac{1}{2}(\mathbf{d} - \mathbf{d^o})^2). \tag{A.4}$$

The maximum of P corresponds to the minimum of the exponent, which means that the maximum probability or most likely state is associated with the minimum of the cost function J, which in matrix notation reads

$$J = (\mathbf{d} - \mathbf{d^o})^T M (\mathbf{d} - \mathbf{d^o}) \tag{A.5}$$

where M is the expected variance in the model/data error. The calculation of such matrices requires long term statistics of the error covariance of the observations and predictions. Because the true states are not known in most cases, empirical relations are used to approximate M. Different weights of the error covariance matrix M are associated with the corrections depending on the distance between the model and observation locations, instrumental errors and model errors. In addition the cost function (A.5) can be written in a more general form adding terms penalizing differences between any *a priori* information available.

The goal of any data assimilation scheme is to minimize the cost function J setting the control variables in order to find the values that yield the minimum difference between

modeled data and observations. In most wave data assimilation studies the control variables have been defined as the wind field, although any other parameter that might influence the state vector could be used, as for example, the superficial current field or the initial wave field. The minimization of the cost function J involves the inversion of (A.5) using the linearized wave model equations (A.3). However this becomes a non-trivial exerercise due to the size of the state vector, with dimension of the order of 10^7 in the case of global wave models. Therefore one seeks the minimization of (A.5) searching for the maximum efficiency and the minimum computational cost.

When all available observations are used for the minimization of the cost function the assimilation scheme is denominated a variational method. In this case the inversion of (A.5) will require a time-dependency of the wave model equations since observations at a later time t will have to be related to the wave state at some previous time $t-1$. This approach allows the correction of the wind field at some point and time away from the observations, for example tracking back a swell component, but evidently with a high computational cost. On the other hand if only the observations at a single time level are used for the minimization of the cost function the approach is denominated a sequential method. Much simpler and computationaly cheaper this method permits the correction only of the wind associated with the wind sea, and hence only locally. In the following sections we will describe in more details the characteristics of sequential and variational methods and their applications in wave data assimilation studies.

A.3 The Optimal Interpolation Scheme

The Optimal Interpolation Scheme (OI) is the widest used method for wave data assimilation due especially to its simplicity and low computational cost compared with other techniques. In this scheme the available SAR spectral information is spread over the grid points using statistical interpolation techniques without taking into account the model constraints. The assimilation is performed in two steps. First a best-guess or analyzed field is calculated by Optimal Interpolation and then the corrections applied to the wind sea part of the spectrum are used to correct the local wind.

The analyzed or best estimate value $\mathbf{x} = (x_i)$ of the true state vector $\mathbf{x}^t = (x_i^t)$ is a linear combination of the model first-guess vector $\mathbf{x}^f = (x_i^f)$ obtained from a previous run and the weighted errors between the observed data $\mathbf{d}^o$ and the corresponding first-guess

values $\mathbf{d}^f$ computed from the model:

$$x_i = x_i^f + \sum_{j=1}^{n_{obs}} W_{ij}(d_j^o - d_j^f) \tag{A.6}$$

where i represents each component of the analyzed field, j the component of every observation and n_{obs} denotes the number of observations. W_{ij} are the interpolation weights determined by the minimization of the mean square error between the true state vector and its best estimation

$$J = < (\mathbf{x} - \mathbf{x}^t)^2 > . \tag{A.7}$$

This cost function (equation A.7) is minimized to obtain the interpolation weight W_{ij} (angle brackets meaning mean values over a large number of realizations). This yields that W_{ij} is a function of the covariance error matrices of the observations and the first-guesses (Komen et al., 1994; Hasselmann et al., 1997). The problem that arises is the computation of these matrices, since long term statistics are needed in order to compare the model predictions with observations. In general empirical relations are used to overcome this problem, and in Voorrips et al. (1997) 2 years of comparison of model results with buoy data are used to determine more refined matrices.

The analyzed data are the result of the Optimal Interpolation scheme (A.6) and can be applied to different types of data, for instance wave heights from altimeters, buoy data and two-dimensional spectra retrieved from SAR images (see for example the description of algorithms for the retrieval of SAR spectra in Hasselmann and Hasselmann, 1991; Krogstad et al., 1994; Hasselmann et al., 1996; Mastenbroek and de Valk, 2000). In Hasselmann et al. (1997) the first step in the assimilation procedure is the optimal interpolation of the two-dimensional SAR wave mode spectrum obtained every 30 s or 200 km along the satellite track. Seeking operational efficiency the number of variables involved in the problem is reduced by partitioning the 2-D spectrum, using a technique introduced by Gerling (1992), in general into 3 or 4 wave systems (wind sea, swell, mixture of wind sea and swell and old wind sea). The wind sea systems are identified by comparing the phase velocity and direction of the spectral peak with the wind speed and direction. Each wave system is assumed to be generated by different physical events, and so are uncorrelated with each others, and each is represented by few parameters: SWH (or spectral energy), mean direction and mean frequency (see more details in Hasselmann et al., 1996). Each wave system of different spectra is cross-assigned

with its counterpart—a wind sea system of a first-guess spectrum is correlated with the same system in the observed spectrum. If the wave system of the first-guess spectrum does not have a match in the observed spectrum it is superimposed on the analyzed spectrum. On the other hand, if the observed spectrum does not have a match in the first-guess spectrum it is superimposed on the first-guess spectrum. So a correspondence between all wave systems of the analyzed and observed spectra is reached and the wave systems that are cross-assigned are optimally interpolated generating an analyzed field of the parameters.

At this point the second step in the assimilation procedure can be implemented with the update of the spectrum and the correction of the wind field. The first-guess spectrum is rotated and rescaled to agree in direction, frequency and energy with the parameters derived from the interpolation and the new analyzed spectrum is created. The wind is corrected using scaling power laws for a growing wind sea spectrum under quasi-equilibrium growth conditions (Hasselmann et al., 1976). The wind field derived after the wave assimilation is interpolated with the first-guess wind yielding an updated wind field. The wave model can now be forced by the updated wind field and the differences between the model and the SAR-retrieved wave spectrum are expected to be smaller.

A test run over a period of two months of assimilation of directional spectra extracted from ERS-1 SAR data is presented in Hasselmann et al. (1997). In that work the optimal interpolation scheme used by ECMWF in the assimilation of altimeter data was modified and applied to the assimilation of the full spectrum retrieved from SAR data. Another example of the application of OI is presented in the work of Voorrips et al. (1997), where wave parameters extracted from pitch-roll buoys in the North Sea are assimilated into a regional version of the WAM model. In Breivik et al. (1998) a routine for the assimilation of retrieved SAR spectra during a test period of 4 months was run parallel to the regular operation of the Norwegian Meteorological Institute (DNMI) second generation wave model using another sequential scheme, the Successive Corrections method. Successive Corrections is used operationally at DNMI so far assimilating only wave heights (Breivik and Reistad, 1994). The OI has also been used operationally in several meteorological centers in their wave forecasting systems. Since August 1993 ERS-1 altimeter wave height data have been assimilated by ECMWF into their WAM wave model (Lionello et al., 1992) while studies for the implementation of assimilation of the full directional SAR wave spectra are ongoing (Janssen and Bidlot, 2001). Observations of SWH from the ERS-2 altimeter are assimilated using OI by the British Meteorological Office (UKMO) in Bracknell into their second generation wave model

(Thomas, 1988; Lorenc et al., 1991) and at the present the assimilation of retrieved SAR wave spectra is an active line of research in this center (James Gunson, personal communication).

On the whole the previous works have shown that the impact of assimilation of SAR spectra into wave models was very modest or neutral. The reason or reasons for this lack of improvement in the forecasting are not clear. One possibility is that the wave models have attained a level of sophistication where there is no clear improvement of the forecasting because of data assimilation. This seems unlikely to be the case. Even third generation models such as WAM with state of the art representation of the physics of wave evolution have room for improvement, specially in the description of the low frequency part of the spectrum. The less well known wave dissipation source function causes a poorer representation of swell compared to the better description of the wind sea part of the spectrum (Komen et al., 1994). Another possible cause could be that methods to extract wave spectra from SAR images are not dealing properly with the complexities of the SAR imaging mechanisms and hence yielding poor retrievals (Voorrips et al., 2001). In addition it is not clear if the lack of improvement in the assimilation exercises are due to the assimilation schemes themselves or to the far fewer SAR observations (both in temporal and spatial coverage) compared to the number of model grid points.

However, besides the fact that these works have found no clear improvement in the forecasting, they have also used significant wave heights as independent data for the validation of the assimilation. The reason is that there is no other source of directional wave information over oceanic basins apart from SAR data. Most of the buoys deployed in the ocean measure only the surface elevation and hence only the frequency spectrum. The only source of wave information with coverage similar to SAR data is derived from altimeters, but the problem of using SWH to assess assimilation experiments is the averaging property of this parameter. More insights about the impact of the assimilation into the forecasting could be gained comparing the directional and spectral misfit between model and another source of directional wave information such as directional buoys. Another point worth mentioning is that the only new information added through the assimilation of SAR data is the the low frequency part of the spectrum since the wave model spectra are used to extend the spectral information beyond the high frequency cut-off. Therefore retrieval methods that do not rely on the wave model spectrum itself as first guess, like the cross-spectral method by Engen and Johnsen (1995), could bring more information to the assimilation procedure and hence improve the forecasting.

A.4 The Adjoint Technique

The basic idea of data assimilation in variational methods is to fit model predictions to observations by modifying the model input rather than the model output. The differences between the model output and observations are measured by a cost function, and the assimilation is performed in order to minimize this cost function respecting the constraints of the model. The change in the wind field needed to generate a change in the wave field is determined by inverting the wave model equation, which has a very high computational cost specially for global operational implementation. The purpose of the Adjoint Method is to determine the minimum of the cost function without explicitly inverting the model equations, in such a way that the model equations and the adjoint model equations are solved in an iterative minimization loop.

Following the notation proposed by Komen et al. (1994) and describing the general data assimilation problem, the cost function J is constructed from three terms

$$J = J^d + J^f + J^c \tag{A.8}$$

taking into account the difference between observed and modeled data J^d, the misfit between the model data and first-guess model values J^f and the difference between the control variables and first-guess control variables J^c (such the wind input and the initial wave field). J is a quadratic function that penalizes deviations of the model from observations and first-guesses, and its minimization yields the values of the control variables that make the model results fit best to the data and first-guesses available. Since J is positive definite, it is differentiable and always has a point of minimum. Then the variations with respect to the control variables ($\partial J/\partial c$) is called the gradient of the cost and must be zero at its minimum.

The minimization of (A.8) is very time consuming in computational terms (actually the linear form of J is calculated by direct minimization) since the model data are implicit functions of the control variables. To avoid the direct inversion of the model equations, the Lagrange function L is constructed using the multipliers method

$$L = J + \lambda_i Ei \tag{A.9}$$

by adding the Lagrange multiplier λ times the models equations (in matrix representation) E to the cost function J (de las Heras, 1994; Komen et al., 1994).

Taking into consideration that the function L is odd its extremum has a stationary point that corresponds to the minimum of the cost function. More specificaly, the total derivative of J is the same as the partial derivative of L with respect to the control variables ($\partial L/\partial c$) and both vanish at the point of minimum. This point can be determined by taking the partial derivatives of L with respect to all the arguments of the problem and setting the results to zero. The variation of the Lagrange function with respect to λ

$$\partial L/\partial \lambda_i = 0 \tag{A.10}$$

yields the model equations, which can be solved forward in time. The derivative of (A.9) with respect to the model data

$$\partial L/\partial x_i = 0 \tag{A.11}$$

is called the adjoint of the wave model and can be solved backward in time. As has already been pointed out

$$\partial L/\partial c = 0 \tag{A.12}$$

is the gradient of J or the cost-function gradient.

The problem of solving the model equations explicitly in order to compute the cost-function gradient is avoided by solving the linearized model equations (A.10—A.12) in an iterative way. As the gradient will be zero only for specific values of the control variables they are used to search the minimum of the cost. Choosing a first-guess for the control variables and solving (A.10) the solution is the model parameter of interest and the cost function J is determined. The adjoint model (A.11) can be solved backward in time to yield the value of λ and the gradient of J can be extracted using (A.12). If the value reached is not acceptable, the control variables can be updated and the procedure repeated until the minimum is approached. Multiple integrations of the model equations and the adjoint model equations are required, which can have a computationally expensive cost in particular for third-generation models in global runs.

The complication of deriving the adjoint model equations from the model equations was avoided by Hersbach (1998). In that work an adjoint model compiler was used to compute the code automatically line by line generating the adjoint of the full-dimensional WAM. The adjoint was used for inverse modeling with the object to get better estimates of several model parameters in the sink and source terms. In this way it is possible to determine whether

misfits between model and data are caused by wrong wind inputs or by deficiencies in the model formulation (or in the linearization of the model equations). So far the adjoint method has been applied in wave data assimilation only to the simpler inverse modeling exercise, with the exception of de las Heras (1994) who worked with a one-dimensional version of the WAM to assimilate wave heights using synthetic data. For short period tests (of one day) the results obtained by de las Heras (1994) using the adjoint method were superior than the results from twin experiments using a simpler optimal interpolation method. For periods longer than one day the behavior of the gradient is more complex and the value of the minimum of the cost function was not attained in many cases.

A.5 The Green's Function Method

In the Adjoint Method the computationally expensive direct inversion of the model equations is avoided by solving the linearized model equations in an iterative way. Despite that, this method still requires an order of magnitude more computer time than the integration of the wave model which seems to be very costly for global operational implementation. The Green's Function Method on the other hand also avoids the direct inversion of the model equations, but does so by relying on a number of physical approximations. The wave spectrum perturbations are expressed by the impulse response (or Green's) function over the wind field perturbations, and are inverted without the need of iterations, implying a computational time of the same order as the integration of the model.

The main assumption is that the wind perturbations that generate the spectrum perturbations are associated with a small region in space and time and therefore can be approximated by a δ-function. This hypothesis is intuitively plausible but it lacks mathematical rigor compared to the Adjoint Method. Once the wave component becomes swell the wind speed has no more influence on it, but on the other hand in the generation region its presence is important during the wave growth. The wave spectrum response to the wind input is to shift the spectral peak towards lower frequencies through nonlinear wave to wave interactions, transferring energy from the region just beyond the spectral peak to the region below the spectral peak which maintains a quasi-equilibrium spectral shape. Thus the impact of the wind is scattered over higher and lower frequencies through this stabilizing effect of the spectrum shape, being only retained and transported when the wave component leaves the generation area, that is as swell, propagating undisturbed. So the most sensitive region of the wave spectrum is the

one that last received the input from the wind in the transition between wind sea and swell.

The assimilation scheme consists of minimizing the differences between model data and observations through the following cost function (Bauer et al., 1996)

$$J = \sum_{r}^{n_{obs}} \left\{ \frac{(d_r^f - d_r^o - d_r)^2}{(\sigma_r^d)^2} \right\} + C \sum_{p} \left\{ u_p^2 + v_p^2 \right\} \tag{A.13}$$

where d_r^f and d_r^o are the first-guess of the model data and the respective observed value, d_r is the modification after the optimization, u_p and v_p are the changes in the wind field in x and y components in a point p in space, n_{obs} is the number of observations, σ_r^d is the standard deviation of the measurements and C is a weighting factor. The Green's Function Method computes the model modifications d_r which are correlated with the modifications in the wind input u_p and v_p respecting the constraints of the model.

In order to minimize the cost function, (A.13) must be expressed in terms of the control variables u_p and v_p, in a way that the response of the wave spectrum $\mathbf{x}$ described by the perturbations in the wind field $\mathbf{u}$ is expressed by the Green's function. In practice, the integration of the response function requires the inversion of the Green's function operator, which is not feasible due to the complexity of this matrix which involves the whole source function. Relying on the assumption that only a specific small region of the wind field causes a perturbation in a component of the wave spectrum, the Green's function can be approximated by a δ-function representing the relation between the wind changes $(u_p, v_p) = [u(\mathbf{x}_p, \mathbf{t}_p), v(\mathbf{x}_p, \mathbf{t}_p)]$ in a point in the past $(\mathbf{x}_p, \mathbf{t}_p)$ and the spectral energy changes in the observation point $(\mathbf{x}_r, \mathbf{t}_r)$. The point $(\mathbf{x}_p, \mathbf{t}_p)$ determines the influence point or the point of the last wind input that must be altered to yield the spectral modification in the component $\mathbf{k}$ and point $\mathbf{x}_r$. The influence point (x_p, t_p) can be determined by tracing back the wave component using the wave age along the great circle path at its group velocity $\mathbf{c_g}$.

So far the Green's function assimilation method was run for synthetic wind cases (Bauer et al., 1996) with no rerun of the wave model in order to check the wave field corrections. A more realistic case was applied to determine the wind field corrections during a storm in the North Atlantic (Bauer et al., 1997). The results were compared with the Optimal Interpolation scheme and the wind corrections have a general good agreement, but again a comparison with the new model output generated by the updated wind field was not performed.

Although quite attractive because it is less expensive in computational terms, the Green's

function method relies on some simplifications, the strongest being about the localization of the wind region of influence. Perturbations in the wave spectrum are assumed to be caused by perturbations in the wind field in some specific region (in space and time) that are approximated by a δ-function, a rather unrealistic supposition. In addition the corrections to the wind are estimated using observations available during one time level in general of 6 hours—like sequential methods—rather than over different times—like variational methods. However since the constraints of the model are maintained the wave spectrum computed after the assimilation is consistent with the model dynamics.

A.6 Discussion

Significant wave heights measured from satellite altimeters have so far been the most widely used information applied in wave models at several weather centers. However significant wave height is a mean parameter. Therefore a greater impact is expected on the wave analysis using techniques for the assimilation of the full two-dimensional spectrum due to the detailed spectral and directional information derived from this information. Global observations of directional spectra are now available with the SAR onboard ERS-1 and ERS-2 and more recently with the launch of ENVISAT carrying the Advanced Synthetic Aperture Radar (ASAR). This fact has opened up challenging possibilities and several studies are undergoing on how to best exploit this information to improve the wave forecasting. In the present work a comprehensive discussion of the theory of wave data assimilation is presented with a review of several assimilation studies developed in the last few years. Futhermore the techniques used so far in the assimilation of the two-dimensional spectrum are examined in more depth.

Research in the area of wave data assimilation is in its early stages of development and implementation but some works have already indicated some exciting prospects for the future. One of the main issues of working with the assimilation of the two-dimensional spectrum is the high number of degrees of freedom involved in the problem. The approach of partitioning the spectrum into a number of wave systems each one represented by a set of parameters like mean direction of propagation, mean energy (SWH) and mean frequency seems reasonable and suits the assimilation problem very well. Another point that deserves to be mentioned is the calculation of the covariance matrices that requires long term statistics of the differences between observation and model. In the study by Voorrips et al. (1997) two years of buoy measurements in the North Sea were used to estimate the interpolation weights. However,

specially due to the lack of long term observations, these interpolation weights are generally approximated by exponential expressions of the ratio between the distance model-observation and a correlation length scale. Thus an improvement of the estimation of the error covariance matrices necessarily requires several runs of the model to compute the statistical correlations.

A very particular characteristic of assimilating data into wave models which has no counterpart in meterorological or oceanic models is the distinction that must be imposed between wind sea and swell. Wind waves are very sensitive to the wind input which ensures that any correction of the wind sea part of the spectrum, if not accompanied by the respective correction in the wind input, reverts quickly to its original (incorrect) state. Therefore the correction of the wind sea part of the spectrum has only local influence. This became clear in the very first exercises on wave data assimilation which pointed out that combined wind and wave assimilation schemes, that is coupled wind-wave models, would be necessary for optimal assimilation purposes. But the use at the present moment of coupled models is a very ambitious task and it seems that it will not be feasible, at least operationally, in the near future.

The effect of swell corrections, on the other hand, can be felt over entire ocean basins over the period of several days. Once the wind waves leave the generation area, becoming swell, they propagate almost undisturbed and the analyzed (corrected) components will have a positive impact on the forecasting. In addition due to nonlinearities in the imaging processes only the low frequency part of the spectrum, before a high wavenumber cut-off, is directly mapped onto SAR images. As a consequence, if the main objective is to improve the wave forecasting rather than correct the wind input, it seems reasonable to assimilate only the swell part of the spectrum which is in the end the only information directly measured by SAR.

Bibliography

M. L. Banner. Equilibrium spectra of wind waves. *Journal of Physical Oceanography*, 20: 996–984, 1990.

M. L. Banner and I. R. Young. Modeling spectral dissipation in the evolution of wind waves. Part I: Assesment of existing model performance. *Journal of Physical Oceanography*, 24: 1550–1571, 1994.

E. Bauer, K. Hasselmann, I. R. Young, and S. Hasselmann. Assimilation of wave data into the wave model WAM using an impulse response function method. *Journal of Geophysical Research*, 101(C2):3801–3816, 1996.

E. Bauer, S. Hasselmann, P. Lionello, and K. Hasselmann. Comparison of assimilation results from an optimal interpolation and the Green's function method using ERS-1 SAR wave mode spectra. In *Proc. 3rd Symp. on Space at the Service of our Environment*, pages 1131–1136, Florence, Italy, 1997.

E. Bauer and P. Heimbach. Annual validation of significant wave heights of ERS-1 Synthetic Aperture Radar wave mode spectra using TOPEX/Poseidon and ERS-1 altimeter data. *Journal of Geophysical Research*, 104(C6):13,345–13,357, 1999.

L. A. Breivik and M. Reistad. Assimilation of ERS-1 altimeter wave heights in an operational numerical wave model. *Weather and Forecasting*, 9:440–450, 1994.

L. A. Breivik, M. Reistad, H. Schyberg, J. Sunde, H. E. Krogstad, and H. Johnsen. Assimilation of ERS SAR wave spectra in an operational wave model. *Journal of Geophysical Research*, 103(C4):7887–7900, 1998.

G. Chen and S. E. Belcher. Effects of long waves on wind-generated waves. *Journal of Physical Oceanography*, 30:2246–2256, 2000.

J. S. Chu, S. R. Long, and O. M. Phillips. Measurements of the interaction of wave groups with shorter wind-generated waves. *Journal of Fluid Mechanics*, 245:191–210, 1992.

G. T. Csanady. *Air-Sea Interaction.* Cambridge University Press, 2001. 239 pages.

M. de las Heras. *On Variational Data Assimilation in Ocean Wave Models.* PhD thesis, University of Utrecht, 1994.

M. de las Heras, G. Burgers, and P. A. E. M. Janssen. Variational wave data assimilation in a third-generation wave model. *Journal of Atmospheric and Oceanic Technology*, 11: 1350–1369, 1994.

F. Dobson, W. Perrie, and B. Toulany. On the deep-water fetch laws for wind-generated surface gravity waves. *Atmosphere-Ocean*, 27(1):210–236, 1989.

M. A. Donelan. *The effect of swell on the growth of wind waves.* Johns Hopkins APL Technical Digest 8(1), 1987. pp. 18–23.

M. A. Donelan. Air-sea interaction. In B. Le Mehaute and D. M. Haines, editors, *The Sea*, volume 9 part A, pages 239–292, 1990.

M. A. Donelan, J. Hamilton, and W. H. Hui. Directional spectra of wind-generated waves. *Philosophical Transactions of the Royal Society of London*, A 315:509–562, 1985.

M. A. Donelan, M. Skafel, H. Graber, P. Liu, D. Schwab, and S. Venkatesh. On the growth rate of wind-generated waves. *Atmosphere-Ocean*, 30(3):457–478, 1992.

E. M. Dunlap, R. B. Olsen, L. Wilson, S. De Margerie, and R. Lalbeharry. The effect of assimilating ERS-1 fast delivery wave data into the north atlantic WAM model. *Journal of Geophysical Research*, 103(C4):7901–7915, 1998.

G. Engen and H. Johnsen. SAR-ocean wave inversion using cross spectra. *IEEE Transactions on Geoscience and Remote Sensing*, 33(4):1047–1056, 1995.

M. A. Gan and V. B. Rao. Surface cyclogenesis over South America. *Monthly Weather Review*, 119:1293–1302, 1991.

T. Gerling. Partitioning sequences and arrays of directional ocean wave spectra into component wave systems. *Journal of Atmospheric and Oceanic Technology*, 9:444–458, 1992.

C. Guedes Soares. Representation of double-peaked sea wave spectra. *Ocean Engineering*, 11 (2):185–207, 1984.

C. Guedes Soares and M. C. Nolasco. Spectral modeling of sea states with multiple wave systems. *Journal of Offshore Mechanics and Arctic Engineering*, 114:278–284, 1992.

H. Günther, S. Hasselmann, and P.A.E.M. Janssen. The WAModel cycle 4 (revised version). Technical report, Deutsches Klimarechenzentrum (DKRZ), Hamburg, Germany, 1992. Tech. Rep. 4.

J. L. Hanson and O. M. Phillips. Wind sea growth and dissipation in the open ocean. *Journal of Physical Oceanography*, 29:1633–1648, 1999.

K. Hasselmann. On the spectral dissipation of ocean waves due to white capping. *Boundary-Layer Meteorology*, 6:107–127, 1974.

K. Hasselmann, T. P. Barnett, F. Bouws, H. Carlson, D. E. Cartwright, K. Enke, J. A. Ewing, H. Gienapp, D. E. Hasselmann, P. Krusemann, A. Meerburg, P. Müller, D. J. Olbers, K. Richter, W. Sell, and H. Walden. Measurements of wind-wave growth and swell decay during the Joint North Sea Wave Project (JONSWAP). *Dtsch. Hydrogr. Z. Suppl.*, A8(12), 1973. 95 p.

K. Hasselmann and S. Hasselmann. On the nonlinear mapping of an ocean wave spectrum into a Synthetic Aperture Radar image spectrum and its inversion. *Journal of Geophysical Research*, 96(C6):10,713–10,729, 1991.

K. Hasselmann, P. Lionello, and S. Hasselmann. An optimal interpolation scheme for the assimilation of spectral wave data. *Journal of Geophysical Research*, 102(C7):15,823–15,836, 1997.

K. Hasselmann, R. K. Raney, W. J. Plant, W. Alpers, R. A. Schuchman, D. R. Lyzenga, C. L. Rufenach, and M. J. Tucker. Theory of Synthetic Aperture Radar ocean imaging: A MARSEN view. *Journal of Geophysical Research*, 90(C3):4659–4686, 1985.

K. Hasselmann, D. B. Ross, and W. Sell. A parametric wave prediction model. *Journal of Physical Oceanography*, 6:200–228, 1976.

S. Hasselmann, C. Brüning, K. Hasselmann, and P. Heimbach. An improved algorithm for the retrieval of ocean wave spectra from Synthetic Aperture Radar image spectra. *Journal of Geophysical Research*, 101(C7):16,615–16,629, 1996.

S. Hasselmann and K. Hasselmann. Computations and parameterizations of the nonlinear energy transfer in a gravity wave spectrum. Part I: A new method for efficient computations of the exact nonlinear energy transfer integral. *Journal of Physical Oceanography*, 14:1369–1377, 1985.

S. Hasselmann, K. Hasselmann, J. H. Allender, and T. P. Barnett. Computations and parameterizations of the nonlinear energy transfer in a gravity wave spectrum. Part II: Parameterisations of the nonlinear energy transfer for application in wave models. *Journal of Physical Oceanography*, 14:1378–1391, 1985a.

S. Hasselmann, P. Heimbach, and C. Bennefeld. Algorithm for retrieving ocean wave spectra from SAR image spectra. Technical report, Deutsches Klimarechenzentrum (DKRZ), Hamburg, Germany, 1998.

P. Heimbach, S. Hasselmann, and K. Hasselmann. Statistical analysis and intercomparison of WAM model data with global ERS-1 SAR wave mode spectral retrievals over 3 years. *Journal of Geophysical Research*, 103(C4):7931–7977, 1998.

H. Hersbach. Application of the adjoint of the WAM model to inverse wave modeling. *Journal of Geophysical Research*, 103(C5):10,469–10,487, 1998.

P. A. E. M. Janssen. Wave-induced stress and the drag of the air flow over sea waves. *Journal of Physical Oceanography*, 19:745–754, 1989.

P. A. E. M. Janssen. Quasi-linear theory of wind-wave generation applied to wave forecasting. *Journal of Physical Oceanography*, 21:1631–1391, 1991.

P. A. E. M. Janssen and J. R. Bidlot. ECMWF wave-model documentation. Technical report, European Centre for Medium-Range Weather Forecasts, 2001. IFS Documentation Cycle CY23r4, 48 pages.

P. A. E. M. Janssen and P. Viterbo. Ocean waves and the atmospheric climate. *Journal of Climate*, 9:1269–1287, 1996.

S. A. Kitaigorodskii. Applications of the theory of similarity to the analysis of wind-generated gravity waves. *Bull. Acad. Sci. USSR Geophys. Ser.*, 1:105–117, 1962.

S. A. Kitaigorodskii. On the theory of the equilibrium range in the spectrum of wind-generated gravity waves. *Journal of Physical Oceanography*, 13:816–827, 1983.

G. J. Komen. The energy balance in short gravity waves. In G. J. Komen and W. A. Oost, editors, *Radar Scattering from Modulated Wind Waves*. Kluwer Academic Publishers, 1988. p. 75–79.

G. J. Komen, L. Cavaleri, M. A. Donelan, K. Hasselmann, S. Hasselmann, and P. A. E. M. Janssen. *Dynamics and Modelling of Ocean Waves*. Cambridge University Press, Great Britain, 1994. 532 p.

G. J. Komen, S. Hasselmann, and K. Hasselmann. On the existence of a fully developed windsea spectrum. *Journal of Physical Oceanography*, 14:1271–1285, 1984.

H. E. Krogstad, O. Samset, and P. W. Vachon. Generalizations of the non-linear ocean-SAR transform and a simplified SAR inversion algorithm. *Atmosphere-Ocean*, 32(1):61–82, 1994.

A. J. Kuik, G. Ph. van Vledder, and L. H. Holthuijsen. A method for the routine analysis of pitch-and-roll buoy wave data. *Journal of Physical Oceanography*, 18:1020–1034, 1988.

I. V. Lavrenov and F. J. Ocampo-Torres. Angular distribution effect on weakly nonlinear energy transfer in the spectrum of wind waves. *Izvestiya, Atmospheric and Oceanic Physics*, 35(2):254–265, 1999.

P. Lionello, H. Günter, and P. A. E. M. Janssen. Assimilation of altimeter data in a global third-generation wave model. *Journal of Geophysical Research*, 97(C9):14,463–14,474, 1992.

P. Lionello, H. Günther, and P.A.E.M. Janssen. A sequential assimilation scheme applied to global wave analysis and prediction. *Journal of Marine Systems*, 6:87–107, 1995.

P. C. Liu. On the slope of the equilibrium range in the frequency spectrum of wind waves. *Journal of Geophysical Research*, 94(C4):5017–5023, 1989.

R. B. Long. The statistical evaluation of directional spectrum estimates derived from pitch/roll buoy data. *Journal of Physical Oceanography*, 10:944–952, 1980.

M. S. Longuet-Higgins. On wave breaking and the equilibrium spectrum of wind-generated waves. *Proc. R. Soc. Lond.*, A310:151–159, 1969.

M.S. Longuet-Higgins, D.E. Cartwright, and N.D. Smith. *Observations of the Directional Spectrum of Sea Waves Using the Motion of a Floating Buoy. Ocean Wave Spectra.* Englewood Cliffs, N.J., Prentice-Hall, 1963. p. 111–136.

A. C. Lorenc, R. S. Bell, and B. Macpherson. The meteorlogical analysis correction data assimilation scheme. *Quarterly Journal of the Royal Meteorological Society*, 117:59–89, 1991.

A. Lygre and H. E. Krogstad. Maximum entropy estimation of the directional distribution in ocean wave spectra. *Journal of Physical Oceanography*, 16:2052–2060, 1986.

S. L. Marple Jr. *Digital Spectral Analysis.* Prentice-Hall Inc., Englewood Cliffs, 1987. 492 p.

D. Masson. On the nonlinear coupling between swell and wind waves. *Journal of Physical Oceanography*, 23:1249–1258, 1993.

C. Mastenbroek and C. F. de Valk. A semiparametric algorithm to retrieve ocean wave spectra from Syntetic Aperture Radar. *Journal of Geophysical Research*, 105(C2):3497–3516, 2000.

T. J. McCarthy. Spectral fitting procedures for double peaked wave spectra. In *Dock and Harbour Engineering Conference*, Suratkal, India, 6-9 December 1989.

H. Mitsuyasu, F. Tasai, T. Suhara, S. Mizuno, M. Ohkusu, T. Honda, and K. Rikiishi. Observations of the directional spectrum of ocean waves using a cloverleaf buoy. *Journal of Physical Oceanography*, 5:750–760, 1975.

F. M. Monaldo and R. C. Beal. Comparison of SIR-C SAR wavenumber spectra with WAM model predictions. *Journal of Geophysical Research*, 103(C9):18,815–18,825, 1998.

M. K. Ochi and E. N. Hubble. On six-parameter wave spectra. In *Proc. 15th Coastal Engineering Conf. A.S.C.E.*, pages 321–328, 1976.

C. E. Parente, N. Violante-Carvalho, J. A. M. Lima, and C. B. Assunção. Wave and wind extreme values in good weather situations in Campos Basin, off Rio de Janeiro. In *Proceedings of the 20th Internationl Conference on Offshore Mechanics and Artic Engineering—OMAE01*, 2001.

O. M. Phillips. The equilibrium range in the spectrum of wind-generated waves. *Journal of Fluid Mechanics*, 4:426–434, 1958.

O. M. Phillips. Spectral and statistical properties of the equilibrium range in wind-generated gravity waves. *Journal of Fluid Mechanics*, 156:505–531, 1985.

O. M. Phillips and M. L. Banner. Wave breaking in the presence of wind drift and swell. *Journal of Fluid Mechanics*, 6(Part 4):625–640, 1974.

W. J. Pierson. Comments on A parametric wave prediction model. *Journal of Physical Oceanography*, 7:127–137, 1977.

W. J. Pierson and L. Moskowitz. A proposed spectral form for fully developed wind seas based on the similarity theory of S. A. Kitaigorodskii. *Journal of Geophysical Research*, 69 (24):5181–5190, 1964.

M. Prevosto, H. E. Krogstad, S. F. Barstow, and C. Guedes Soares. Observations of the high-frequency range of the wave spectrum. *Journal of Offshore Mechanics and Arctic Engineering*, 118:89–95, 1996.

I. S. Robinson. *Satellite Oceanography.* Ellis Horwood Ltd., Chichester, UK, 1985. 455 p.

G. Rodriguez and C. Guedes Soares. A criterion for the automatic identification of multimodal sea wave spectra. *Applied Ocean Research*, 21:329–333, 1999a.

G. Rodriguez and C. Guedes Soares. Uncertainty in the estimation of the slope of the high frequency tail of wave spectra. *Applied Ocean Research*, 21:207–213, 1999b.

G. Rodriguez, C. Guedes Soares, and F. J. Ocampo-Torres. Experimental evidence of the transition between power law models in the high frequency range of the gravity wave spectrum. *Coastal Engineering*, 38:249–259, 1999.

R. Romeiser. Global validation of the wave model WAM over a one-year period using geosat wave height data. *Journal of Geophysical Research*, 98(C3):4713–4726, 1993.

R. L. Snyder, F. W. Dobson, J. A. Elliott, and R. B. Long. Array measurements of atmospheric pressure fluctuations above surface waves. *Journal of Fluid Mechanics*, 102:1–59, 1981.

SWAMP Group. *Ocean Wave Modeling.* Plenum Press, New York (USA), 1985. 256 p.

J. P. Thomas. Retrieval of energy spectra from measured data for assimilation into a wave model. *Quarterly Journal of the Royal Meteorological Society*, 114:781–800, 1988.

Y. Toba. Local balance in the air-sea boundary processes, III. On the spectrum of wind waves. *J. Oceanogr. Soc. Japan*, 29:209–220, 1973.

H. L. Tolman. Effects of numerics on the physics in a third-generation wind-wave model. *Journal of Physical Oceanography*, 21:1095–1111, 1992.

M. J. Tucker. Interpreting directional data from large pitch-roll-heave buoys. *Ocean Engineering*, 16(2):173–192, 1989.

N. Violante-Carvalho. Investigation of the wave climate in Campos Basin, Rio de Janeiro–Brazil and its correlation with the meteorological situations—*in Portuguese*. Master's thesis, Rio de Janeiro University- COPPE/UFRJ, 1998.

N. Violante-Carvalho, L. M. P. Nunes, and W. Tavares Jr. Typical conditions and extreme values of wind speed in Campos Basin. Technical Report 005/97, Brazilian Oil Company – PETROBRAS, 1997.

N. Violante-Carvalho, F. J. Ocampo-Torres, and I. S. Robinson. Buoy observations of the influence of swell on wind waves in the open ocean. *Applied Ocean Research*, submitted, 2002a.

N. Violante-Carvalho, C. E. Parente, I. S. Robinson, and L. M. P. Nunes. On the growth of wind generated waves in a swell dominated region in the South Atlantic. *Journal of Offshore Mechanics and Arctic Engineering*, 124:14–21, 2002b.

A. C. Voorrips, A. W. Heemink, and G. J. Komen. Wave data assimilation with the kalman filter. *Journal of Marine Systems*, 19:267–291, 1999.

A. C. Voorrips, V. K. Makin, and S. Hasselmann. Assimilation of wave spectra from pitch-and-roll buoys in a north sea wave model. *Journal of Geophysical Research*, 102:5829–5489, 1997.

A. C. Voorrips, C. Mastenbroek, and B. Hansen. Validation of two algorithms to retrieve ocean wave spectra from ERS Synthetic Aperture Radar. *Journal of Geophysical Research*, 106(C8):16,825–16,840, 2001.

WAMDI Group. The WAM model—a third generation ocean wave prediction model. *Journal of Physical Oceanography*, 18:1775–1810, 1988.

J. W. Wright, W. J. Plant, W. C. Keller, and W. L. Jones. Ocean wave-radar modulation transfer functions from the west coast experiment. *Journal of Geophysical Research*, 85: 4957–4966, 1980.

C. Wunsch. *The Ocean Circulation Inverse Problem.* Cambridge University Press, 1996. 458 pages.

L. R. Wyatt, S. P. Thompson, and R.R. Burton. Evaluation of high frequency Radar wave measurements. *Coastal Engineering*, 37:259–282, 1999.

I. R. Young. On the measurement of directional wave spectra. *Applied Ocean Research*, 16: 283–294, 1994.

I. R. Young. Observations of the spectra of hurricane generated waves. *Ocean Engineering*, 25(4–5):261–276, 1998.

I. R. Young. *Wind Generated Ocean Waves.* Elsevier, 1999. 288 p.

I. R. Young and G. Ph. van Vledder. A review of the central role of nonlinear interactions in wind-wave evolution. *Philosophical Transactions of the Royal Society of London*, A 342: 505–524, 1993.

I. R. Young and L. A. Verhagen. The growth of fetch limited waves in water of finite depth. Part 2. Spectral evolution. *Coastal Engineering*, 29:79–99, 1996.

I. R. Young, L. A. Verhagen, and M. L. Banner. A note on the bimodal directional spreading of fetch-limited wind waves. *Journal of Geophysical Research*, 100(C1):773–778, 1995.

Index